

Ga^{III} and Zr^{IV} Complexes as Phosphatase Analogues

Fergal Coleman

Thesis for the Degree of Ph.D.



September, 2011

School of Chemistry

National University of Ireland, Galway

Abstract

In purple acid phosphatase (PAP)-catalysed phosphate monoester hydrolysis, it is accepted that the ferric ion of the active site can mediate the reaction through Lewis acid activation of the substrate and through nucleophilic attack on phosphorus by coordinated hydroxide. These modes are antagonistic, OH bound to a strongly acidic Fe^{III} center will not be an efficient nucleophile, whereas OH coordinated to a less acidic Fe^{III} centre will be a better nucleophile. Ligand electron donating strength influences the acidity of the metal ion. Employing Ga^{III} as a model for the Fe^{III} site, a series of Ga^{III} complexes of tripodal ligands of various electron-donating capacity were synthesised and their activities towards the hydrolysis of the phosphate diester bis(2,4-dinitrophenyl) phosphate (BDNPP), compared. It was observed that complexes with stronger ligand electron-donating groups provided greater rate accelerations. It is proposed that in the PAP models, the efficiency of the coordinated hydroxide nucleophile prevails over Lewis acid activation in deciding the intrinsic reactivity in PAP-mediated phosphate ester hydrolysis.

In RNase and Dnase activity, divalent Mg is frequently required as metal cofactor. This is explained by the high natural abundance and favorable chemical properties of Mg. However, the activity of Mg in model systems is greatly reduced relative to enzymatic systems. The low dielectric constants of enzyme active sites is considered to be better-mimicked by organic solvents like alcohols or DMSO than by aqueous solvent. Dinuclear Mg^{II} and Zn^{II} complexes were synthesised and their activities towards the RNA model 2-hydroxypropyl-p-nitrophenyl phosphate (HPNP) in DMSO were tested. However, no activity was observed due to poor association between the negatively charged complexes and anionic phosphate ester.

A dinuclear Zr^{IV} complex of the ligand 5-methyl-2-hydroxy-1,3-xylene- α,α -diamine- $\text{N},\text{N},\text{N}',\text{N}'$ -tetraacetic acid (HXTA) has been generated and its activity towards phosphate mono- and diester hydrolysis tested between pH 5.5 and 8.5. At neutral pH, monoester hydrolysis was observed to be ~60-fold faster than for an analogous diester. A possible explanation for this observation is that monoanionic phosphate diesters are weak ligands and so, binding to the catalyst is poor relative to phosphate monoesters. Metal ion cooperativity, through synthesis of an analogous mononuclear complex was studied. Ligand electron donating effects were investigated.

Acknowledgements.

I would like to thank my research supervisor, Dr. Andrea Erxleben, for her guidance, support, helpfulness and enthusiasm throughout my postgraduate studies.

I would like to thank Prof. Michael J. Hynes for his work on and contribution to kinetic studies, molecular modelling and potentiometric titrations.

I would like to thank all the postgrads and postdocs for many memorable moments, some great Friday nights in the bar and a great four years.

I would like to thank all of the technical staff, especially Jim Cotter, a gentleman and a scholar, and Seamus Collier, for never taking things too seriously!

Finally, I would like to thank Fiona Kirby and my family for their love, support and encouragement throughout my academic studies.

Glossary of Symbols and Abbreviations.

4-NPP	4-nitrophenyl phosphate
Å	Angstrom
anal.	analysis
AP	alkaline phosphatase
Asp	aspartate
ATP	adenosine triphosphate
BDNPP	bis(2,4-dinitrophenyl) phosphate
BNPP	bis(4-nitrophenyl) phosphate
BTP	bis-tris propane
calcd.	calculated
cAMP	cyclic adenosine monophosphate
d(ApA)	2'-deoxyadenylyl (3'→5')-2'-deoxyadenosine
dAp	2'-deoxyadenylyl 5'-phosphate
DFT	density functional theory
DMP	dimethyl phosphate
DMSO	dimethyl sulfoxide
DNA	deoxyribonucleic acid
DPP	diphenyl phosphate
Glu	glutamate
His	histidine
HPNP	2-hydroxypropyl 4-nitrophenyl phosphate
HXTA	5-methyl-2-hydroxy-1,3-xylene- α,α -diamine- N,N,N',N'-tetraacetic acid
k	rate constant
K _a	acid dissociation constant
kbPAP	kidney bean purple acid phosphatase
K _{eq}	equilibrium constant
k _{obs}	pseudo first order rate constant
M	molarity (moles/litre)
MeOH	methanol
μM	micromolar

mM	millimolar
MNPP	mono(4-nitrophenyl) monophenyl phosphate
mol	mole(s)
nm	nanometre
PAP	purple acid phosphatase
PP	phenyl phosphate
RNA	ribonucleic acid
RNase	ribonuclease
Ser	serine
T	temperature
THF	tetrahydrofuran
TSP	3-trimethylsilyl-1-propanesulfonic acid
Tyr	tyrosine
UpU	uridyl 3',5'-uridine

Table of Contents.

Abstract	i
Glossary of Symbols and Abbreviations	iii
Table of Contents	v

Chapter 1. Introduction.

1.1. Phosphate Esters in Biology	1
1.2. DNA and RNA	1
1.3. Mechanisms of Phosphate Ester Hydrolysis	4
1.3.1. Metal-Catalysed Phosphate Ester Hydrolysis	5
1.4. Phosphoesterases	7
1.4.1. Alkaline Phosphatase	7
1.4.2. DNA Polymerase I.	8
1.4.3. Ribozymes	9
1.5. Metal-Catalysed Phosphate Ester Hydrolysis	11
1.5.1. Lewis Acid Activation	11
1.5.2. Metal Hydroxide Activation	12
1.5.3. Metal Hydroxide Activation Coupled with Lewis Acid Activation	12
1.5.4. Leaving Group Activation	13
1.5.5. Dinuclear Complexes	14
1.5.6. Lanthanide Complexes	14
1.5.6.1. Hydrolytic Cleavage by Cerium Ions	15
1.5.6.2. Hydrolytic Cleavage by Lanthanide Complexes	16
1.5.7. Oxidative Cleavage of Nucleic Acids	17
1.5.8. Biomimetic Systems	18
1.5.8.1. Alkaline Phosphatase Models	19

1.5.8.2.	Phospholipase C and P1 Nuclease Models	20
1.6.	Aims	21
1.7.	References	22
Chapter 2. Ga^{III} Complexes as Models for the Fe^{III} Site in Purple Acid Phosphatase.		
2.1.	Introduction	25
2.1.1.	Mechanism of PAP – Catalysed Phosphate Ester Hydrolysis	25
2.1.2.	PAP Biomimetics	27
2.1.2.a.	Models for the Mechanism involving a Terminal-OH Nucleophile	27
2.1.2.b.	Models for the Mechanism Involving a μ -OH Nucleophile.	28
2.1.3.	Aims	30
2.2.	Results	33
2.2.1.	Synthesis of Ligands	34
2.2.2.	Gallium Complexes	37
2.2.3.	Solution Behaviour of the Complexes	42
2.2.4.	BDNPP Hydrolysis	44
2.2.5.	Solvent Deuterium Isotope Effect	50
2.2.6.	Substrate Binding	52
2.2.7.	DFT Calculations	53
2.3.	Discussion	56
2.4.	References	59
Appendix 2.1. Crystallographic Data		61

Chapter 3. Hydrolysis of an RNA Mimic by Mg^{II} and Zn^{II} Complexes in Non-Aqueous Media.

3.1.	Introduction	62
3.1.1.	Ribonucleases	63
3.1.1.a.	Ribonuclease A	63
3.1.1.b.	Ribonuclease H	64
3.1.1.c.	Ribonuclease P	65
3.1.2.	Model Systems	66
3.1.3.	Aims	67
3.2.	Results	69
3.2.1.	Synthesis and Characterisation of the Mg ^{II} and Zn ^{II} Complexes of HXTA	69
3.2.2.	Phosphodiesterase Activity	73
3.3.	Discussion	74
3.4.	References	76
	Appendix 3.1. Crystallographic Data	78

Chapter 4. Hydrolysis of Phosphate Esters: Selective Hydrolysis of Phosphate Monoesters over Diesters by Zirconium(IV) Complexes.

4.1.	Introduction	80
4.1.1.	Mechanisms of Phosphate Monoester Hydrolysis	81
4.1.2.	Metal-Catalysed Phosphate Monoester Hydrolysis	82
4.1.3.	Zr ^{IV} -Mediated Phosphate Ester Hydrolysis	86
4.1.4.	Aims	89
4.2.	Results	90
4.2.1.	Complexes	90
4.2.2.	Phosphate Ester Hydrolysis	94
4.2.2.1.	Phosphate Diester Hydrolysis	95

4.2.2.2.	Phosphate Monoester Hydrolysis	96
4.2.2.3.	Thermodynamics of Phosphate Ester Hydrolysis	100
4.2.2.4.	Hydrolysis of Phenyl Phosphate	103
4.2.2.5.	Dependence of the Hydrolysis Rate on the Ligand : Zr ^{IV} Ratio	104
4.2.2.6.	Inhibition by Phosphate	105
4.3.	Discussion	106
4.4.	References	111
Appendix 4.1.	Kinetic Plots for Phosphate Diester Hydrolysis	113
Appendix 4.2.	2 nd order plot for the hydrolysis of 4-NPP by Zr ₂ L ²	114
 Chapter 5. Experimental.		
5.1.	General Information	115
5.2.	Kinetic Studies	116
5.3.	Materials	116
5.3.1.	Chapter 2: Synthetic Procedures	117
5.3.2.	Chapter 3: Synthetic Procedures	118
5.3.3.	Chapter 4: Synthetic Procedures	119
5.4.	References	119

Chapter 1. Introduction.

1.1. Phosphate Esters in Biology.

Phosphate esters are ubiquitous in nature. Many of the most important biomolecules are organophosphates (e.g. in DNA, RNA, cAMP, and phospholipids). They play important roles in biology, and are involved in every aspect of cellular function. One of the most important reactions in biological chemistry is phosphorylation whereby a phosphoryl group is transferred from one group to another. Transfer of a phosphoryl group from ATP to a suitable acceptor is the primary source of energy in cells. Other processes which rely upon phosphorylation include; the activation of nucleosides to provide building blocks for DNA and RNA, the biosynthesis of amino acids and the activation/deactivation of many enzymes involved in controlling cell metabolism and in signal transduction. cAMP is believed to play an important role in the transmission of genetic information.

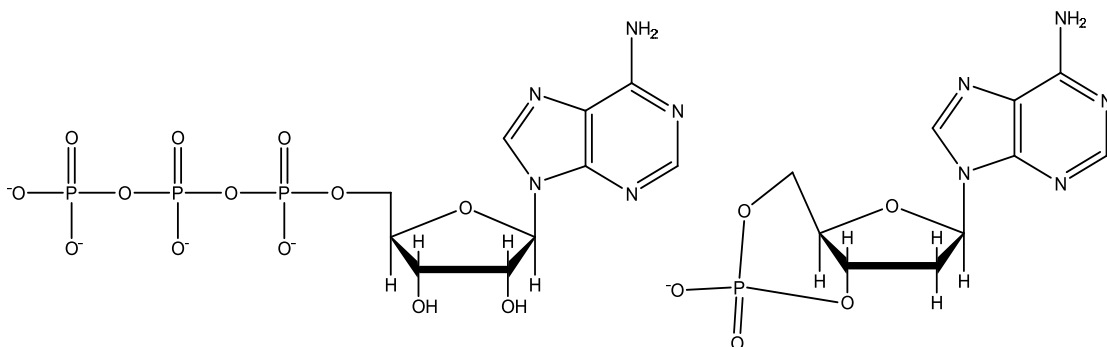


Figure 1.1: Structure of ATP and 3',5'-cAMP.

1.2. DNA and RNA.

Deoxyribonucleic acid (DNA) and ribonucleic acid (RNA) are the polymeric biomolecules responsible for the storage and transfer of genetic information in living organisms. DNA and RNA are constructed from individual building blocks called

nucleosides linked by phosphate ester bonds. Nucleosides are in turn composed of a sugar and a heterocyclic base group. The sugar group in DNA is deoxyribose and the sugar group in RNA is ribose. In the case of both biopolymers there are four nucleobases, the sequence of which encodes the genetic information. The base groups unique to DNA are adenine, guanine, cytosine and thymine. In RNA, the thymine is replaced by uracil.

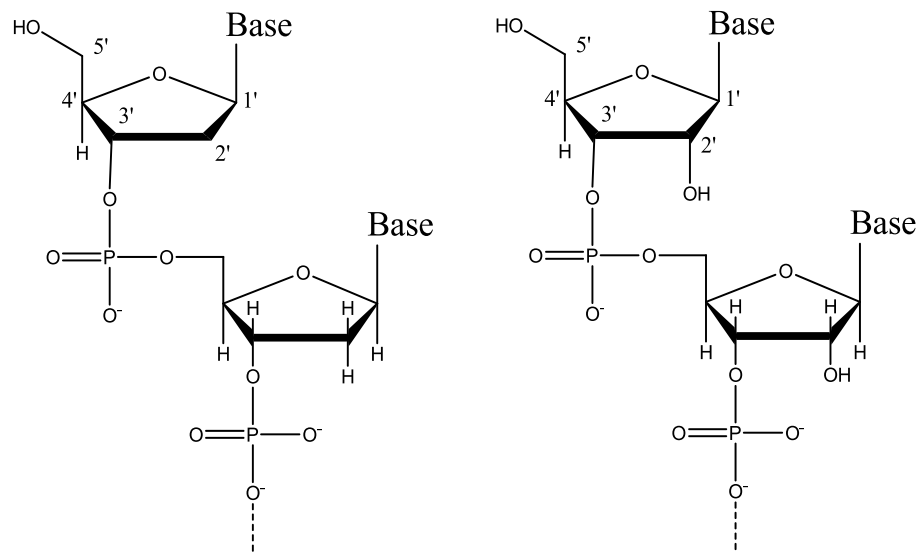


Figure 2: Primary structures of DNA (left) and RNA (right).

The sugar groups are connected at the 3' and 5' positions by phosphate diester linkages (**Figure 1.2**). Watson and Crick, in 1953, showed each polymeric strand in DNA is coiled in a helix and linked to another strand by hydrogen bonds between the base groups.¹ Each base pairs up selectively with another base, adenine with thymine (uracil in the case of RNA) and guanine with cytosine (**Figure 1.3**).

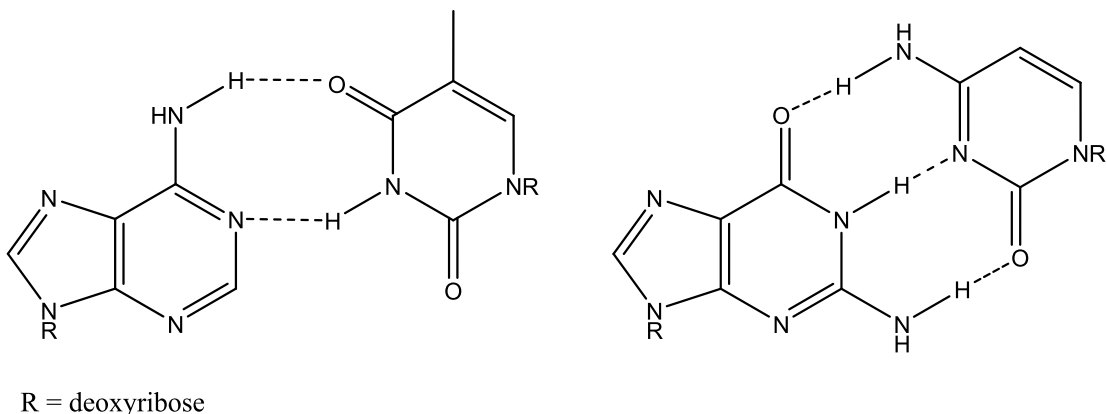


Figure 1.3: Adenine – Thymine and Guanine – Cytosine base pairing in DNA.

These macromolecules are very stable with respect to hydrolysis of the phosphate diester linkage in the absence of a suitable hydrolase. The half-life of one phosphate diester linkage in DNA with respect to solvent catalysed hydrolysis at 25°C is estimated to be of the order of tens to hundreds of billions of years.² The half-life for the hydrolysis of RNA under the same conditions is estimated to be significantly shorter at ~110 years.³ RNA, while still a very stable molecule with respect to hydrolysis is significantly more reactive than DNA. This disparity in reactivity is due to the 2'-OH group of ribose in RNA, which acts as an intramolecular nucleophile (**Figure 1.4**).

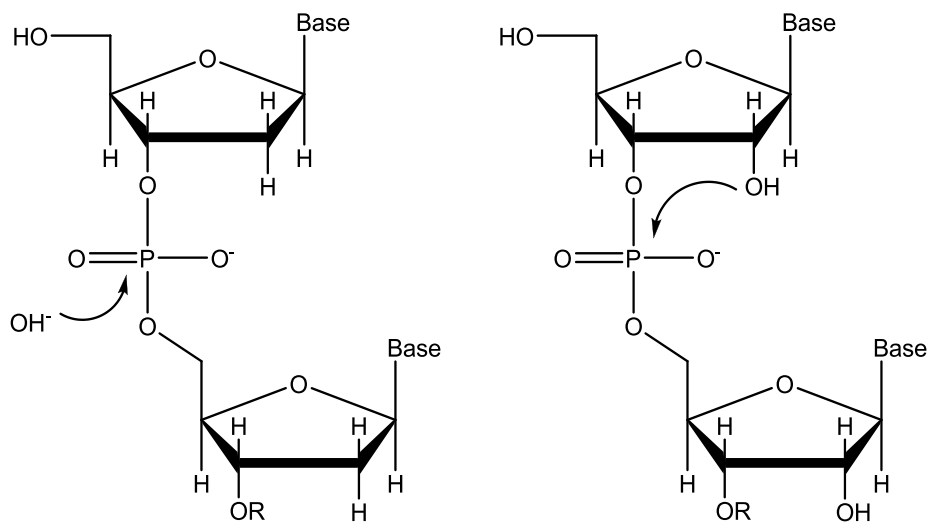


Figure 1.4: Mechanism of base catalysed hydrolysis of DNA (left) and RNA (right).

1.3. Mechanisms of Phosphate Ester Hydrolysis.

There are two general mechanisms by which phosphate esters undergo hydrolysis. The first involves an associative pathway via a penta-covalent intermediate. The second involves a dissociative pathway via a trigonal metaphosphate species, analogous to an S_N1 process in carbon chemistry. A concerted process is also available whereby no intermediates are formed and the nucleophile and leaving group form a pentacoordinate species in a single transition state. In many cases it is unclear which pathway the hydrolysis reaction follows.

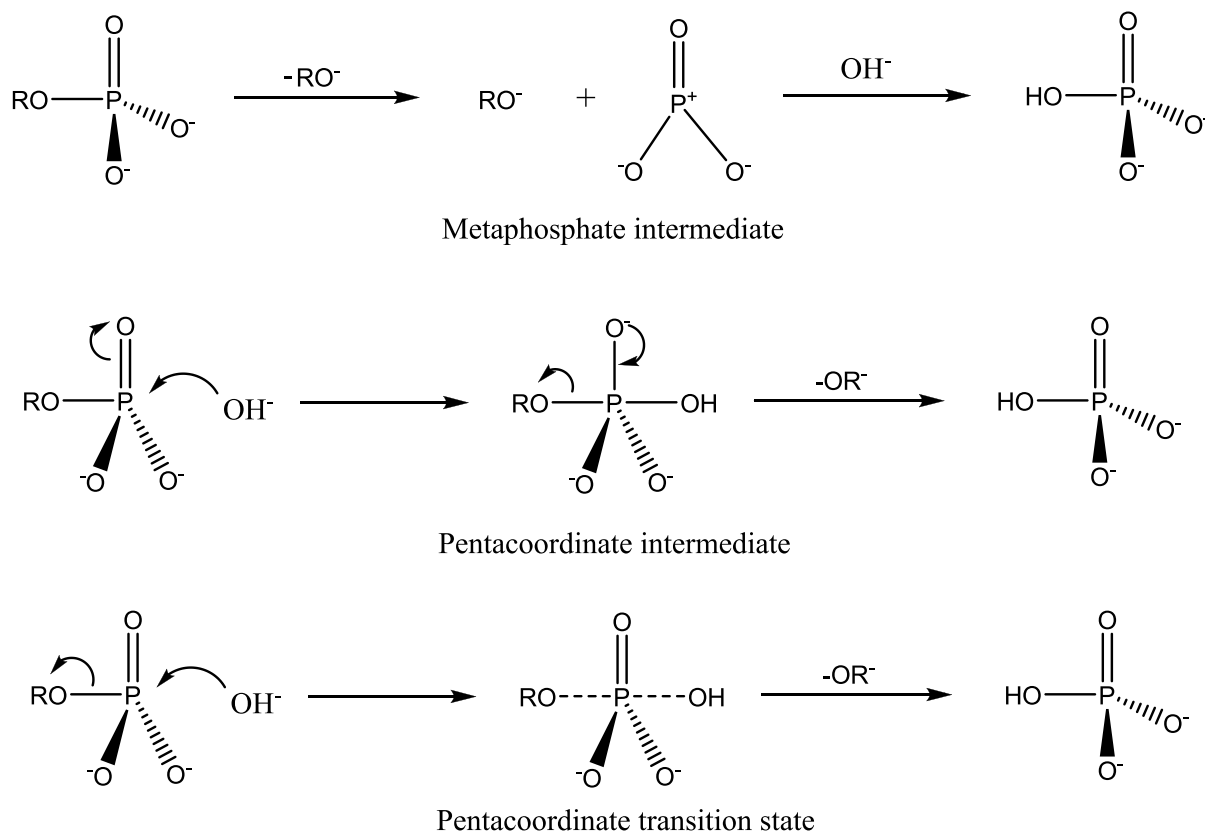


Figure 1.5: Dissociative, associative and concerted mechanisms for phosphate ester hydrolysis.

1.3.1. Metal-Catalysed Phosphate Ester Hydrolysis.

Many natural nucleases contain one or more metal ions, usually Zn(II), Mg(II), Ca(II) or Mn(II), in their active sites. Often, many metal centers are involved in the catalytic process. A number of different mechanisms by which mononuclear (**Figure 1.6**) and dinuclear (**Figure 1.7**) complexes catalyse phosphomonoester hydrolysis have been proposed.³

These are; a) Lewis acid activation whereby the metal ion activates the phosphorus towards nucleophilic attack; b) nucleophilic attack by metal coordinated hydroxide; c) leaving group activation where the metal ion is coordinated by the leaving group oxygen. Additionally, indirect modes of activation include; metal coordinated hydroxide

acting as a general base catalyst and metal coordinated water acting as a general acid catalyst; d) and e) respectively.

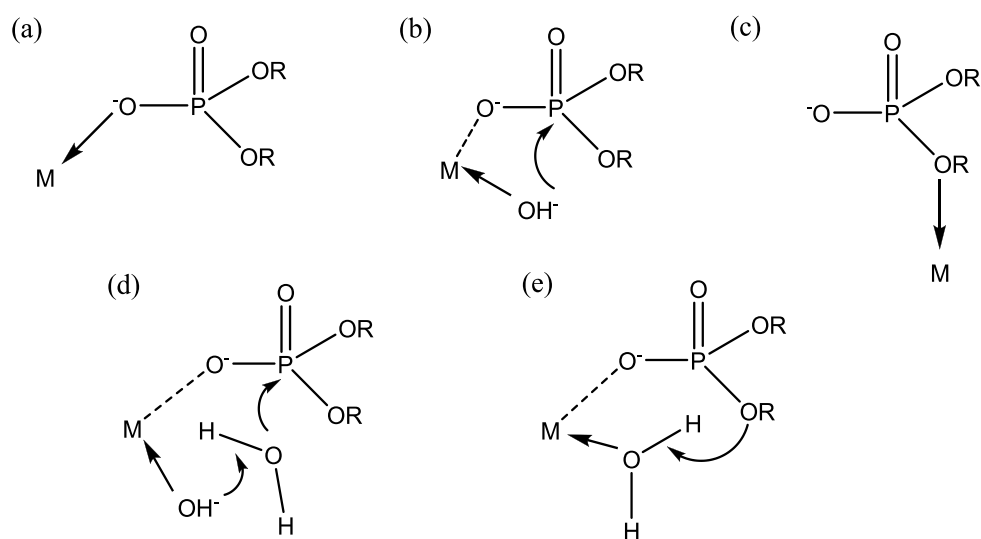


Figure 1.6: Proposed mechanisms of catalytic hydrolysis by mononuclear metal complexes.

Dinuclear catalysts are generally found to be much more reactive than their mononuclear counterparts, due to positive cooperation.³ Below are some pathways by which two metal ions may cooperate positively.

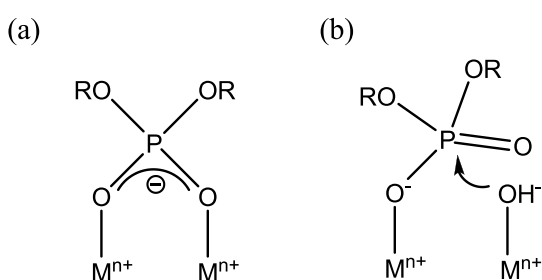


Figure 1.7: Proposed mechanisms of catalytic hydrolysis by dinuclear metal complexes.

Modes of activation include; a) double Lewis acid activation where the phosphate bridges the metal centres; b) single Lewis acid activation combined with metal-bound hydroxide attack. Double Lewis acid activation acting alone suffices to hydrolyse RNA rapidly, which already possesses a well-placed nucleophile at the 2' position of the sugar group. However, DNA hydrolysis requires both Lewis acid and nucleophile activation.³

1.4. Phosphoesterases.

Huge rate accelerations are required to hydrolyze DNA (10^{17} -fold), RNA (10^8 -fold) or other phosphate ester substrates within minutes.³ There are phosphorylases capable of these incredible rate enhancements. Many of these enzymes require a binuclear metal site for activity e.g. DNA polymerase I. Purple acid phosphatases (PAPs) are a class of binuclear metalloenzyme that catalyse phosphomonoester hydrolysis. There are at least 15 confirmed examples of such enzymes. Much work has been carried out in elucidating mechanistic information in the mode of action of these catalysts. Both natural and synthetic phosphorylases have been studied extensively due to their fundamental importance to a large number of biological processes.

1.4.1. Alkaline Phosphatase.

Alkaline phosphatase (AP) is one of the most intensely studied enzymatic phosphorylases. This enzyme is a non-specific phosphomonoesterase and it is found in prokaryotes and eukaryotes. AP is a homodimer with each monomeric unit possessing a three metal cluster in the active site consisting of two zinc ions and one magnesium ion.⁴ The Zn atoms are 3.8 Å apart, are not bridged in the resting state and are in close proximity to the nucleophilic residue Ser102. The Mg ion in the active site does not play a central role in the catalytic step. The two Zn ions are bidentately bridged by the phosphate substrate. Evidence for retention of phosphorus stereochemistry and of a phosphorylated enzyme intermediate suggests that the reaction proceeds via two consecutive nucleophilic attacks. The two zinc ions act in unison, one ion activating

Ser102 as nucleophile and the second activating a water molecule towards displacing the phosphate group from the serine residue (**Figure 1.8**).⁴⁻⁷

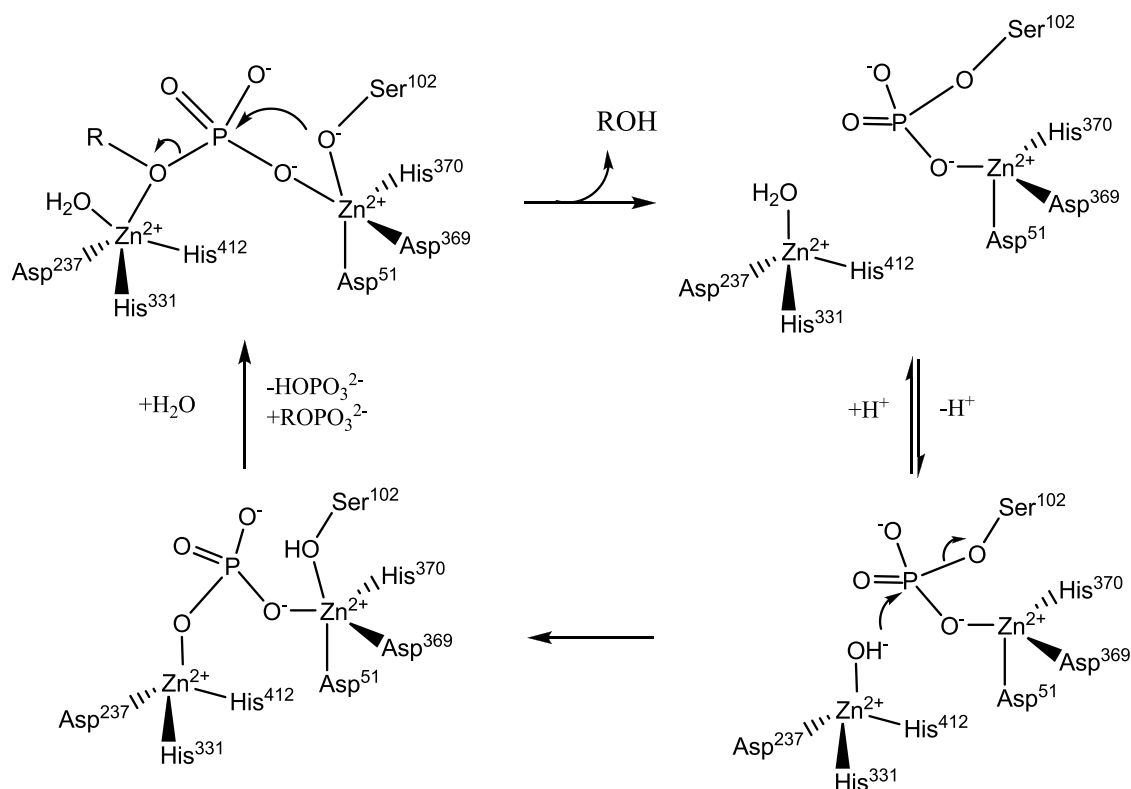


Figure 1.8: Active site structure and proposed mechanism for phosphate ester hydrolysis by AP.

1.4.2. DNA Polymerase I.

DNA polymerase I is an enzyme which catalyses the transfer of nucleotides to the 3' end of template primer DNA. It is an essential enzyme in that it is responsible for replicating and maintaining the integrity of the genetic code. DNA polymerase enzymes are often capable of nuclease as well as polymerase activity. Polymerase I has both 3'-5' exonuclease activity and corresponding 5'-3' exonuclease activity on single strand DNA.

DNA polymerase I from *E. coli* is a well studied enzyme. Cleavage of this enzyme yields a large C-terminal fragment which retains polymerase, 3'-5' and 5'-3' exonuclease activity.⁶

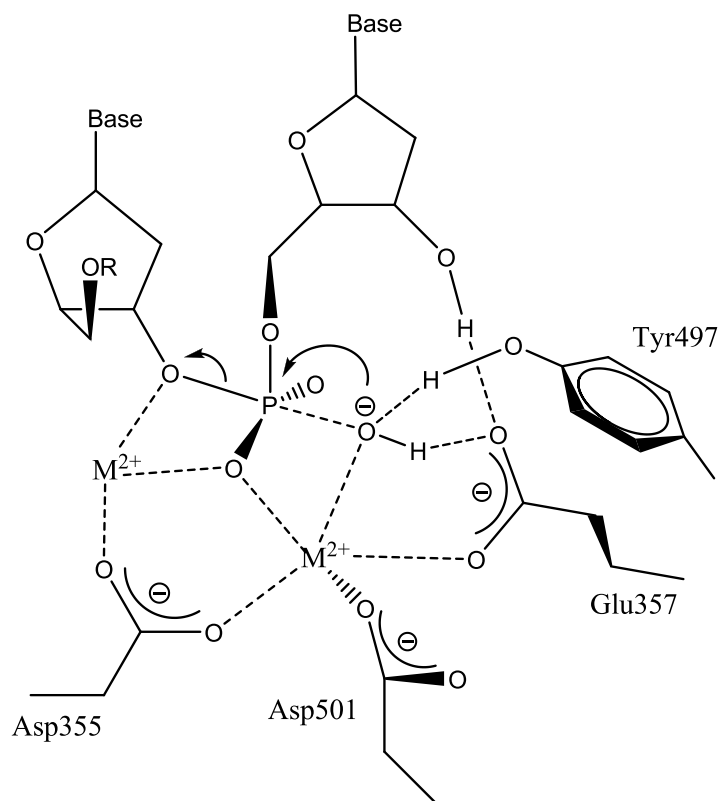


Figure 1.9: Proposed mechanism for the hydrolysis of DNA by DNA polymerase I (*E. coli*).

A crystal structure of the 3'-5'-exonuclease fragment was obtained and a mechanism extrapolated.⁸ From the proposed mechanism of hydrolysis in **Figure 1.9**, it can be seen that this enzyme activates the phosphodiester towards hydrolysis in three ways; (a) Coordination to the divalent ions in a bridging fashion leads to Lewis acid activation of the substrate (b) Activation of a terminal metal-bound OH towards nucleophilic attack on the substrate; (c) The leaving group oxygen is coordinated to a metal ion which stabilizes the developing negative charge. These factors combine synergistically enabling the efficient hydrolysis of DNA.

1.4.3. Ribozymes.

Ribozymes composed entirely of RNA, catalyse a range of reactions including phosphate ester hydrolysis. As well as playing an important role in stabilising the

ribozyme structure, metal ions are central to phosphorylase activity. Ribozymes generally depend on the Mg^{2+} ion for structure and function, however, Mn^{2+} -ribozyme systems are known to mediate phosphate diester hydrolysis. Ribozymes are known for their ability to bind another strand of RNA and specifically cleave the phosphodiester backbone through one of two mechanisms⁹ (**Figure 1.10**). Ribozymes are also known to self-cleave.

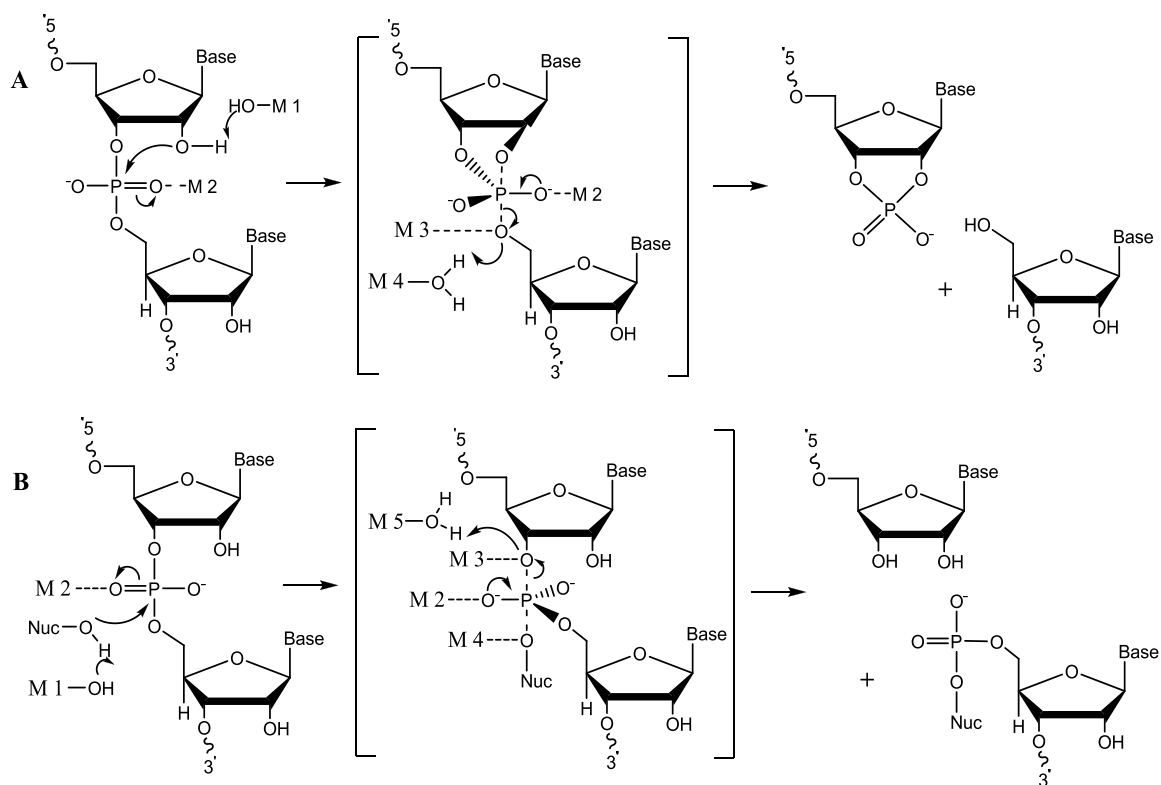


Figure 1.10: Mechanisms for ribozyme-catalysed phosphate ester hydrolysis.

In mechanism **A**, the internal 2' hydroxyl group is activated towards nucleophilic attack on the phosphorus centre, generating the 2'-3'-cyclic phosphate and 5'-OH species. Hammerhead, hairpin and tRNA ribozymes are found to catalyse phosphate ester hydrolysis by this mechanism. In the second mechanism **B**, an external nucleophile attacks the phosphorus centre in an S_N2 displacement. This mechanism is relevant to group I and group II intron ribozyme catalysed cleavage of RNA. Single metal ions may perform several roles in these systems; activation of external/internal nucleophiles;

Lewis acid activation of substrate; stabilisation of developing negative charge on the leaving group; they can act as a general acid by donating a proton to the leaving group.

1.5. Metal-Catalysed Phosphate Ester Hydrolysis.

The highly efficient way in which nature's enzymes catalyse a diverse array of reactions has inspired the field of biomimetic chemistry, a term coined by Breslow.¹⁰ Synthesis of artificial enzymes that catalyse the hydrolysis of phosphate esters has been attracting increasing attention in view of their potential applications. These catalysts may be employed as biomimetic enzymes in gaining insight into the mechanisms of the corresponding exonuclease or restriction enzyme or as conformational probes in the determination of DNA structure. Other applications include as customized restriction enzymes or as antibiotic and chemotherapeutic drugs.¹¹ The discovery that lanthanide and some transition metal ion complexes can promote the hydrolysis of DNA sparked great interest in the field.

1.5.1. Lewis Acid Activation.

Lewis acid activation of the substrate is a common method of catalysis. The phosphate ester coordinates to the metal ion, electron density is withdrawn from the phosphorus centre, making nucleophilic attack by solvent hydroxide or metal coordinated hydroxide favorable. The contribution of Lewis acid activation towards phosphoester hydrolysis was quantified in a substitutionally inert Ir^{III} complex. It was shown that coordination of the phosphotriester to the trivalent metal ion provides a 400-fold rate enhancement in the rate of hydrolysis relative to uncoordinated trimethyl phosphate¹² (**Figure 1.11**). The reaction occurs via intermolecular attack on phosphorus by solvent hydroxide.

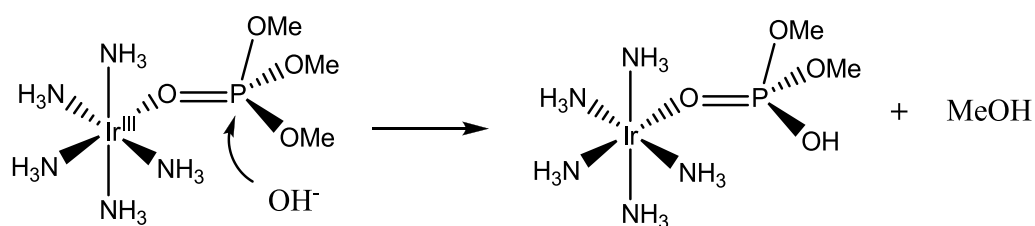


Figure 1.11: Lewis acid activation in the hydrolysis of trimethyl phosphate.

1.5.2. Metal Hydroxide Activation.

Another role of the metal ion in phosphate ester hydrolysis is in the generation of a hydroxide nucleophile. The pK_a for $2H_2O \rightleftharpoons OH^- + H_3O^+$ is lowered upon coordination to a metal ion.¹³ Thus, metal ions serve to increase the concentration of hydroxide species at neutral pH. However, metal-coordinated hydroxide is approximately 100 times less nucleophilic than free hydroxide.¹⁴ Metal hydroxide activation, acting independently can give up to 8 orders of magnitude rate acceleration.³

The efficacy of metal hydroxide activation is greatly enhanced by substrate binding. Binding of the substrate brings the electrophilic centre into close proximity with the attacking hydroxo nucleophile, greatly increasing the probability of nucleophilic attack on phosphorus.

1.5.3. Metal Hydroxide Activation Coupled with Lewis Acid Activation.

Coupling these modes of activation is the chief mechanism by which many artificial phosphorylases operate. Coordination of the phosphate ester to the metal ion results in activation of the phosphorus centre towards nucleophilic attack. Subsequent nucleophilic attack by an adjacent metal hydroxide group leads to cleavage of the phosphate ester group. Synergism is often observed as the metal hydroxide group is ideally placed to carry out nucleophilic attack on an activated substrate. Chin and co-workers reported the hydrolysis of the hydrolytically stable phosphate diester dimethyl phosphate (DMP) at neutral pH by a Co(III) complex (**Figure 1.12 (complex A)**).¹⁵ There are two vacant coordination sites cis to each other in the coordination sphere of complex A. The phosphate diester displaces one of the aqua ligands upon coordination and the adjacent metal-hydroxo group acts as an intramolecular nucleophile. The half-life of DMP is estimated to be 600,000 years at 100°C with respect to water hydrolysis. The cobalt-bound phosphate diester is hydrolysed with a half-life of 40 days at neutral pH and 60°C. The metal in complex B is coordinated by an analogous pentadentate ligand leaving only a single vacant coordination site. As a result, complex B can provide either Lewis acid activation or metal-hydroxide activation, not both. No hydrolysis of DMP was observed for this complex.

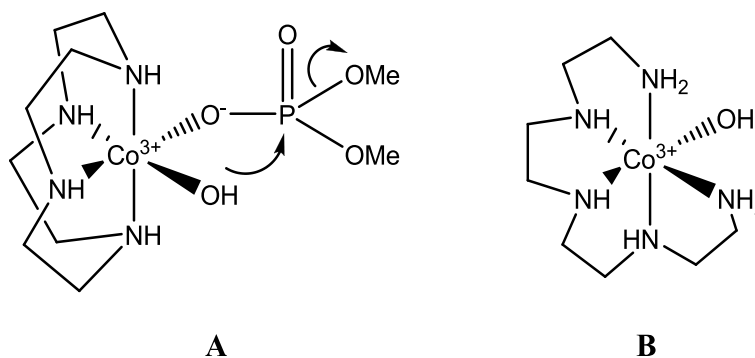


Figure 1.12: Hydrolysis of the phosphate diester dimethyl phosphate by a Co(III) complex.

1.5.4. Leaving Group Activation.

Coordination of the leaving group oxygen to a metal ion can greatly enhance the rates of phosphate ester hydrolysis. In a mechanism for the DNA polymerase I catalysed hydrolysis of DNA, it was proposed that the leaving group oxygen is coordinated to a Mg^{2+} ion in the active site.⁵ However, designing model compounds that mimic this mode of activation has proven difficult due to the low affinity of this non-basic oxygen towards metal coordination. Bruice and coworkers compared the rates of hydrolysis of bis(8-hydroxyquinoline) phosphate and bis(6-hydroxyquinoline) phosphate in the presence of metal ions (**Figure 1.13**).¹⁴

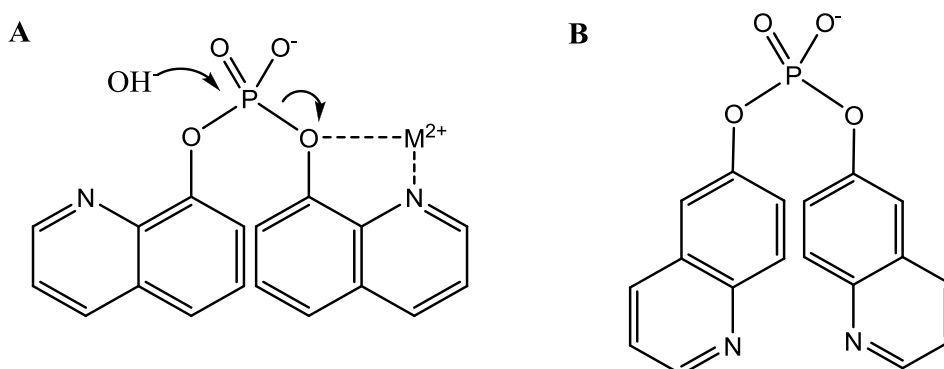


Figure 1.13: Leaving group activation in the hydrolysis of bis(8-hydroxyquinoline) phosphate (A) and bis(6-hydroxyquinoline) phosphate (B).

It was observed that the hydrolysis of bis(6-hydroxyquinoline) phosphate is much slower than the hydrolysis of bis(8-hydroxyquinoline) phosphate in the presence of metal ions. Coordination of a divalent metal ion to the oxygen of the quinoline leaving group leads to stabilisation of the developing negative charge in the transition state.

1.5.5. Dinuclear Complexes.

As with natural phosphorylases, two or more metal ions are often employed in artificial catalysts in order to take advantage of all the different modes of activation that can be provided (Lewis acid, nucleophile and leaving group activation). A synergistic effect is often observed in these systems. For example, in a study comparing the activity of a dinuclear Cu^{2+} complex with that of an analogous mononuclear complex, the dinuclear complex was shown to be ~20-fold more active in the hydrolysis of bis(4-nitrophenyl) phosphate (BNPP) (**Figure 1.14**).¹⁶

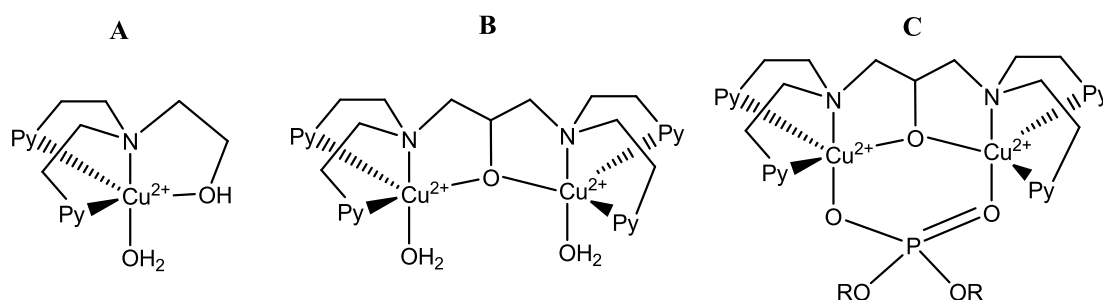


Figure 1.14: Mono- and dinuclear Cu^{2+} complexes for the hydrolysis of BNPP.

In the hydrolysis of BNPP by the bimetallic complex, the phosphate diester bridges the copper ions (**Figure 1.14 (C)**). Each divalent ion acts as a Lewis acid activator (double Lewis acid activation).

1.5.6. Lanthanide Complexes.

There has been much interest in the development of lanthanide complexes as artificial phosphorylases. Lanthanide ions, as hard Lewis acids with high coordination numbers, fast ligand exchange rates and no accessible redox chemistry (except for cerium) are ideally suited as mediators for phosphate ester hydrolysis.¹⁷ The high Lewis acidity of these ions serves to lower the pK_a values of coordinated water molecules, increasing the

availability of hydroxide species at lower pH. Fast ligand exchange rates promote high catalytic turnover. The redox inactivity of these ions is also important with regards to molecular biology. In the hydrolysis of DNA for example, selective hydrolytic cleavage is preferable over oxidative cleavage for two main reasons; (1) oxidative cleavage mechanisms often produce diffusible radicals resulting in unselective cleavage and multiple cleavage sites, (2) oxidative cleavage products are inconsistent with those produced by natural hydrolases and thus fragments cannot be further enzymatically religated.⁷ In theory, a synthetic hydrolase could be used as an artificial restriction enzyme. Sequence specificity could be achieved by encoding sequence specificity into the hydrolase or linking it to an appropriate DNA binding agent.

1.5.6.1. Hydrolytic Cleavage by Cerium Ions.

Chin and co-workers reported the cleavage of the dinucleotide dApdA (2'-deoxyadenyl(3'-5')-2'-deoxyadenosine) by Ce(III) involving air-oxidation of Ce(III) to Ce(IV) and the formation of a peroxo complex (**Figure 1.15**).¹⁸

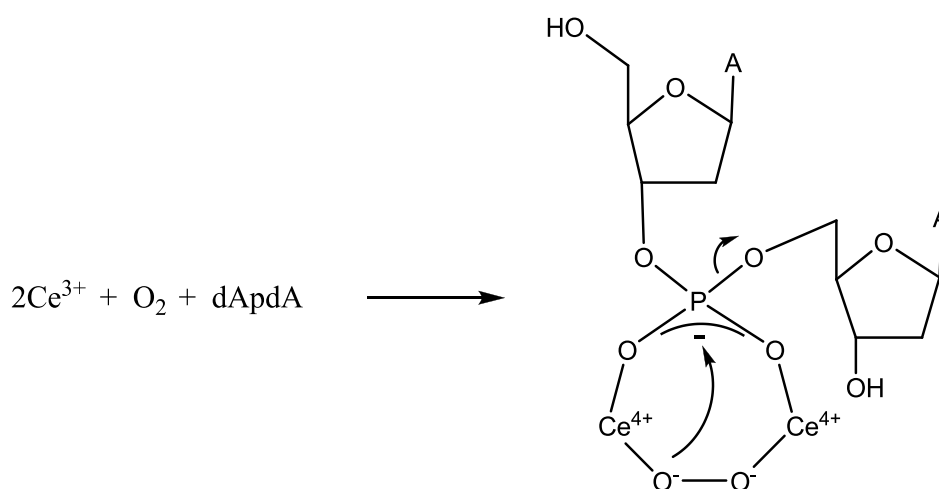


Figure 1.15: Hydrolysis of a dinucleotide by Ce^{3+} and molecular oxygen.

A mechanism whereby Ce(III) is oxidised to Ce(IV) followed by intramolecular Ce peroxide attack on the coordinated phosphate diester was proposed. This mechanism combines Lewis acid activation of the substrate with intramolecular attack by a coordinated nucleophile.

1.5.6.2. Hydrolytic Cleavage by Lanthanide Complexes.

When complexed to 1,3-bis[tris(hydroxymethyl)methylamino]-propane (BTP) (**Figure 1.16 (A)**), it was found that the early Ln(III) ions were more active than the late with respect to bis(4-nitrophenyl)phosphate (BNPP) (**Figure 1.16(B)**) hydrolysis.¹⁹

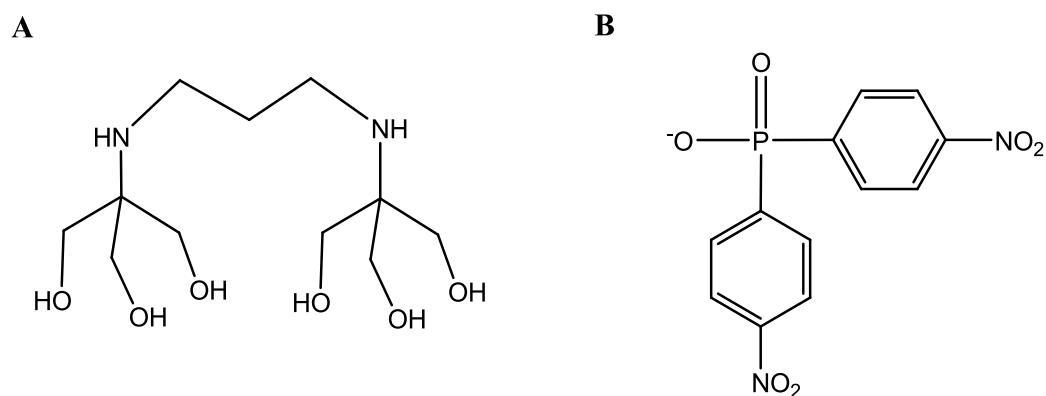


Figure 1.16: 1,3-bis[tris(hydroxymethyl)methylamino]-propane (BTP) (A) and bis(4-nitrophenyl)phosphate (BNPP) (B).

This trend correlates with the increasing pK_a values of Ln(III)-coordinated water ligands and correspondingly increasing nucleophilicity of Ln(III)-bound OH. The limiting factor for these Ln(III)-BTP systems is the activation of the Ln-bound OH towards nucleophilic attack on phosphorus.

Cerium is the only lanthanide capable of accessing the tetravalent state in aqueous solution. The Ce(IV) ion has proven to be extremely active towards phosphate ester hydrolysis, enhancing BNPP hydrolysis by a factor of $>10^{10}$ and DNA hydrolysis by $>10^{11}$.¹⁷

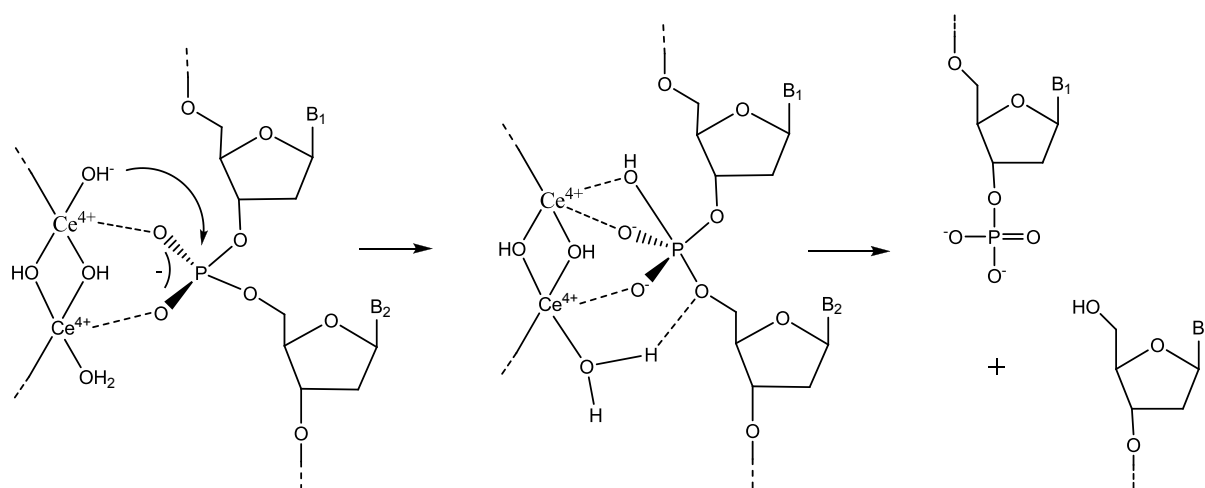


Figure 1.17: Proposed mechanism for cerium(IV) ion promoted hydrolysis of DNA at pH 2.²⁰

Ce(IV) is a hard cation and has a high affinity for hard oxygen donors. In solution, formation of hydroxo-bridged species occurs. Upon coordination of the hydroxo-bridged dicerium species to the phosphate diester backbone of DNA (**Figure 1.17**), the phosphorus centre is strongly activated through double Lewis acid activation by these tetravalent cations.²⁰ Although the metal-bound hydroxo group is a weaker nucleophile than free OH⁻, the high state of activation of the phosphorus allows the reaction to proceed efficiently. Furthermore, the negatively charged transition state is stabilised through inductive electron withdrawal by the cerium cations.

1.5.7. Oxidative Cleavage of Nucleic Acids.

Oxidative cleavage of nucleic acids by redox active coordination compounds is also known.²¹ This class of chemical nuclease operates by oxidative attack on the ribose or deoxyribose moiety.²² Oxidative cleaving agents, owing to their sugar-directed reactivity, can cleave DNA at all sequence positions regardless of the adjacent nucleobase.

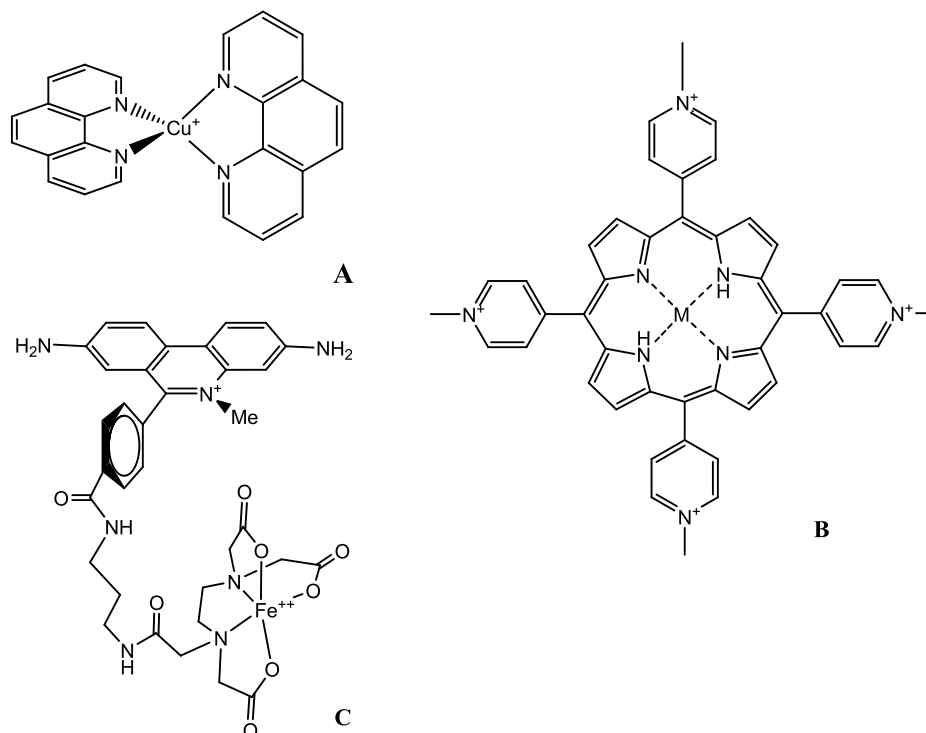


Figure 1.18: Redox active chemical nucleases.

A few examples of coordination compounds that promote DNA cleavage under physiological conditions are shown in **Figure 1.18**.²³⁻²⁵ The first coordination complex to oxidatively cleave DNA was reported in 1979 by Sigman *et al* (**Figure 1.18 (A)**).²³ The first step in the nucleolytic reaction mediated by this 1,10-phenanthroline copper complex involves reversible non-covalent binding to DNA. In the second step, the cuprous ion is oxidized by hydrogen peroxide, resulting in a copper-oxo species. This copper oxo species in turn attacks the DNA leading to a series of reactions that ultimately results in DNA strand scission.²¹

1.5.8. Biomimetic Systems.

Biomimetic hydrolysis of phosphate esters is of increasing importance in biotechnology and medicine. Given the high efficiency with which phosphorylases operate, the design of small molecule compounds that mimic the structural characteristics of the active core in these enzymes is a good place to start with respect to enhancing the activity of metal catalysts. Also, mechanistic information garnered from biomimetic compounds can be

utilised to better understand the mechanisms and structure-function relationships in these enzymes.

1.5.8.1. Alkaline Phosphatase Models.

The mechanism of alkaline phosphatase catalysed phosphoester hydrolysis involves two steps (see 1.3.2). In the first step, a serine residue is activated towards nucleophilic attack by a Zn^{II} ion, generating the phospho-enzyme intermediate. The second zinc ion activates a water molecule towards nucleophilic attack in the second step, while the developing negative charge on the leaving group is stabilised by the former zinc ion (Figure 1.19 (A)).⁴⁻⁷

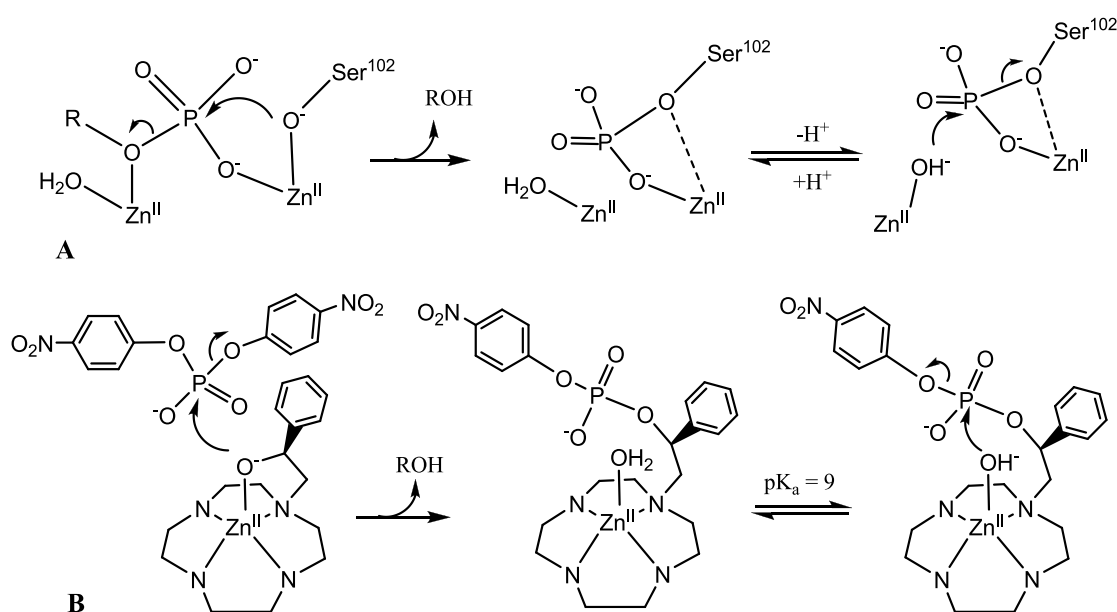


Figure 1.19: Analogous mechanisms for phosphate ester hydrolysis by AP (A) and by a biomimetic zinc coordination compound (B) on the activated substrate BNPP.

This mechanism is well-mimicked by the zinc(II) macrocyclic tetraamine complex with an alcohol pendant arm shown in Figure 1.19 (B).²⁶ The alcohol pendant group is activated by Zn(II) towards nucleophilic attack on the phosphate diester, resulting in the cleavage of a phosphoester bond and the generation of a phosphoryl intermediate. A

zinc-bound water is deprotonated, generating a terminal hydroxo group, which is ideally positioned to carry out intramolecular nucleophilic attack on phosphorus, cleaving the second phosphoester bond.

1.5.8.2. Phospholipase C and P1 Nuclease Models.

Not many biomimetic systems are available for the study of trinuclear zinc enzymes such as phospholipase C and P1 nuclease. Furthermore, little is known about their mode of action.²⁷ These enzymes are very similar structurally at their trinuclear zinc active site, differing only in one ligand (Glu vs. Asp) at Zn2 (**Figure 1.20**).^{28,29} For this reason, their mechanisms of phosphoester hydrolysis are expected to be similar.

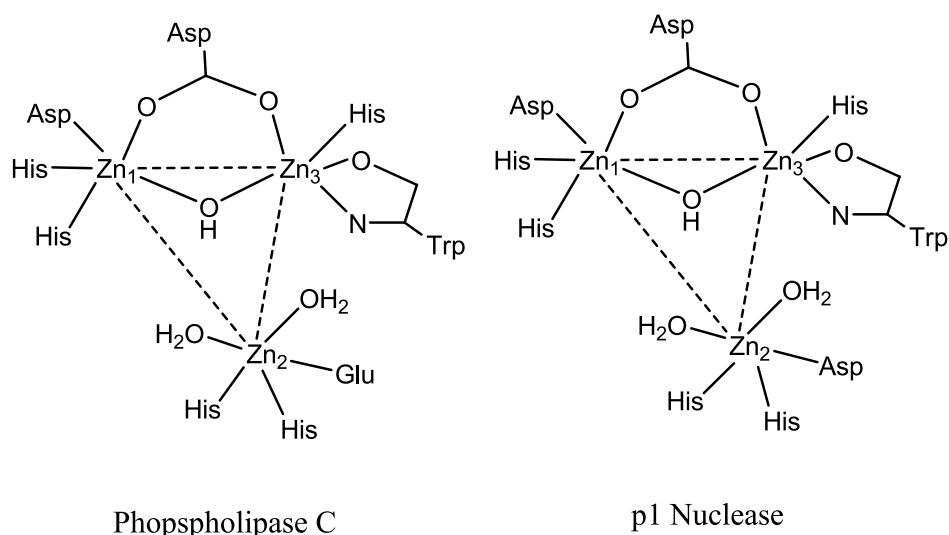


Figure 1.20: Trinuclear active sites of phospholipase C and P1 nuclease.

Zacharias *et al.* have reported the crystal structure of a trinuclear zinc complex that is structurally analogous with the enzyme P1 nuclease (**Figure 1.21**).³⁰ In the same study, a Zn₂Cu complex of the same ligand was prepared. The high activity of the Zn₃ complex in the cleavage of calf-thymus DNA compared to the Zn₂Cu analog demonstrates the importance of the homo-trinuclear composition.

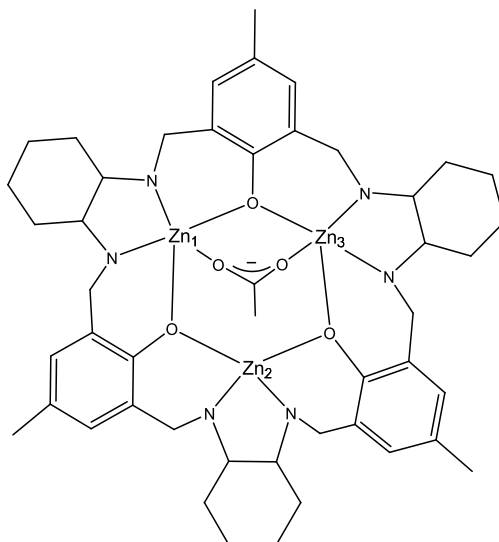


Figure 1.21: Trinuclear Zn complex as a structural analog of the trinuclear active site of P1 nuclease.

1.6. Aims.

In order to better understand the role of the metal ion in phosphate ester hydrolysis and the factors which promote catalytic activity in different systems, a number of different studies would be undertaken.

The first study is directed towards understanding the role of the ferric ion in the active site of purple acid phosphatase (PAP) in phosphomonoester hydrolysis. The active site in PAP contains a bimetallic core consisting of a ferric ion and another divalent ion (Fe, Zn or Mn) bridged by a hydroxo group. Ga^{III} complexes are employed as models for the Fe^{III} site in PAP in order to gain some insight into substrate and nucleophile activation in PAP. This study comprises chapter 2.

Though frequently a mediator in RNase and DNase activity, high activity for divalent magnesium in model systems is not known. Organic solvents such as alcohols or DMSO are considered to better represent the environment, in terms of polarity, inside the active site of an enzyme. In the second study a dinuclear Mg^{II} complex would be generated and

its activity towards phosphate diester hydrolysis in DMSO compared with that of an analogous Zn^{II} complex.

In the final study, the objective was to generate an efficient catalyst for phosphate monoester hydrolysis. Mono- and dinuclear Zr^{IV} complexes are generated and their activities towards phosphate mono- and diester hydrolysis investigated. Tetravalent zirconium is a known mediator of phosphate diester and ATP hydrolysis, however, no detailed study of phosphate monoester hydrolysis by a Zr^{IV} complex has previously been described.

1.7. References.

- (1) Watson, J. D.; Crick, F. H. C. *Nature* **1953**, *171*, 737.
- (2) Wolfenden, R.; Ridgway, C.; Young, G. *J. Am. Chem. Soc.* **1998**, *120*, 833.
- (3) Williams, N. H.; Takasaki, B.; Wall, M.; Chin, J. *Acc. Chem. Res.* **1999**, *32*, 485.
- (4) Coleman, J. E. *Annu. Rev. Biophys. Biomol. Struct.* **1992**, *21*, 441.
- (5) Strater, N.; Lipscomb, W. N.; Klabunde, T.; Krebs, B. *Angew. Chem. Int. Ed.* **1996**, *35*, 2024.
- (6) Wilcox, D. E. *Chem. Rev.* **1996**, *96*, 2435.
- (7) Hegg, E. L.; Burstyn, J. N. *Coord. Chem. Rev.* **1998**, *173*, 133.
- (8) Steitz, T. A.; Steitz, J. A. *Proc. Natl. Acad. Sci. U.S.A.* **1993**, *90*, 6498.
- (9) Pyle, A. M. *Science* **1993**, *261*, 709.
- (10) Breslow, R. *Acc. Chem. Res.* **1980**, *13*, 170.
- (11) Mancin, F.; Scrimin, P.; Tecilla, P.; Tonellato, U. *Chem. Commun.* **2005**, 2540.
- (12) Hendry, P., Sargeson, A. M. *Chem. Commun.* **1984**, 164.
- (13) Buckingham, D. A.; Harrowfield, J. M.; Sargeson, A. M. *J. Am. Chem. Soc.* **1974**, *96*, 1726.
- (14) Browne, K. A., Bruice, T. C. *J. Am. Chem. Soc.* **1992**, *114*, 4951.
- (15) Kim, J. H., Chin, J. *J. Am. Chem. Soc.* **1992**, *114*, 9792.
- (16) Selmeczi, K., Giorgi, M., Speier, G., Farkas, E., Réglér, M. *Eur. J. Inorg. Chem.* **2006**, 1022.

- (17) Franklin, S. J. *Curr. Opin. Chem. Biol.* **2001**, *5*, 201.
- (18) Takasaki, B. K., Chin, J. *J. Am. Chem. Soc.* **1994**, *116*, 1121.
- (19) Gómez-Tagle, P., Yatsimirsky, A. K. *J. Chem. Soc., Dalton Trans.* **1998**, 2957.
- (20) Komiyama, M., Takeda, N., Shigekawa, H. *Chem. Commun.* **1999**, 1443.
- (21) Sigman, D. S.; Mazumder, A.; Perrin, D. M. *Chem. Rev.* **1993**, *93*, 2295.
- (22) Sigman, D. S. *Biochemistry* **1990**, *29*, 9097.
- (23) Sigman, D. S.; Graham, D. R.; D'Aurora, V.; Stern, A. M. *J. Biol. Chem.* **1979**, *254*, 12269.
- (24) Ward, B.; Skorobogaty, A.; Dabrowiak, J. C. *Biochemistry* **1986**, *25*, 6875.
- (25) Hertzberg, R. P.; Dervan, P. B. *J. Am. Chem. Soc.* **1982**, *104*, 313.
- (26) Kimura, E., Kodama, Y., Koike, T., Shiro, M. *J. Am. Chem. Soc.* **1995**, *117*, 8304.
- (27) Weston, J. *Chem. Rev.* **2005**, *105*, 2151.
- (28) Hough, E.; Hansen, L. K.; Birknes, B.; Jynge, K.; Hansen, S.; Hordvik, A.; Little, C.; Dodson, E.; Derewenda, Z. *Nature* **1989**, *338*, 357.
- (29) Romier, C.; Dominguez, R.; Lahm, A.; Dahl, O.; Suck, D. *Proteins* **1998**, *32*, 414.
- (30) Korupoju, S. R.; Mangayarkarasi, N.; Zacharias, P. S.; Mizuthani, J.; Nishihara, H. *Inorg. Chem.* **2002**, *41*, 4099.

Chapter 2. Ga^{III} Complexes as Models for the Fe^{III} Site in Purple Acid Phosphatase.

Results Published:

Coleman, F.; Hynes, M. J.; Erxleben, A. *Inorg. Chem.* **2010**, *49*, 6725-6733.

Ga^{III} Complexes as Models for the M^{III} Site of Purple Acid Phosphatase: Ligand Effects on the Hydrolytic Reactivity Toward bis(2,4-dinitrophenyl) phosphate.

Chapter 2. Ga^{III} Complexes as Models for the Fe^{III} Site in Purple Acid Phosphatase.

2.1. Introduction.

Purple acid phosphatases (PAP) are enzymes found in animals, plants, fungi and bacteria. They are binuclear metallohydrolases with an Fe^{III}M^{II} core, the divalent ion being Fe, Zn or Mn. They catalyse the hydrolysis of a wide range of phosphomonoester substrates in the pH range 4-7.¹ PAP's display a characteristic purple colour in their active form owing to a tyrosinate-to-Fe^{III} charge transfer. Crystal structures of red kidney bean², rat^{3,4}, pig⁵, human⁶ and sweet potato⁷ PAP have been reported. Despite the overall low sequence homology, seven conserved amino acid residues were revealed in the active site. In the resting state, Fe^{III} is coordinated by a histidine, an aspartate and a tyrosine residue. The divalent ion is coordinated by two histidine residues and an asparagine. The metal ions are bridged by the carboxylate group of an aspartate residue and a modelled bridging hydroxo group. The coordination sphere of the Fe^{III} ion is completed by a modelled terminal hydroxo group.^{8,9}

2.1.1. Mechanism of PAP – Catalyzed Phosphate Ester Hydrolysis.

A proposed mechanism for the hydrolysis of a phosphomonoester by kidney bean purple acid phosphatase (kbPAP) is shown (**Figure 2.1**).² The active site of kidney bean purple acid phosphatase is occupied by Fe(III) and Zn(II) ions. The enzyme exhibits a bell-shaped pH-rate profile for phosphomonoester hydrolysis with kinetic pK_a values of 4.8 and 6.9.² The lower kinetic pK_a value is due to deprotonation of Fe(III)-bound water, the higher pK_a is attributed to the deprotonation of the oxygen of the phosphate substrate. This higher pK_a may also be attributed to the deprotonation of the mechanistically important His296. Initial coordination of the phosphate monoester to the divalent metal ion results in the activation of the substrate towards nucleophilic attack. Nucleophilic attack by the terminal Fe^{III}-bound hydroxo group occurs. The pentacoordinate transition state is stabilised by the metal ions and hydrogen bonding interactions with His202 and His296. It is proposed that

the release of the leaving group is aided by the transfer of a proton from protonated His296.

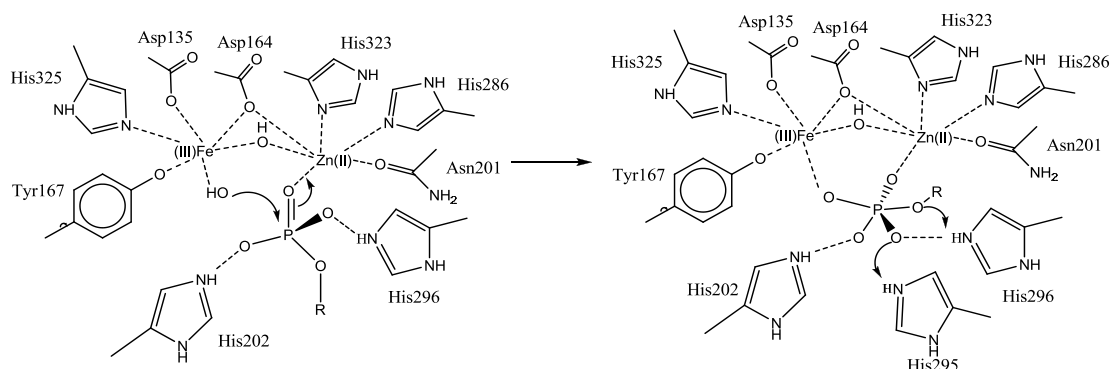


Figure 2.1: Proposed mechanism for the hydrolysis of a phosphate monoester by kidney bean purple acid phosphatase at the Fe(III)Zn(II) site.²

In an alternative mechanism,¹⁰⁻¹³ the phosphate monoester binds in a bidentate bridging mode to both the Fe³⁺ and M²⁺ ions. The suitably placed μ -OH group attacks phosphorus leading to hydrolysis (**Figure 2.2**).

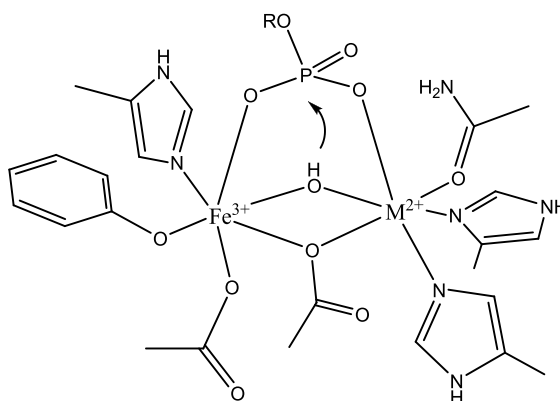


Figure 2.2: Alternative mechanism whereby the phosphate ester bidentately bridges the two metal ions and the bridging hydroxo group acts as a nucleophile.¹¹

The lower nucleophilicity of a μ -OH group relative to a terminally bound OH is an argument against this mechanism. However, it was proposed that coordination of the phosphate monoester leads to a shift of the μ -OH bridge towards the divalent ion, transforming it into a quasi-terminal binding group, with increased nucleophilicity.¹⁰ Replacement of the ferric ion in uteroferrin PAP by Ga^{III} has been undertaken.¹³ The pH-dependence of the Ga^{III}- substituted enzyme with respect to phosphomonoester

hydrolysis supports a mechanism whereby the phosphomonoester coordinates the metal ions in a μ -1,3 fashion and the μ -OH acts as the reaction-initiating nucleophile. In the same work, it was found that the native enzyme ($\text{Fe}^{\text{III}}\text{-Fe}^{\text{II}}$ active site) carried out hydrolysis by the former mechanism. A one enzyme-two mechanisms hypothesis was proposed whereby the identity of the attacking nucleophile varies depending upon the metal ion composition, the geometry of the second coordination sphere and also the substrate itself.¹³

2.1.2. PAP Biomimetics.

2.1.2.a. Models for the Mechanism Involving a Terminal-OH Nucleophile.

Neves, Schenk and coworkers synthesised an $\text{Fe}^{\text{III}}(\mu\text{-OH})\text{Zn}^{\text{II}}$ complex as a model for the active site of PAP (**Figure 2.3**).¹⁴ Kinetics of phosphate ester hydrolysis were performed on the activated phosphate diester bis(2,4-dinitrophenyl) phosphate (BDNPP). Potentiometric titration combined with kinetic data revealed that the catalytically active species for hydrolysing BDNPP is $[(\text{OH})\text{Fe}(\mu\text{-OH})\text{Zn}(\text{OH}_2)]$.

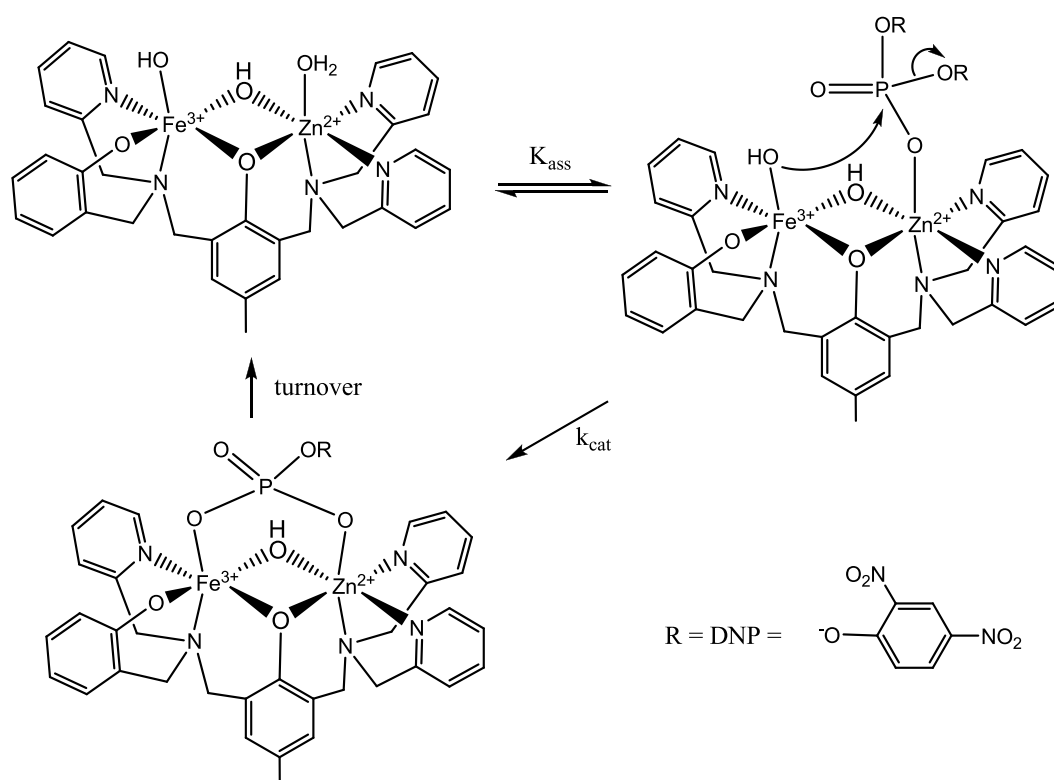


Figure 2.3: Hydrolysis of the phosphate diester BDNPP by a binuclear phosphorylase that is structurally similar to the active site of PAP.

The mechanism in action here is a good mimic for the former mechanism in section 2.1.1. i.e. coordination of the phosphate ester to the divalent ion and nucleophilic attack by terminal OH of the ferric ion. The μ -1,3-coordinated phosphomonoester product undergoes substitution by two water molecules to regenerate the active species.

2.1.2.b. Models for the Mechanism Involving a μ -OH Nucleophile.

Schenk and coworkers synthesised a $\text{Ga}^{\text{III}}\text{-Zn}^{\text{II}}$ analog of the complex shown in **Figure 2.3** as a biomimetic model for the heterovalent active site of PAP.¹³ The Ga^{III} ion is coordinated with an N_2O_2 ligand donor set while the divalent ion is coordinated by a softer N_3O donor set. The remaining coordination sites are occupied by aqua ligands. The origin of the reaction-initiating nucleophile could not be determined, however from potentiometric studies, the catalytically active species was found to be of the type $[(\text{OH})\text{Ga}^{\text{III}}(\mu\text{-OH})\text{Zn}^{\text{II}}(\text{OH}_2)]$.

In the same study, using ion replacement techniques, Fe^{III} was replaced with Ga^{III} in the active site of PAP from pig uterine fluid (**Figure 2.4**).¹³ It was shown that the mechanism for the $\text{Ga}^{\text{III}}\text{-Zn}^{\text{II}}$ derivative of uteroferrin involves coordination of the phosphomonoester in a μ -1,3 bridging manner and that nucleophilic attack by the bridging hydroxo species leads to phosphate ester hydrolysis. Furthermore, it was found that replacement of the native ferric ion with Ga^{III} leads to increased catalytic activity.

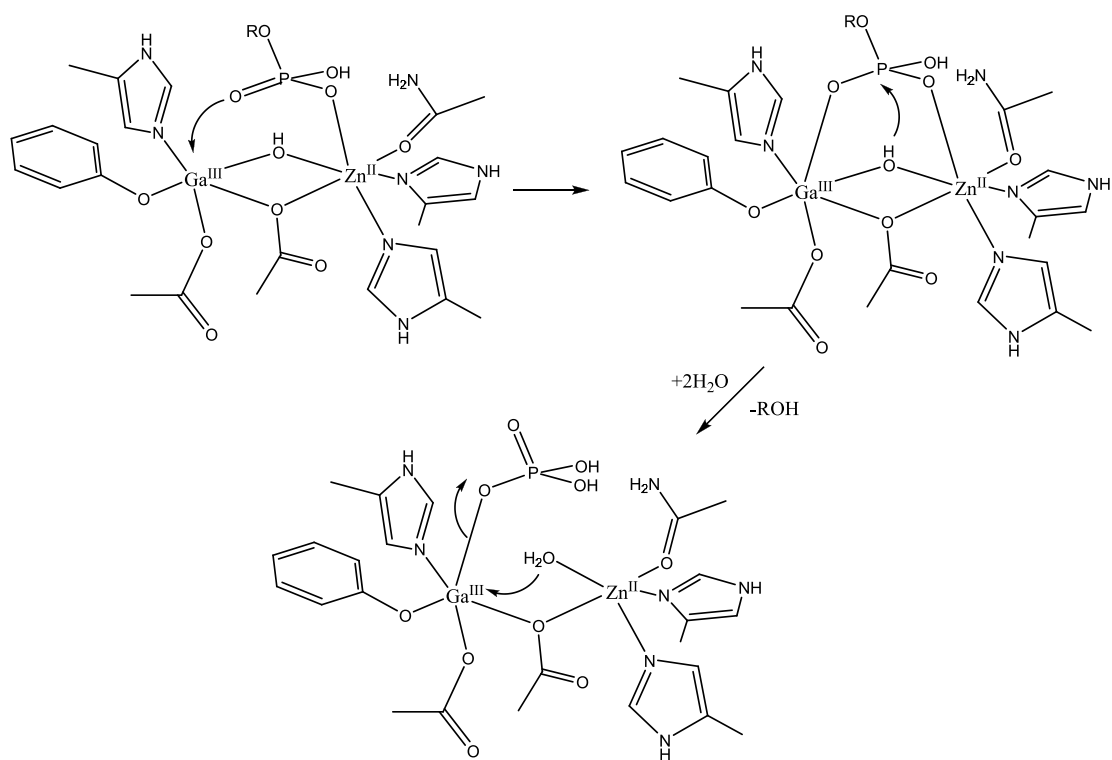


Figure 2.4: Phosphomonoester hydrolysis by Ga^{III}-substituted PAP from pig uterine fluid.¹³

2.1.3. Aims.

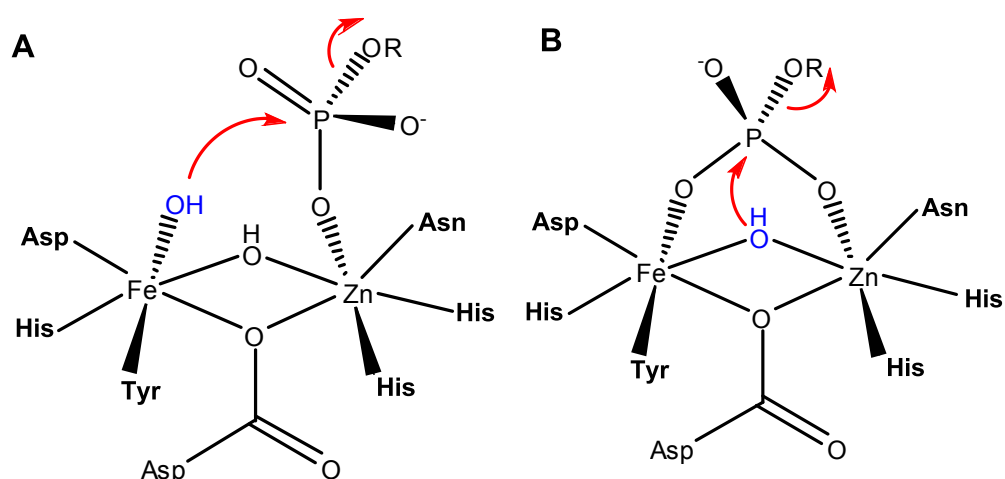


Figure 2.5: Mechanisms of PAP-catalysed phosphate monoester hydrolysis.

Two different proposals assign the mechanism to (a) coordination of the phosphomonoester to the divalent ion and nucleophilic attack by Fe^{III} -bound terminal OH (**Figure 2.5 (A)**)^{2,15-17} and (b) coordination of the phosphomonoester in a bidentate bridging manner and nucleophilic attack by $\mu\text{-OH}$ (**Figure 2.5 (B)**).^{7,10-12,18} In the latter mechanism, the role of the ferric ion is two-fold. Fe^{III} is directly coordinated to the substrate and acts as a Lewis acid. Fe^{III} is also coordinated to the attacking nucleophile, thereby directly influencing its nucleophilicity. The efficiency of the reaction is therefore, regulated by the Lewis acidity of the Fe^{III} ion.

The Lewis acidity of the Fe^{III} ion is modulated by the ligand donor set. The stronger the Lewis acidity of the ferric ion, the higher the Lewis acid activation of the substrate but the lower the nucleophilicity of the attacking nucleophile. The central question to be addressed in this work is the understanding of the relative importances of these opposing factors i.e. Lewis acid activation of the substrate versus nucleophile efficiency of the bridging hydroxo group.

The role of Lewis acid activation versus nucleophile efficiency has been studied in model systems (**Figure 2.6**).

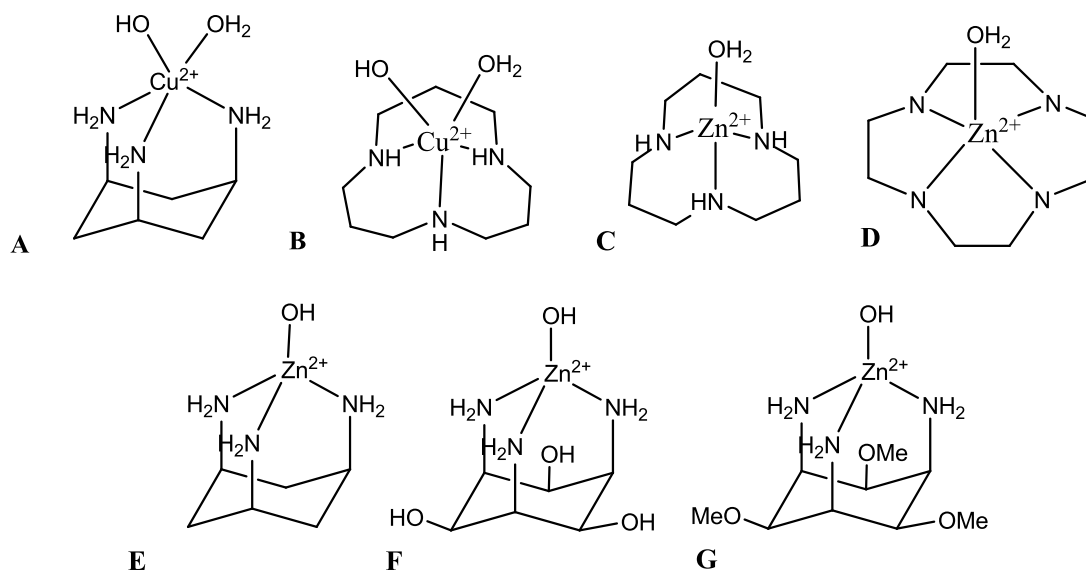


Figure 2.6: Series of complexes used in studying the relative importances of substrate activation versus nucleophile efficiency.¹⁹⁻²¹

Fujii and coworkers found an inverse correlation between the pK_a of coordinated water and the estimated rate constant for the hydrolysis of a model substrate by Cu^{II} complexes **A** and **B** (**Figure 2.6**).¹⁹ The estimated rate constant increased in line with the Lewis acidity of the metal ion. Similarly, for Zn^{II} complexes **C** and **D** (**Figure 2.6**), activation of the substrate was the chief factor in promoting phosphate di- and triester hydrolysis.²⁰ However, in a more recent study by Mancin and coworkers on the Zn^{II} complexes **E**, **F** and **G** (**Figure 2.6**), it was observed that the activation of the nucleophile prevails in determining their intrinsic reactivities.²¹

It was the aim of this work to determine the chief mode of activation in the modulation of phosphate ester hydrolysis by the Fe^{III} ion in PAP by employing Ga^{III} as a mimic for this ion. Ga^{III} is an excellent mimic of Fe^{III}, with similar ionic radius and Lewis acidity. It has been shown to replace Fe^{III} in non-natural forms of PAP.^{13,22} Ga^{III} complexes are characterised by a well defined coordination chemistry and furthermore Ga^{III} displays no relevant redox activity. This redox inactivity

facilitates detailed kinetic studies without interference from competing oxidative-cleaving pathways.

A series of Ga^{III} complexes with tripodal ligands were synthesised and their activities towards the hydrolysis of the activated phosphate diester bis(2,4-dinitrophenyl) phosphate (BDNPP) (**Figure 2.7 (A)**) were studied. These ligands coordinate in a tetradentate fashion, leaving two vacant cis coordination sites on Ga^{III} , occupied by solvent molecules. This allows for coordination of the phosphate diester substrate and subsequent nucleophilic attack by a cis hydroxo group (**Figure 2.7 (B)**).

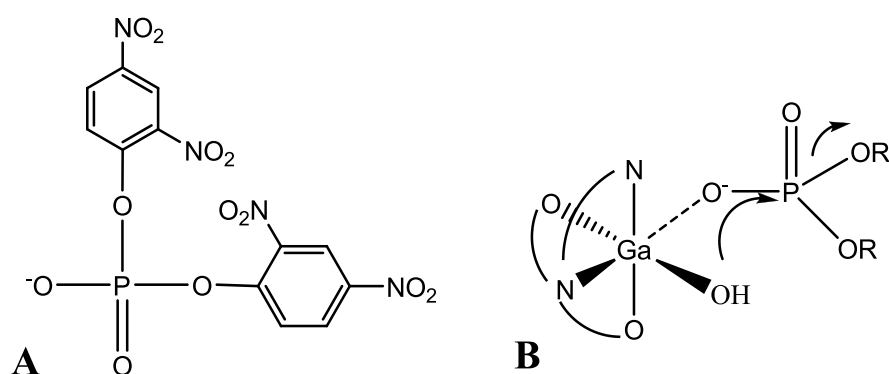


Figure 2.7: BDNPP (A) and substrate coordination and nucleophilic attack by Ga-bound OH (B).

The aim of this study was to determine the effect of different ligand donor groups on the Lewis acidity of the Ga^{III} centre and in turn, how this affects the rate of phosphate diester hydrolysis in these systems i.e. substrate activation versus nucleophile efficiency.

The ferric ion in the active site of PAP is coordinated by the phenolate of a tyrosine residue. In hydrolytically active enzymes, the metal is usually coordinated to carboxylate as negatively charged oxygen donor. The presence of the phenolate donor group is believed to stabilise the trivalent state of the iron. The donor strength of the phenolate also influences the Lewis acidity and may therefore be important for catalytic activity. The second aim of this study was to assess the influence that the phenolate donor group might have on the catalytic activity of these enzymes.

2.2. Results.

In this study, the activities of a number of Ga^{III} complexes of tripodal ligands with respect to phosphate diester hydrolysis were investigated. The tripodal ligands chosen for this study each contain unique combinations of donor groups including; phenolate, carboxylate, pyridyl and primary amine donors (**Figure 2.8**). Each of these ligands when complexed with Ga^{III} influences its Lewis acidity to a different degree, generating a series of Ga^{III} complexes across which the Lewis acidity of the central metal ion is varied.

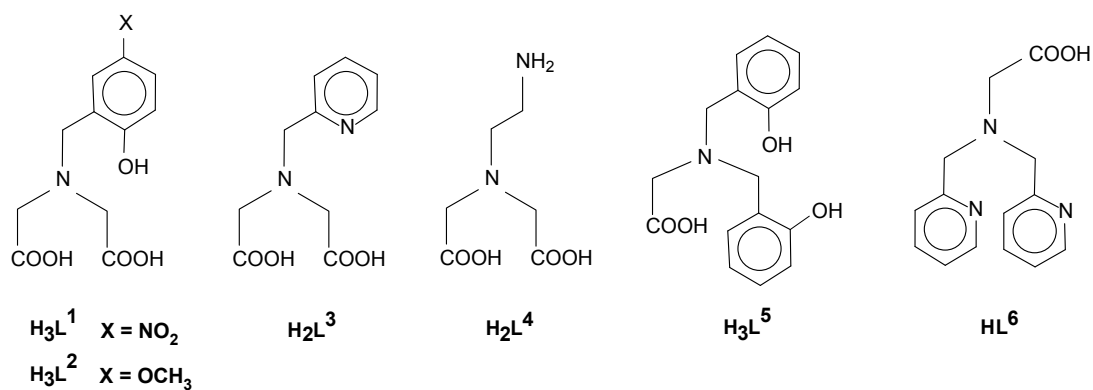


Figure 2.8: Tripodal ligands employed in this study.

2.2.1. Synthesis of Ligands.

Ligands $\mathbf{H}_3\mathbf{L}^1$ and $\mathbf{H}_3\mathbf{L}^2$ were prepared by a solvent free Mannich reaction (**Figure 2.9**).²³ In a typical procedure the appropriate p-phenol, paraformaldehyde and ethyl iminodiacetate were stirred at 50°C for 16 hours under N_2 . The diester product was purified by silica gel chromatography. Ester hydrolysis was carried out by heating the ester in 5 M HCl at 50°C overnight.

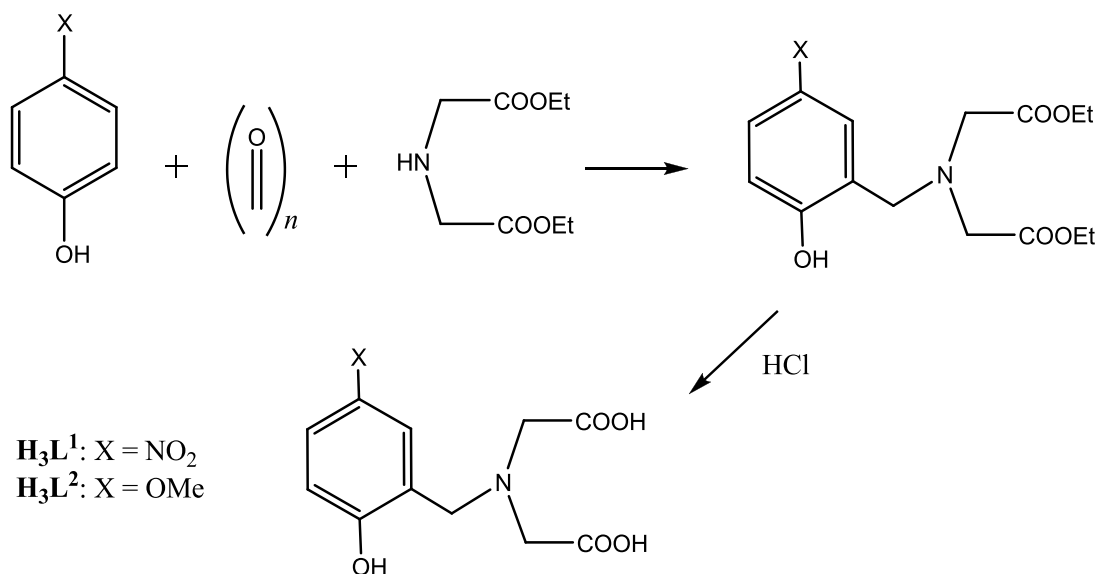


Figure 2.9: Synthetic route to ligands $\mathbf{H}_3\mathbf{L}^1$ and $\mathbf{H}_3\mathbf{L}^2$.

Ligands $\mathbf{H}_2\mathbf{L}^3$ and \mathbf{HL}^6 were synthesised by the route shown in **Figure 2.10**.^{24,25}

Iminodiacetic acid and 2-picolylchloride and potassium carbonate in 1.5 M KOH were stirred at 80°C for 18 hours. Needle-shaped crystals of $\mathbf{H}_2\mathbf{L}^3$ were isolated from solution at pH 3.5.

\mathbf{HL}^6 was prepared by a similar procedure by stirring glycine and 2-picolyl chloride in 3 M NaOH at 60°C for 2 hours.

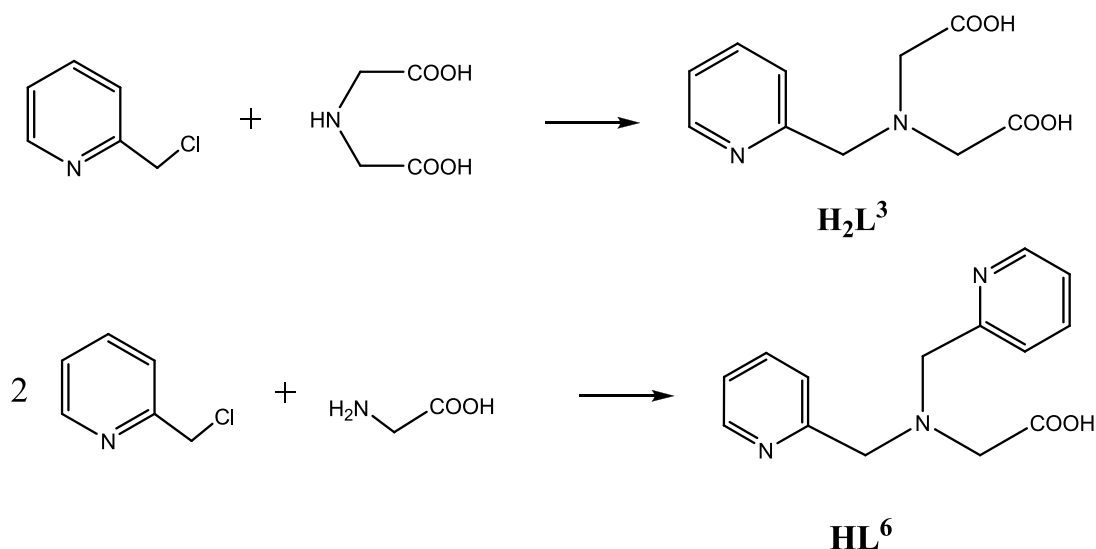


Figure 2.10: Synthetic route to ligands **H₂L³** and **HL⁶**.

The procedure of Martell was followed for the synthesis of **H₂L⁴** (**Figure 2.11**).²⁶ Ethyl acetate and ethylenediamine were refluxed for 20 hours to give N-acetyethylenediamine which was purified by reduced pressure distillation. N-Acetyethylenediamine and bromoacetic acid were stirred in 3.5 M NaOH at 35°C for 1 hour. The protecting acetyl group was removed by saponification with 5 M NaOH.

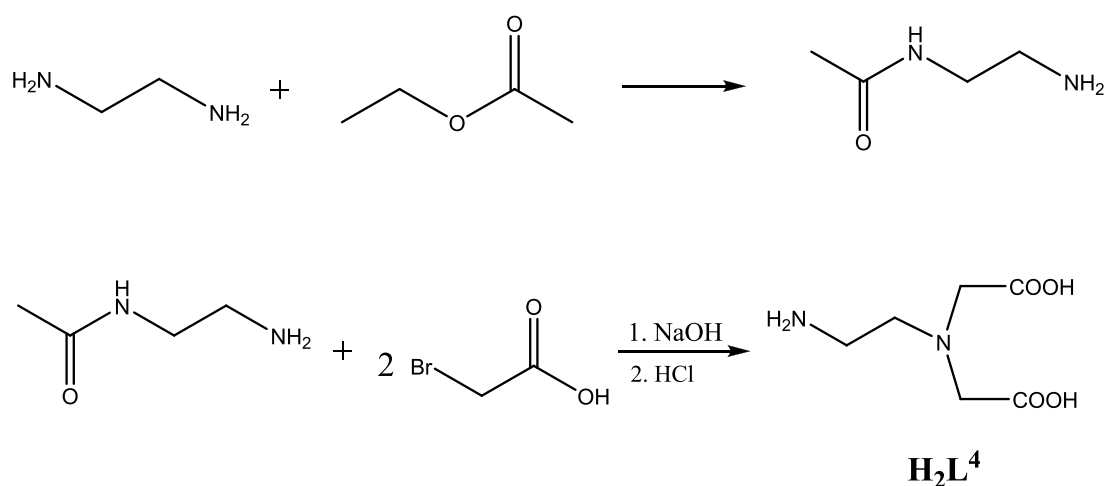


Figure 2.11: Synthetic route for the synthesis of **H₂L⁴**.

H₃L⁵ was synthesised by the route shown in **Figure 2.12**.²⁷ Glycine and salicylic acid were stirred in a methanolic solution of LiOH, resulting in the formation of the imine which was reduced with NaBH₄ to give N-(2-hydroxybenzyl)aminoacetic acid (**A**, **Figure 2.12**). 2-Bromomethyl phenyl acetate, N-(2-hydroxybenzyl)aminoacetic acid and Et₃N were stirred for 24 hours at room temperature. The obtained ester was hydrolysed with stirring in a methanolic solution of KOH.

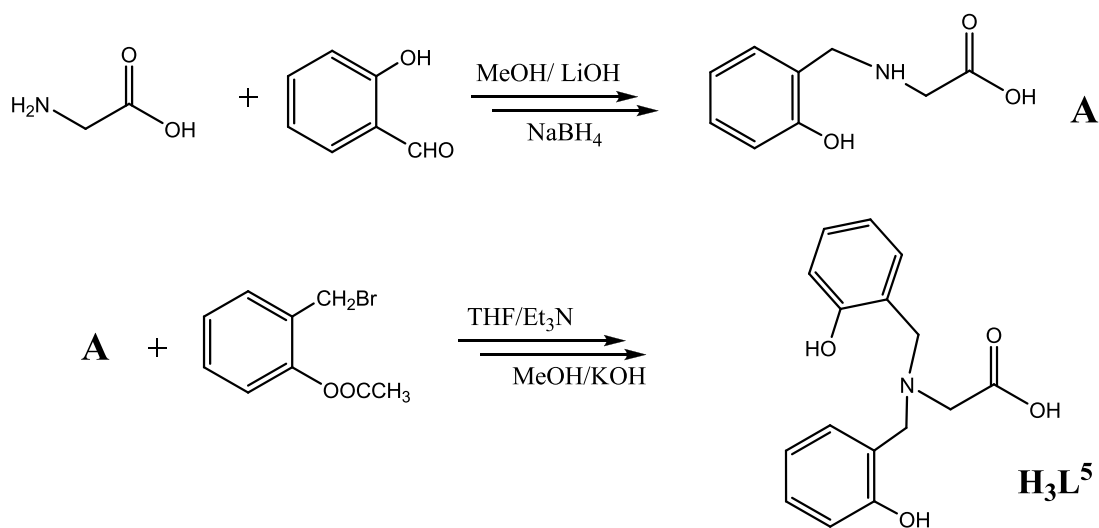


Figure 2.12: Synthetic route to **H₃L⁵**.

2.2.2. Gallium Complexes.

[GaL¹(H₂O)₂] (**1**) and [GaL²(H₂O)₂] (**2**) were prepared according to the literature.²⁸ The Ga^{III} complexes of the ligands **H₂L³**, **H₂L⁴** and **HL⁶** were isolated in crystalline form from slightly acidic solution as hydroxo-bridged dimers, [GaL³(μ-OH)]₂·4H₂O (**3**), [GaL⁴(μ-OH)]₂·4H₂O (**4**) and [GaL⁶(μ-OH)]₂(NO₃)₂·3H₂O (**6**). [GaL⁵(H₂O)₂] (**5**) was generated in situ by mixing equimolar amounts of **H₃L⁵** and Ga(NO₃)₃, binding in the pH range 3 – 9 was confirmed by ¹H NMR spectroscopy. The ¹H NMR spectrum of **5** is shown in **Figure 2.13**. In the case of ligand **H₂L⁴**, the mononuclear 2:1 complex [Ga(**HL⁴**)₂]Cl·2H₂O (**4a**) was isolated from more strongly acidic solution due to protonation of the primary amine group, rendering the ligand unable to coordinate in a tetradentate mode. X-ray structures of complexes **3**, **4**, **4a** and **6** are shown below (**Figures 2.14 – 2.17**).

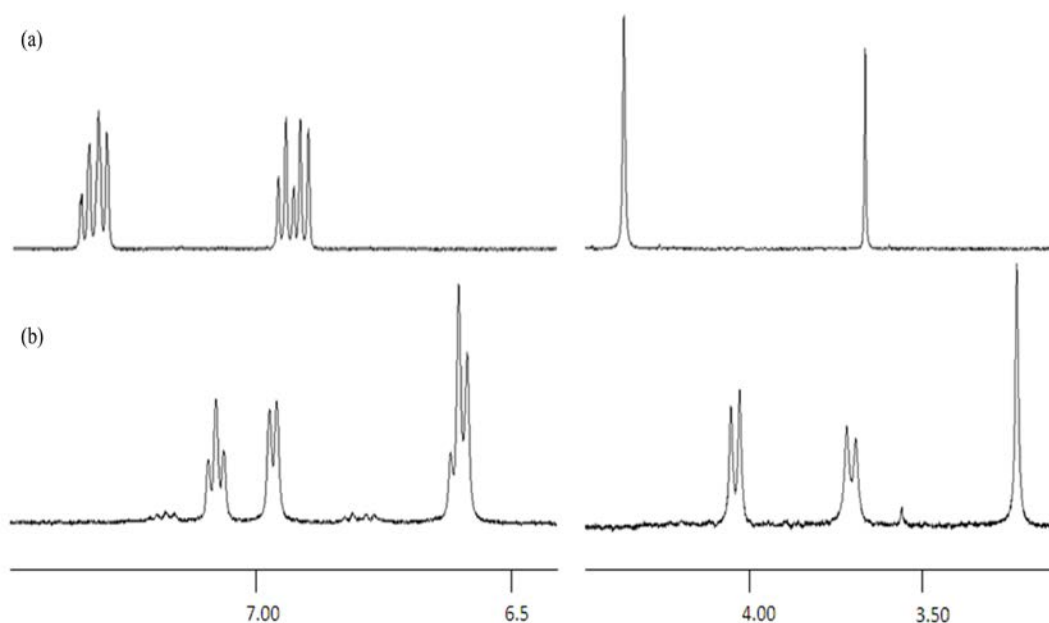


Figure 2.13: ¹H NMR spectrum (D₂O) of **H₃L⁵** (a) and complexed **5** (b).

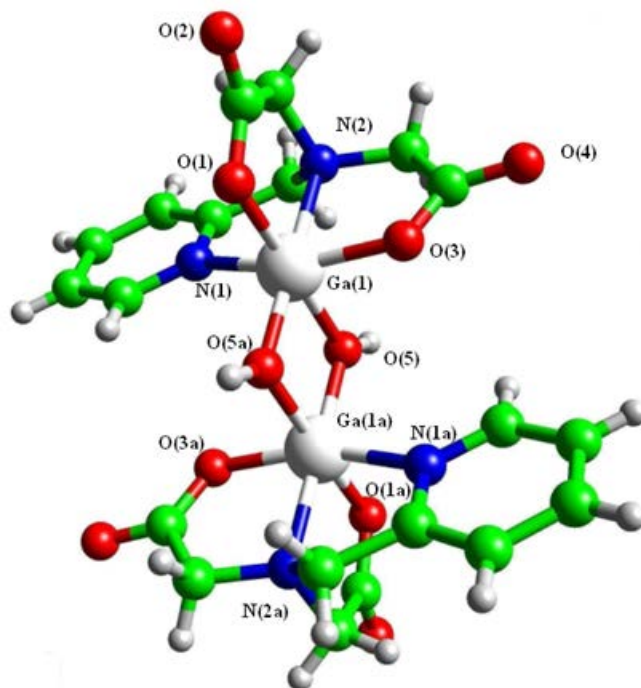


Figure 2.14: Molecular structure of $[\text{GaL}^3(\mu\text{-OH})]_2 \cdot 4\text{H}_2\text{O}$ (3) with the atom numbering scheme. Water molecules of crystallization are omitted for clarity.

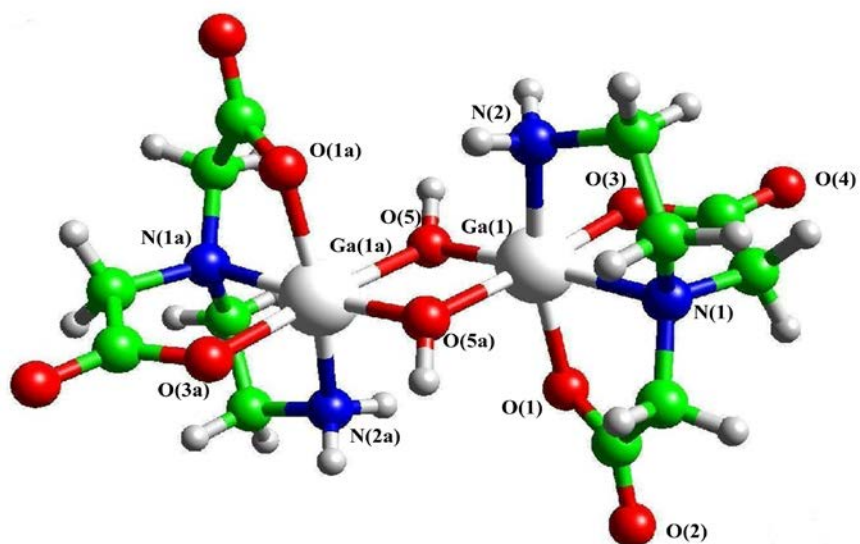


Figure 2.15: Molecular structure of $[\text{GaL}^4(\mu\text{-OH})]_2 \cdot 4\text{H}_2\text{O}$ (4) with the atom numbering scheme. Water molecules of crystallization are omitted for clarity.

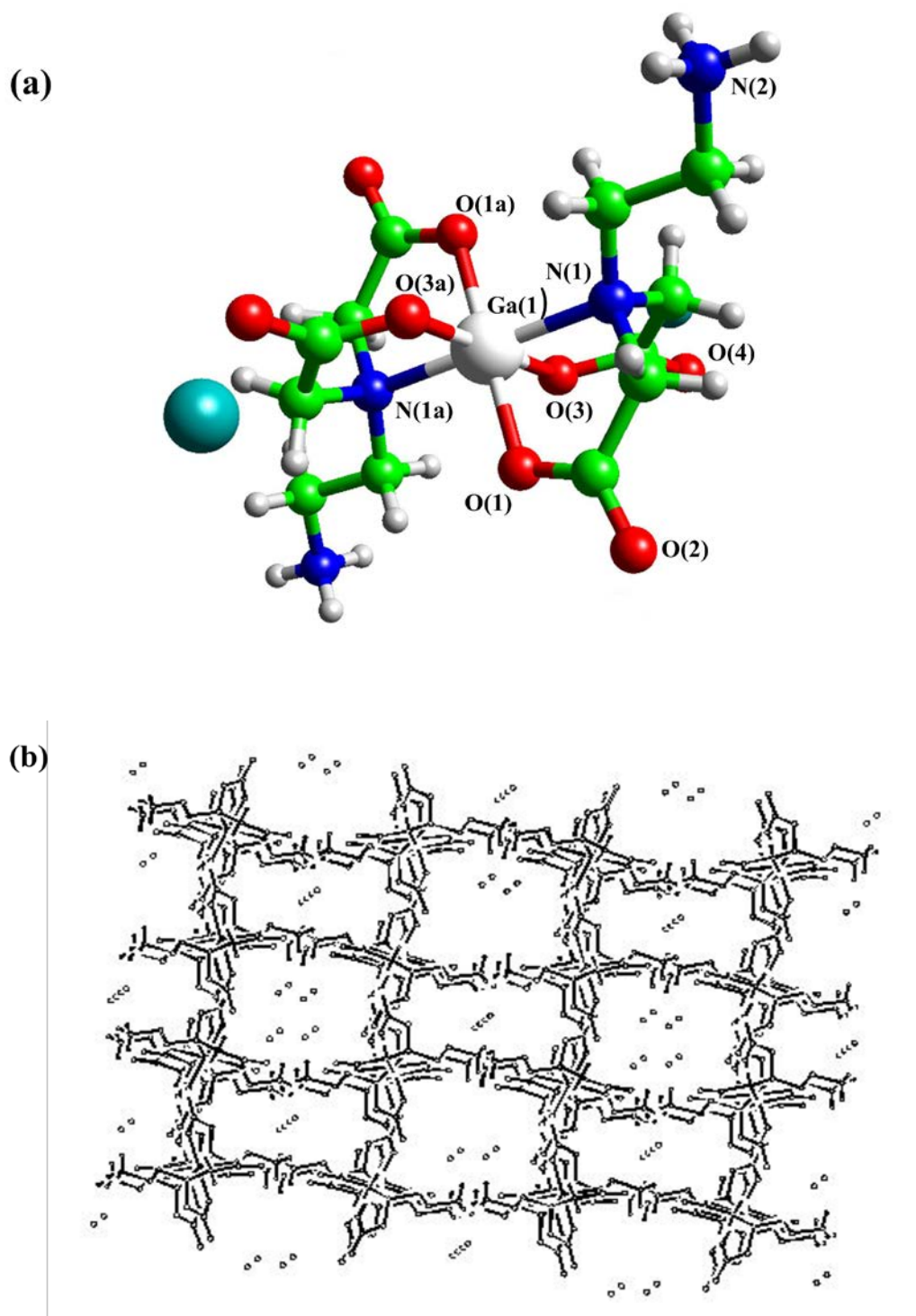


Figure 2.16: (a) View of $[\text{Ga}(\text{HL}^4)_2]\text{Cl}\cdot 2\text{H}_2\text{O}$ (**4a**) with the atom numbering scheme. Water molecules of crystallization are omitted for clarity. (b) Crystal packing of **4a**. The view is along the *b* axis.

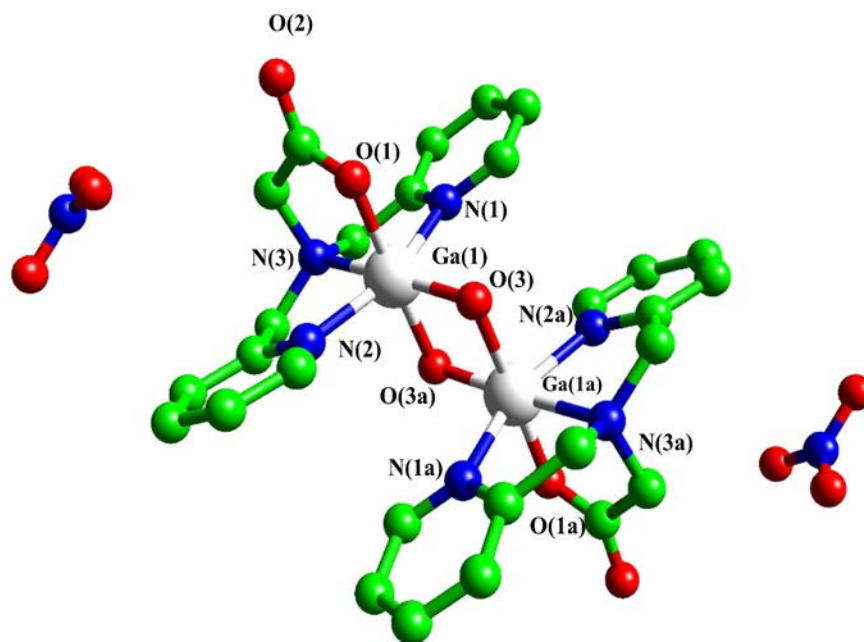


Figure 2.17: View of $[\text{GaL}^6(\mu\text{-OH})]_2(\text{NO}_3)_2 \cdot 3\text{H}_2\text{O}$ (**6**) with the atom numbering scheme. Hydrogen atoms and water molecules of crystallisation are omitted for clarity.

The Ga^{III} complexes of H_2L^3 , H_2L^4 and HL^6 were crystallised as hydroxo bridged dimers, all in the monoclinic crystal system and space group $P2_1/c$. Hydroxo bridged dimers **3** and **4** are neutral while **6** is a dication. In each structure, Ga is located in a slightly distorted octahedral environment, coordinated by the respective tetradentate tripodal ligand and the two bridging hydroxo groups. Ga - Ga distances range from 2.951 Å to 2.982 Å. The hydroxo bridges in each structure are unsymmetrical, the Ga - O bond length is shorter where it is *trans* to tertiary amine than where it is *trans* to carboxylate (**Table 1**). The bond angles around the bridging oxygen atoms range from 99.2 to 100.9°. Ga - N bond lengths are greater for tertiary amino nitrogen than for primary amino nitrogen (**4**) and pyridyl nitrogen (**3** and **6**).

The 2:1 complex **4a** crystallised in the orthorhombic crystal system in the space

group *Pccn*. Each ligand coordinates tridentately through two carboxylate groups and the tertiary amine nitrogen. The non-coordinating primary amine group is protonated. The structure is centrosymmetric with gallium located at the inversion centre. Hydrogen bonding is observed between the ammonium groups, carboxylate oxygens and methylene groups (N(2)⋯O(4) 2.842(2) Å, N(2)-H⋯O(4) 139°, -x, ½ + y, ½ - z; C(3)⋯O(2) 3.345(2) Å, C(3)-H(a)⋯O(2) 179°, -½ + x, -y, ½ -z; C(3)⋯O(2) 3.243 Å, C(3)-H(b)⋯O(2) 169°, ½ - x, y, ½ + z). There are two types of channel present. Water molecules of crystallization are located in the large channels while chloride counterions are located in the smaller channels. The water molecules of crystallization and the chloride anions form hydrogen bonds with the non-coordinating, protonated amino groups (N(2)⋯O(1w) 2.823(2) Å, ½ - x, ½ - y, z; N(2)⋯Cl 3.182(1) Å, ½ - x, y, ½ + z). Selected bond distances and angles are presented in **Table 1**.

Table 1: Selected bond lengths [Å] and angles [°] in compounds **3** – **6**.

3			
Ga(1)–N(1)	2.084(2)	Ga(1)–N(2)	2.105(2)
Ga(1)–O(1)	1.975(2)	Ga(1)–O(3)	1.967(2)
Ga(1)–O(5)	1.982(2)	Ga(1)–O(5a) ^a	1.903(2)
Ga(1)⋯Ga(1a) ^a	2.9600(6)		
N(1)–Ga(1)–N(2)	78.21(9)	N(1)–Ga(1)–O(3)	159.69(9)
N(1)–Ga(1)–O(5)	90.14(8)	N(1)–Ga(1)–O(5a) ^a	102.25(9)
N(2)–Ga(1)–O(1)	84.92(8)	N(2)–Ga(1)–O(3)	81.75(8)
4			
Ga(1)–N(1)	2.068(2)	Ga(1)–N(2)	2.029(2)
Ga(1)–O(1)	1.982(2)	Ga(1)–O(3)	1.983(2)

Ga(1)–O(5)	1.863(1)	Ga(1)–O(5a) ^b	2.002(2)
Ga(1)⋯Ga(1a) ^b	2.951(1)		
N(1)–Ga(1)–N(2)	84.20(8)	N(1)–Ga(1)–O(3)	83.45(7)
N(1)–Ga(1)–O(5)	174.52(7)	N(1)–Ga(1)–O(5a) ^b	100.21(7)
N(2)–Ga(1)–O(1)	162.45(8)	N(2)–Ga(1)–O(3)	91.11(8)
4a			
Ga(1)–N(1)	2.086(3)	Ga(1)–O(1)	1.948(3)
Ga(1)–O(3)	1.948(3)		
N(1)–Ga(1)–O(1)	85.3(1)	N(1)–Ga(1)–O(3)	85.3(1)
O(1)–Ga(1)–O(3)	89.0(2)		
6			
Ga(1)–N(1)	2.062(3)	Ga(1)–N(2)	2.061(3)
Ga(1)–N(3)	2.086(2)	Ga(1)–O(1)	1.976(2)
Ga(1)–O(3)	1.884(2)	Ga(1)–O(3a) ^a	1.982(2)
Ga(1)⋯Ga(1a) ^a	2.982(1)		
N(1)–Ga(1)–N(2)	159.2(1)	N(1)–Ga(1)–N(3)	80.2(1)
N(1)–Ga(1)–O(1)	85.8(1)	N(2)–Ga(1)–O(1)	89.0(1)
N(2)–Ga(1)–O(3)	101.1(1)	O(3)–Ga(1)–O(3a) ^a	79.12(9)

^a -1-x,1-y,1-z; ^b 1-x,1-y,1-z

2.2.3. Solution Behaviour of the Complexes.

As confirmed by ¹H NMR spectroscopy, no dissociation of complexes into free ligand and metal ion was observed in the pH range 3-9. Dissolving the hydroxo-bridged complexes [GaL³(μ-OH)]₂·4H₂O (**3**), [GaL⁴(μ-OH)]₂·4H₂O (**4**) and [GaL⁶(μ-OH)]₂(NO₃)₂·3H₂O (**6**) at 1 mM concentration gave solutions with pH values of between 5 and 6. Potentiometric titration revealed the dissociation of the hydroxo-bridged dimers into their monomeric components in solution (**Figure 2.19**). One titratable proton per gallium was observed, in the pH range 3 - 10, with pK_a values of 7.38(2) (**3**), 7.78(2) (**4**), and 6.72(3) (**6**). Acid dissociation constants for

complexes **1** and **2** were previously reported.²⁸ Two titratable protons per Ga^{III} were revealed for **5**; 7.37(2) and 9.29(3). The titration curves for complexes **3,4,5** and **6** are presented in **Figure 2.18**.

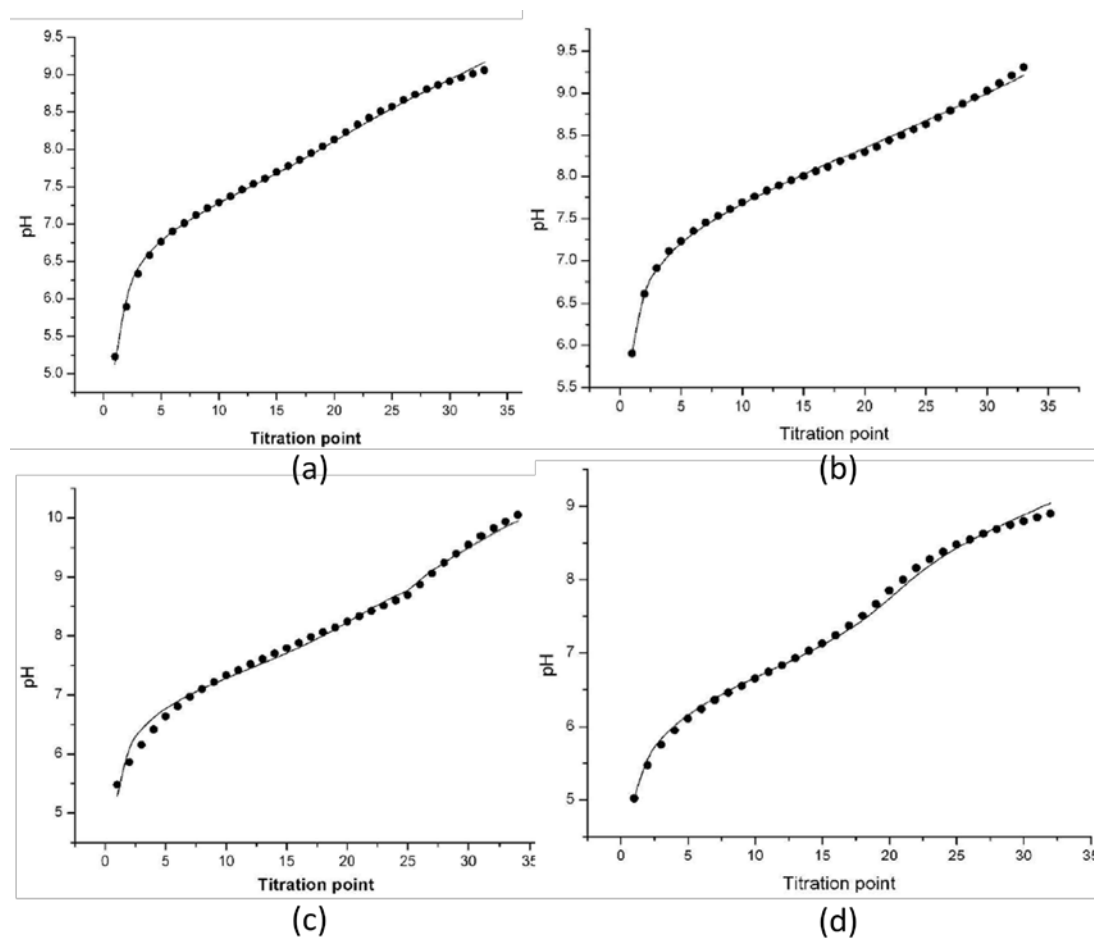


Figure 2.18: Titration curves of **3** (a), **4** (b), **5** (c) and **6** (d).

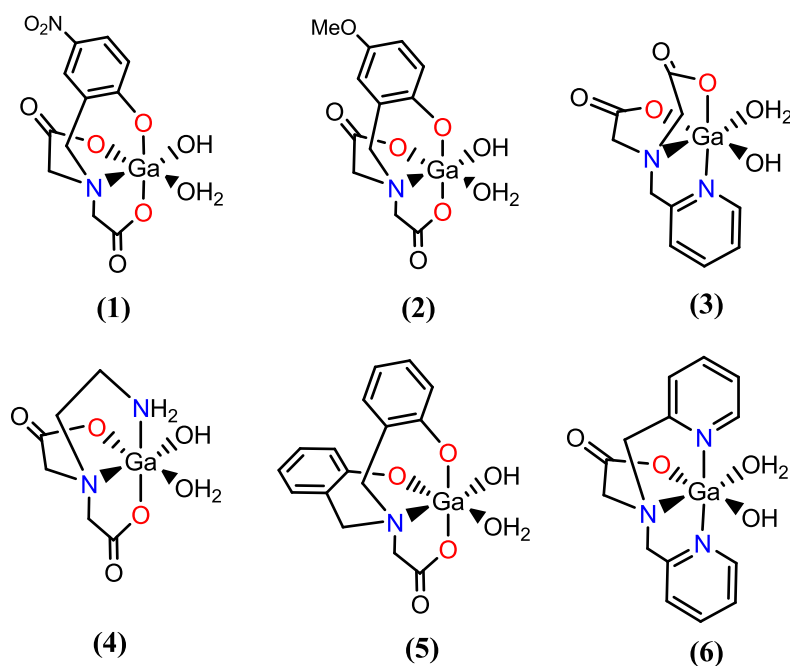


Figure 2.19: Ga^{III} complexes depicted in their monomeric aqua-hydroxy forms in solution (charges are omitted).

2.2.4. BDNPP Hydrolysis.

Activity of the complexes towards phosphate diester hydrolysis was studied using the activated phosphate diester bis(2,4-dinitrophenyl) phosphate (BDNPP). Phosphate monoester hydrolysis is extremely slow and metal catalysis even for activated esters is challenging. As is often done in the literature, a diester substrate is used to model phosphate monoester hydrolysis. The hydrolysis of this substrate can be conveniently monitored by measuring the increase in absorbance at 400 nm due to the reaction product 2,4-dinitrophenolate (**Figure 2.20**).

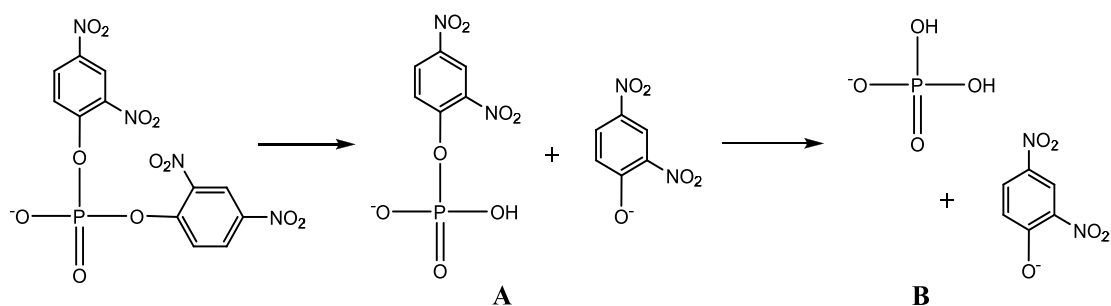


Figure 2.20: Hydrolysis of BDNPP to give the phosphomonoester (A) and free phosphate (B).

The method of initial rates was used to determine the pseudo-first-order rate constants by following the reaction to < 5 % conversion. This method ensures that the rate constants determined are due predominantly to phosphate diester hydrolysis, the initial hydrolysis product (**Figure 2.20 (A)**). In each catalytic run, the reaction rates were corrected for the spontaneous hydrolysis of BDNPP at the relevant pH. In the case of complex **6**, the study of BDNPP hydrolysis was hampered by long induction periods which cannot be explained at present. Complexes **1-5** exhibited bell-shaped pH-rate profiles with maxima at pH 7.0 (**1**), 7.5 (**2**), 6.4 (**3**), 6.7 (**4**) and 8.5 (**5**) (**Figure 2.21**).

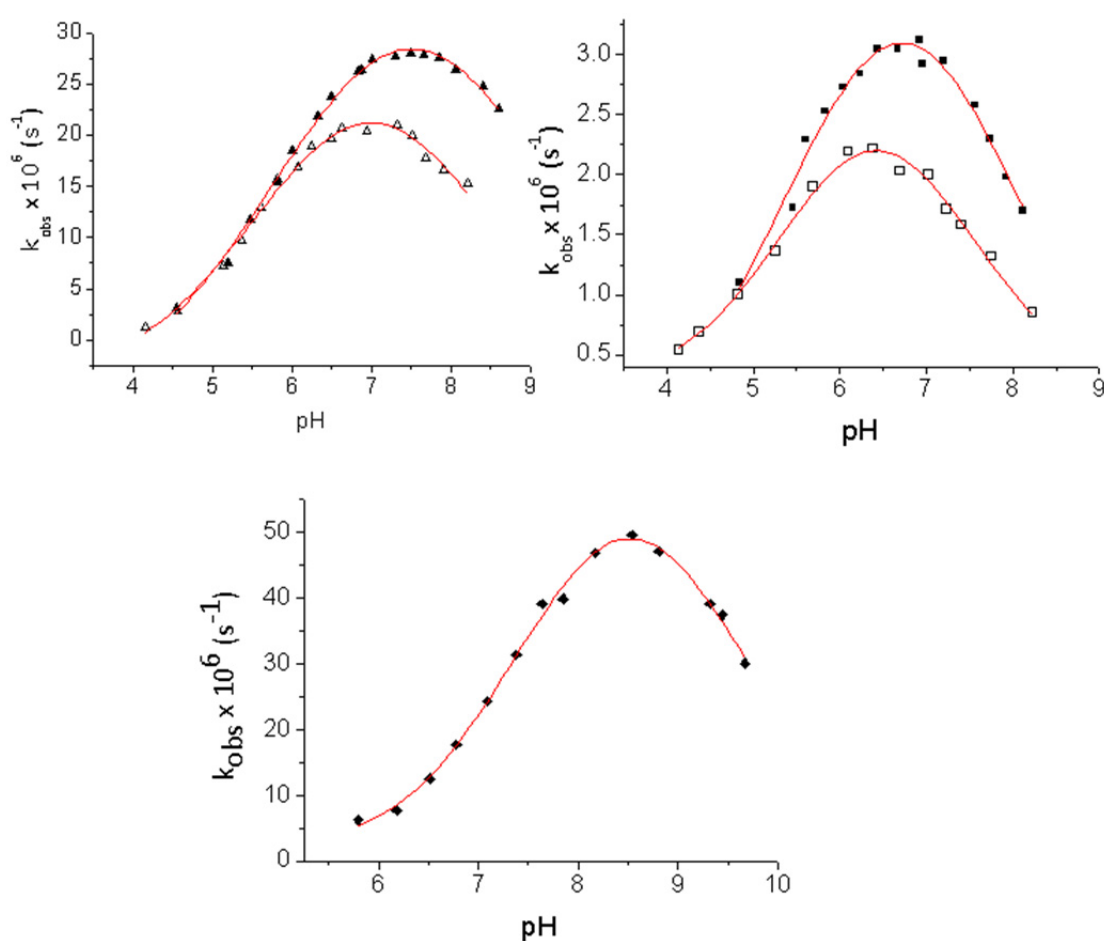


Figure 2.21: Rate-pH profiles for the cleavage of BDNPP (5×10^{-5} M) with 2 mM solutions of **1** (\triangle), **2** (\blacktriangle), **3** (\circ), **4** (\blacksquare) and **5** (\blacklozenge) at 37 °. [buffer] = 50 mM (buffer = PIPBS (pH 4 – 5), MES (pH 5 – 6.5), HEPES (pH 6.8 – 8), EPPS (pH 7.5 – 8.5) and CHES (pH 8.5 – 9.5); $I = 0.1$ M (NaClO_4)).

The bell-shaped pH-rate profiles strongly suggest that the active species for hydrolysing BDNPP are the aqua-hydroxo forms of the complexes. **Table 2** presents the pK_a values of Ga^{III} -coordinated water, determined potentiometrically and kinetically.

Table 2: pK_a values determined potentiometrically and kinetically.

Complex	pK_{a1}	pK_{a2}	$pK_{a1}^{'a}$	$pK_{a2}^{'a}$
1	5.54(2) ^b		5.43	8.59
2	6.42(1) ^b		5.90	8.99
3		7.38(2) ^c	5.69	7.12
4		7.78(2) ^c	5.72	7.72
5	7.37(2) ^c	9.29(3) ^c	7.26	9.72
6	6.72(3) ^c			

^a Kinetic data. ^b Potentiometric data, ref. ²⁸. ^c Potentiometric data, this work.

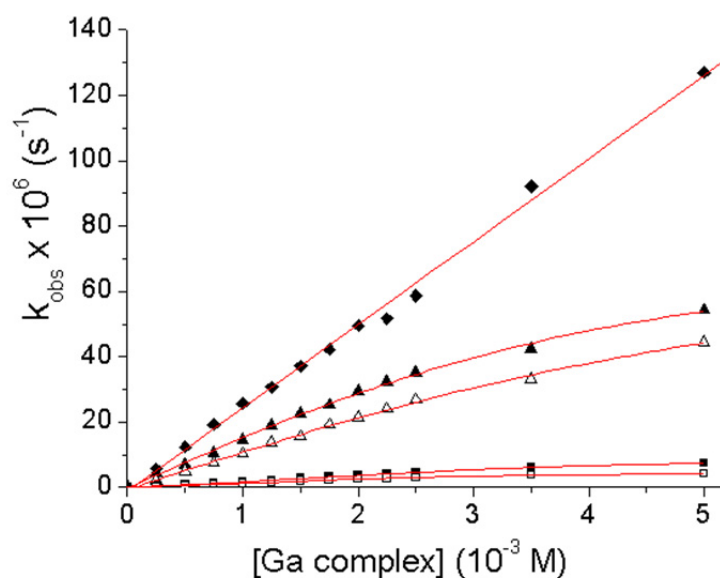


Figure 2.22: Dependence of the rate of cleavage of BDNPP (5×10^{-5} M) on the concentration of **1** (Δ), **2** (\blacktriangle), **3** (\circ), **4** (\blacksquare) and **5** (\blacklozenge) at 37° , and at the respective optimum pH for each complex. [buffer] = 50 mM, $I = 0.1$ M ($NaClO_4$).

The dependence of the rate of BDNPP hydrolysis with complex concentration was also studied (**Figure 2.22**). A deviation from linearity occurs at higher complex concentrations. This is due to the formation of the inactive hydroxo-bridged dimer species at higher concentration (**Figure 2.23**).

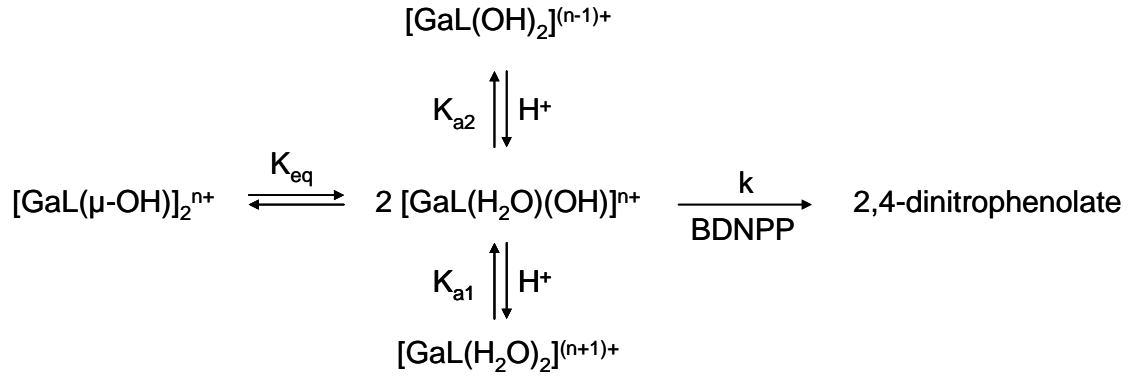


Figure 2.23: Solution equilibria of complexes 1–5 and phosphate diester hydrolysis.

Taking into account the equilibrium shown in (**Figure 2.23**), the following equations were derived:

$$k_{\text{obs}} = A + k [\text{Ga}(\text{H}_2\text{O})(\text{OH})], \text{ where } A \text{ is a constant} \quad (1)$$

$$[\text{Ga}]_t = 2 [\text{Ga}_2\text{L}_2(\mu\text{-OH})_2] + [\text{GaL}(\text{H}_2\text{O})(\text{OH})] + [\text{GaL}(\text{H}_2\text{O})_2] + [\text{GaL}(\text{OH})_2] \quad (2)$$

$$[\text{Ga}]_t = \frac{2[\text{GaL}(\text{H}_2\text{O})(\text{OH})]^2}{K_{\text{eq}}} + [\text{GaL}(\text{H}_2\text{O})(\text{OH})] \left(1 + \frac{[\text{H}^+]}{K_{a1}} + \frac{K_{a2}}{[\text{H}^+]} \right) \quad (3)$$

Hence,

$$[\text{GaL}(\text{H}_2\text{O})(\text{OH})] = \frac{-\left(1 + \frac{[\text{H}^+]}{K_{a1}} + \frac{K_{a2}}{[\text{H}^+]} \right) \pm \sqrt{\left(1 + \frac{[\text{H}^+]}{K_{a1}} + \frac{K_{a2}}{[\text{H}^+]} \right)^2 + \frac{8}{K_{\text{eq}}} [\text{Ga}]_t}}{\frac{4}{K_{\text{eq}}}} \quad (4)$$

and

$$k_{\text{obs}} = A + k \frac{-\left(1 + \frac{[\text{H}^+]}{K_{a1}} + \frac{K_{a2}}{[\text{H}^+]} \right) \pm \sqrt{\left(1 + \frac{[\text{H}^+]}{K_{a1}} + \frac{K_{a2}}{[\text{H}^+]} \right)^2 + \frac{8}{K_{\text{eq}}} [\text{Ga}]_t}}{\frac{4}{K_{\text{eq}}}} \quad (5)$$

Fitting the kinetic data according to **eq. 5** gave the equilibrium constants for dimer dissociation into monomers (K_{eq} (M)) and the catalytic rate constants for BDNPP hydrolysis $\{k$ ($\text{M}^{-1}\text{s}^{-1}$) $\}$, presented in **Table 3**.

Table 3: Equilibrium constants, catalytic rate constants and kinetic pK_{a} values for the hydrolysis of BDNPP by complexes **1-5**.

Complex	K_{eq} (M)	k ($\text{M}^{-1}\text{s}^{-1}$)	pK_{a1}	pK_{a2}
$[\text{GaL}^1(\text{H}_2\text{O})(\text{OH})]^-$	0.541	2.12×10^{-2}	5.43	8.59
$[\text{GaL}^2(\text{H}_2\text{O})(\text{OH})]^-$	1.03×10^{-2}	3.05×10^{-2}	5.90	8.99
$[\text{GaL}^3(\text{H}_2\text{O})(\text{OH})]$	1.34×10^{-3}	3.61×10^{-3}	5.69	7.12
$[\text{GaL}^4(\text{H}_2\text{O})(\text{OH})]$	2.28×10^{-3}	3.86×10^{-3}	5.72	7.72
$[\text{GaL}^5(\text{H}_2\text{O})(\text{OH})]^-$	7.85	4.64×10^{-2}	7.26	9.72

Equilibrium constants for the dissociation of the dimers into monomeric units decrease in the order **5** > **1** > **2** > **4** > **3**. As expected, the anionic complexes (in their respective aqua-hydroxo forms) **1**, **2** and **5** show a lower tendency towards dimer formation. Species distribution plots for the new gallium complexes, **3**, **4** and **5**, presented in **Figure 2.24** were computed using a program based on the comics algorithm.²⁹

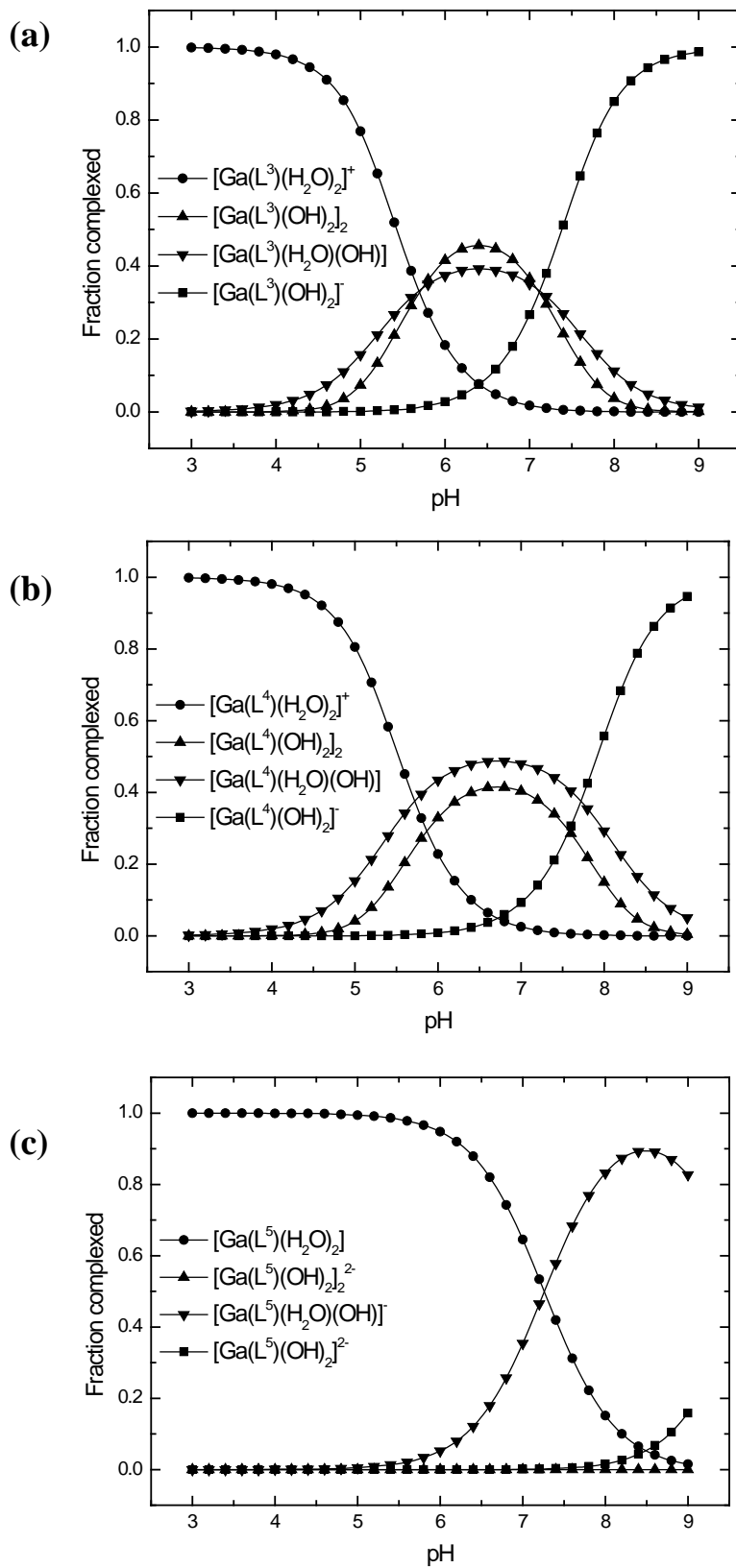


Figure 2.24: Species distribution of **3** (a), **4** (b) and **5** (c) as a function of pH. Species diagrams are based on pK_a and K_{eq} values calculated from kinetic data.

2.2.5. Solvent Deuterium Isotope Effect.

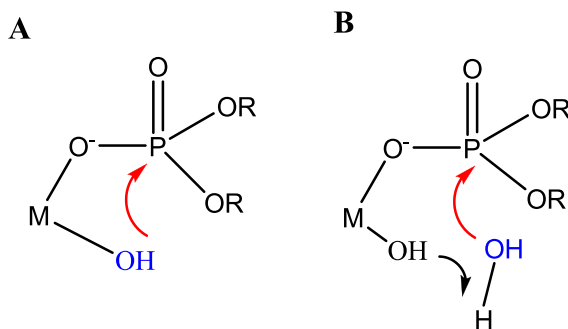


Figure 2.25: Nucleophilic (A) and general base (B) mechanisms.

Kinetic data obtained was consistent with a nucleophilic mechanism (**Figure 2.25 (A)**) and a general base mechanism (**Figure 2.25 (B)**). In order to distinguish between these mechanisms, the solvent deuterium isotope effect was employed. In a nucleophilic mechanism, coordination of the substrate to the Ga^{III} centre results in substrate activation. Subsequent nucleophilic attack by the cis- hydroxo group leads to cleavage of the phosphate diester bond. In a general base mechanism, the cis-hydroxo group deprotonates solvent water, generating OH^- , which in turn carries out nucleophilic attack on the substrate. The solvent deuterium isotope effect is a classical method used to differentiate between these mechanisms.^{30,31} In general, a $k_{\text{H}}/k_{\text{D}}$ value of between 0.8 and 1.5 indicates a nucleophilic mechanism, no proton transfer involved in the rate-determining step. In all cases, $k_{\text{H}}/k_{\text{D}}$ values in this range were obtained; 1.26 (**1**), 1.08 (**2**), 0.95 (**3**), 0.90 (**4**), 0.84 (**5**). The solvent deuterium isotope effect was determined by measuring the rate constant in D_2O and $k_{\text{H}}/k_{\text{D}}$ values were calculated by taking the initial rates at the corresponding pL values (L = H, D) ($\text{pD} = \text{pH} + 0.4$). $k_{\text{H}}/k_{\text{D}}$ was determined for a range of pL values for each complex and the mean value across the range reported (**Figure 2.26**).

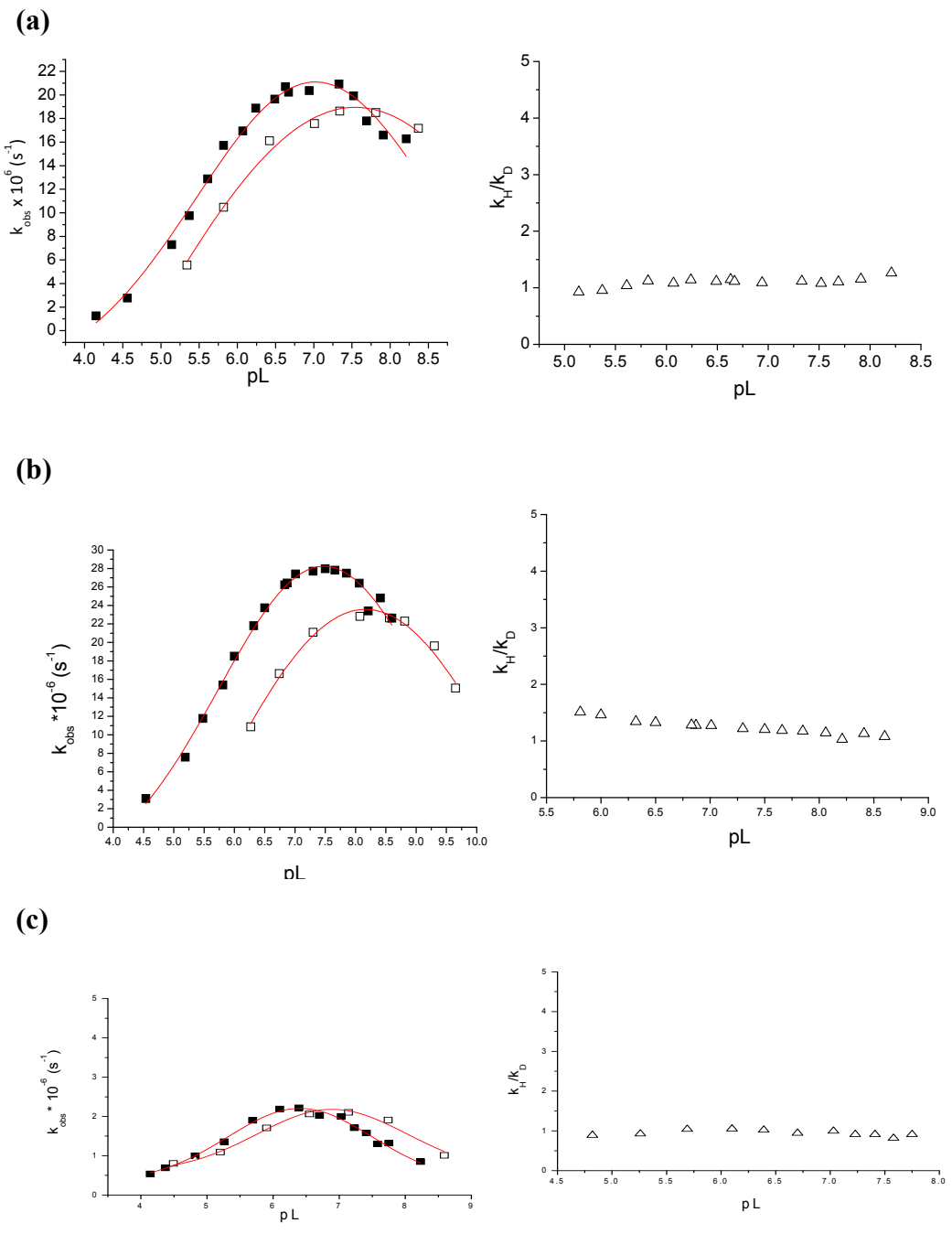
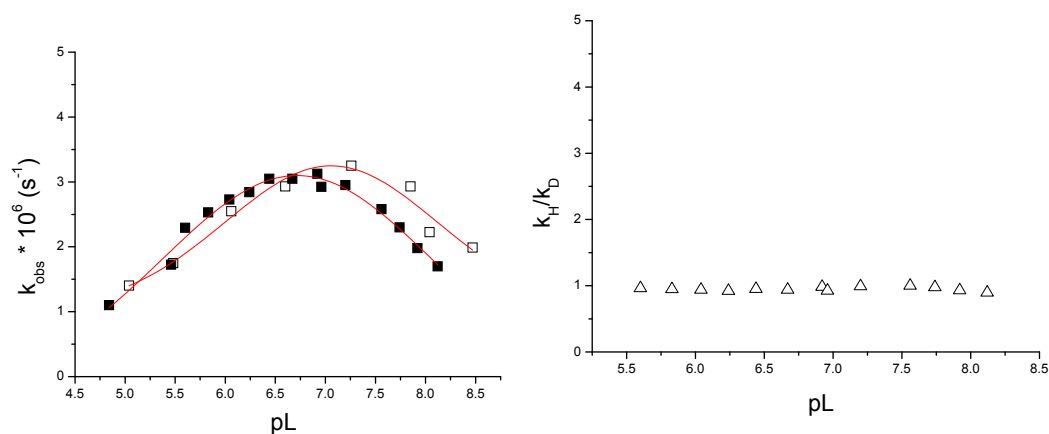


Figure 2.26 continued on next page.

(d)



(e)

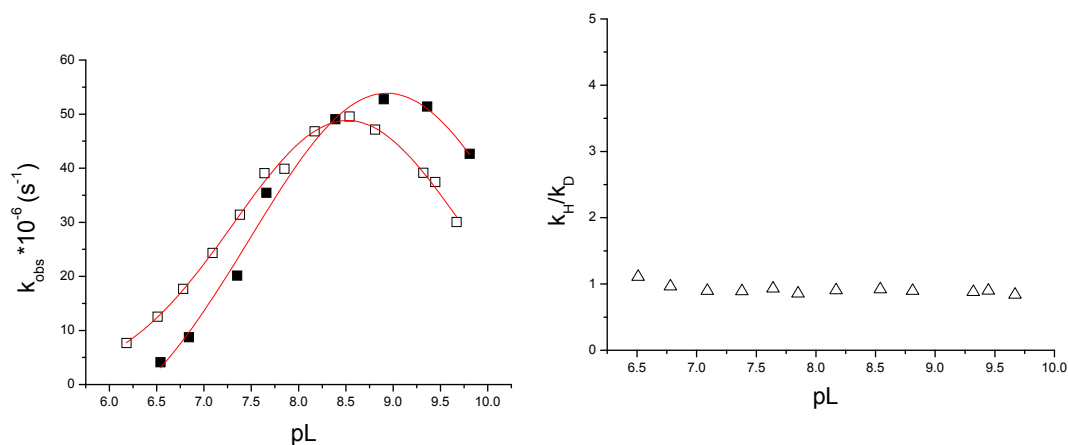


Figure 2.26: pL-rate profile (L = H, D) for the hydrolysis of BDNPP (5×10^{-5} M) in H₂O (■), D₂O (□) at 37°C; 50 mM HEPES and 2 mM **1** (a), **2** (b), **3** (c), **4** (d) and **5** (e). (Δ) Isotope effect ($k_{\text{H}}/k_{\text{D}}$) calculated by taking k 's at corresponding pL values (pD = pH + 0.4). Reaction rates were corrected for the uncatalysed reaction in H₂O and D₂O.

2.2.6. Substrate Binding.

Substrate binding to the complexes in their aqua-hydroxo forms was investigated using the hydrolytically stable phosphate diester dimethylphosphate (DMP) (**Figure 2.27**). Binding constants were estimated using ¹H NMR spectroscopy. Addition of 1 equivalent of DMP to a 2 mM solution of complex at the pD of optimum activity for each complex resulted in a new doublet appearing downfield (~0.2 – 0.5 ppm) from

the free DMP peak. The presence of two signals indicates that the phosphate diester complex is kinetically inert on the NMR timescale. Binding was studied at the optimum pD from the pH- rate profile for each complex. Binding constants are 60 M^{-1} (**3**), 7 M^{-1} (**1**) and 2.5 M^{-1} (**5**). The measurement of binding constants for **2** and **4** was not possible due to severe signal overlap. Due to the limited solubility of the complexes, the ^{31}P NMR could not be recorded.

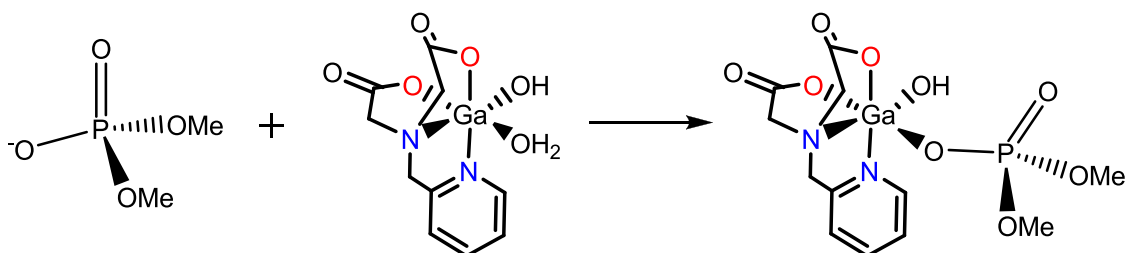


Figure 2.27: Binding of DMP with $[\text{GaL}^3(\text{H}_2\text{O})(\text{OH})]$ (charges are omitted).

2.2.7. DFT Calculations.

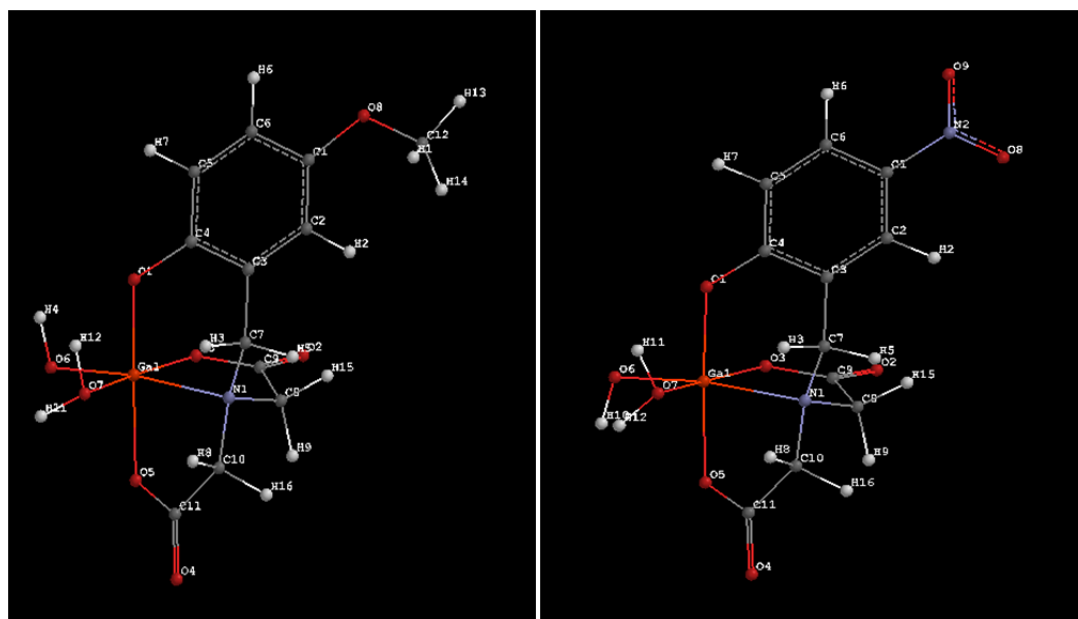
The nucleophilicity of a metal-bound hydroxide depends on the M-OH bond strength. Bond strength can be correlated with bond length. DFT calculations at the B3LYP/6-31G* level were carried out on $[\text{GaL}^1(\text{H}_2\text{O})(\text{OH})]^-$, $[\text{GaL}^2(\text{H}_2\text{O})(\text{OH})]^-$, $[\text{GaL}^3(\text{H}_2\text{O})(\text{OH})]$, $[\text{GaL}^4(\text{H}_2\text{O})(\text{OH})]$, and $[\text{GaL}^5(\text{H}_2\text{O})(\text{OH})]^-$ in water to determine Ga-OH bond lengths.³² On the basis of X-ray structures of **1**,²⁸ **3** and **4**, it was assumed that the phenolate oxygen, the tertiary amine and a carboxylate coordinate meridionally in **1** and **2**, while in **3** and **4**, the primary amine/pyridine, the tertiary amine and a carboxylate coordinate meridionally. No X-ray data was available for **5**, so calculations on both possible structural arrangements were undertaken i.e. phenolate trans to phenolate and phenolate trans to carboxylate. The order in which aqua ligands on Ga^{III} are deprotonated is unclear. Both scenarios were considered, i.e. hydroxo groups were placed trans to the tertiary amine and trans to carboxylate for complexes **1-4**. For complex **5**, the hydroxo group was placed trans to tertiary amine (for both ligand binding modes i.e. phenolate trans to phenolate and phenolate trans to carboxylate), phenolate oxygen and the carboxylate group. The results are

presented in **Table 4**. The DFT optimized structure for complexes **1-5** are depicted in **Figure 2.28**.

Table 4: Ga-OH bond distances (Å) determined from the B3LYP/6-31G*-optimized structures of the $[\text{GaL}(\text{H}_2\text{O})(\text{OH})]^{n-}$ species.

	OH trans to nitrogen H ₂ O trans to oxygen	OH trans to oxygen H ₂ O trans to nitrogen
$[\text{GaL}^1(\text{H}_2\text{O})(\text{OH})]^-$	1.865	1.875
$[\text{GaL}^2(\text{H}_2\text{O})(\text{OH})]^-$	1.872	1.885
$[\text{GaL}^3(\text{H}_2\text{O})(\text{OH})]$	1.841	1.854
$[\text{GaL}^4(\text{H}_2\text{O})(\text{OH})]$	1.859	1.873
$[\text{GaL}^5(\text{H}_2\text{O})(\text{OH})]^-$	1.907 ^a	1.896 ^a
	1.894 ^b	1.893 ^b

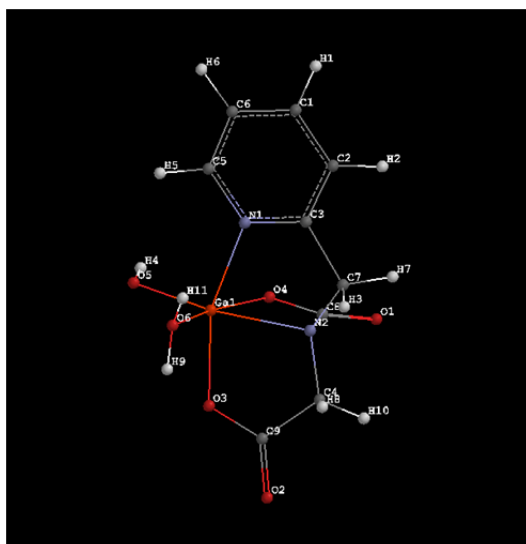
^a Phenolate trans to phenolate. ^b Phenolate trans to carboxylate.



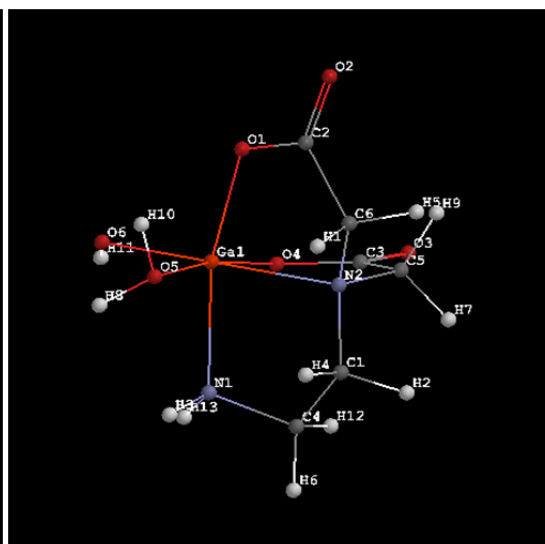
$[\text{GaL}^1(\text{H}_2\text{O})(\text{OH})]^-$

$[\text{GaL}^2(\text{H}_2\text{O})(\text{OH})]^-$

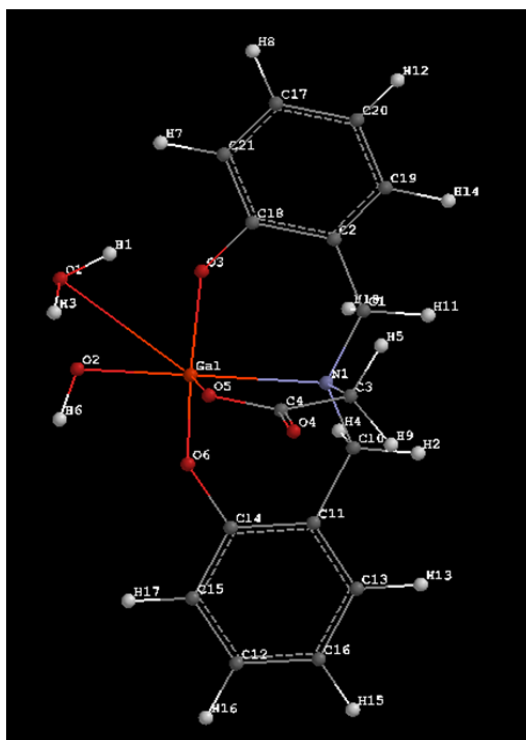
Figure 2.28 continued on the next page.



[GaL³(H₂O)(OH)]



[GaL⁴(H₂O)(OH)]



[GaL⁵(H₂O)(OH)]⁻

Figure 2.28: Optimized structures of the aqua hydroxo species of **1** – **5** with OH *trans* to tertiary amine for each complex.

It is well-established that the acidity of a metal-bound aqua ligand is influenced by the strength of the interaction between the metal and the donor atom in the *trans* position. The weaker is this interaction, the stronger will be the interaction between

the metal and the aqua ligand, lowering its pK_a . X-ray crystal structure data of **1**, **3** and **4** reveal that the Ga-N_{tert.am} bond is always longer than the Ga-O bonds, suggesting that water trans to the tertiary amine will be deprotonated first. However, for both structural possibilities considered (OH trans to tertiary amine and OH trans to oxygen), the trend is the same; Ga-OH bond lengths increasing from a minimum of 1.841 to 1.907 Å in the order [GaL³(H₂O)(OH)] < [GaL⁴(H₂O)(OH)] < [GaL¹(H₂O)(OH)]⁻ < [GaL²(H₂O)(OH)]⁻ < [GaL⁵(H₂O)(OH)]⁻.

2.3. Discussion

The bell-shaped pH-rate profiles obtained for the hydrolysis of BDNPP by each of the complexes implies that the active species in each case is the aqua-hydroxo species where the pH of optimum activity lies between the acid dissociation constants of metal-bound water ligands. A well established mechanism involving coordination of the substrate to Ga^{III} and subsequent nucleophilic attack by the cis-hydroxo group leading to phosphate diester hydrolysis is tenable. A mechanism whereby a solvent water molecule is deprotonated by a metal-bound hydroxide, and consequent nucleophilic attack by solvent OH⁻ was also considered. However, this mechanism was discounted following solvent deuterium isotope effect studies.

The optimum pH and the catalytic rate constant at the optimum pH for each complex increases in the order **3** < **4** < **1** < **2** < **5**. The difference in rate acceleration between the most and least active complexes is approximately one order of magnitude. Kinetic pK_a values for the deprotonation of the first aqua ligand of each complex increase in the order **1** < **4** \approx **3** < **2** < **5** while the values for deprotonation of the second aqua ligand increase in the order **3** < **4** < **1** < **2** < **5**. The acidity of a metal-bound water ligand can be considered a measure of the Lewis acidity of the metal centre. Although the pK_{a1} and pK_{a2} values do not offer a clear-cut picture of the order of increasing Lewis acidity of the central metal ion, the two most active complexes contain the least acidic Ga^{III} centres. These complexes, with more weakly acidic Ga^{III}, offer the least in substrate activation and on the other hand, provide greater activation of hydroxide towards nucleophilic attack.

It should also be said that the correlation between catalytic activity and the basicity of the nucleophile is not a proportionate one. As the nucleophilicity of a metal-hydroxide is generally related to its basicity, it is apparent that there are other contributing factors involved, for example substrate binding, substrate activation and steric factors.

The nucleophilicity of the attacking nucleophile was indirectly probed using DFT calculations on each of the complexes in their monomeric aqua-hydroxo forms. The nucleophilicity of a metal-bound hydroxide depends on the M-OH bond strength. Ga-OH bond lengths were found to increase/weaken in the order $[\text{GaL}^3(\text{H}_2\text{O})(\text{OH})] < [\text{GaL}^4(\text{H}_2\text{O})(\text{OH})] < [\text{GaL}^1(\text{H}_2\text{O})(\text{OH})]^- < [\text{GaL}^2(\text{H}_2\text{O})(\text{OH})]^- < [\text{GaL}^5(\text{H}_2\text{O})(\text{OH})]^-$ in accordance with the order of increasing catalytic activity. This result further confirms that nucleophile efficiency is the overriding factor.

Substrate binding to the complexes in their aqua-hydroxo forms was investigated using the hydrolytically stable phosphate diester dimethylphosphate (DMP). It was shown that substrate affinity followed the trend $[\text{GaL}^3(\text{H}_2\text{O})(\text{OH})] (60 \text{ M}^{-1}) > [\text{GaL}^1(\text{H}_2\text{O})(\text{OH})]^- (7 \text{ M}^{-1}) > [\text{GaL}^5(\text{H}_2\text{O})(\text{OH})]^- (2.5 \text{ M}^{-1})$. As expected the anionic complexes, **1** and **5**, bound the substrate less strongly. Complex **5**, although displaying the weakest substrate affinity is the most active catalyst, indicating that nucleophile efficiency prevails over weak substrate binding as it does over substrate activation in these systems.

It is apparent that the most active catalysts contain strongly electron donating phenolate groups in the coordination sphere of gallium. Furthermore, the most active catalyst contains two phenolate donor groups. Strong metal-ligand interactions are known to weaken metal-water/hydroxide interactions in organometallic complexes containing water/hydroxide coordination sites. From X-ray crystallography data for the mono- and dinuclear complexes **1**, **3** and **4**, it is clear that the metal-ligand interaction is stronger for the phenolate donor ligands than for neutral nitrogen donors. Comparing **1** which contains a $\text{N}_{tert.am}(\text{COO})_2\text{O}_{Phe}$ donor set with **3** and **4** which possess $\text{N}_{tert.am}(\text{COO})_2\text{N}_{py}$ and $\text{N}_{tert.am}(\text{COO})_2\text{N}_{prim.am}$ donor sets respectively, the Ga- O_{Phe} bond distance (1.884(2) Å²⁸) is significantly shorter than the Ga- N_{py} (2.084(2) Å) and the Ga- $\text{N}_{prim.am}$ (2.029(2) Å) bond lengths. The stronger metal-

ligand interactions in the phenolate donor complexes relative to complexes with neutral nitrogen donors result in the weakening of the metal-hydroxide bond, enhancing its nucleophilicity. Furthermore, a direct comparison of complexes **1** and **2** underscores the influence of ligand donor properties. Both complexes contain the $N_{tert.am}(COO)_2O_{Phe}$ donor set, however complex **1** contains a strongly electron withdrawing p-NO₂ and complex **2** a strongly electron donating p-OMe group on the aromatic ring. Complex **2** is the more active catalyst, further demonstrating the positive effect that strongly electron donating groups confer on the nucleophilicity of the metal hydroxide group. The model studies and DFT calculations show that replacing a pyridine donor group with phenolate results in an increase of about 0.03 Å in the Ga-OH bond distance, leading to an almost 10-fold enhancement in the rate of phosphodiester hydrolysis.

With respect to the mechanism of action of PAP phosphomonoester hydrolysis, involving coordination of the phosphomonoester to the divalent ion and nucleophilic attack by Fe^{III}-bound OH (**Figure 2.5 (A)**), it appears that the role of phenolate is not insignificant. Together with stabilising the trivalent ferric ion, it is also possible that phenolate may also play a critical role in activating the terminal hydroxide towards nucleophilic attack on phosphorus. Where the mechanism in **Figure 2.5 (B)** is operative, with the ferric ion providing potentially both substrate and nucleophile activation, it appears that the latter is the chief contribution.

2.4. References

- (1) Mitic, N.; Smith, S. J.; Neves, A.; Guddat, L. W.; Gahan, L. R.; Schenk, G. *Chem. Rev.* **2006**, *106*, 3338.
- (2) Klabunde, T., Strater, N., Frohlich, R., Witzel, H., Krebs, B. *J. Mol. Biol.* **1996**, *259*, 737.
- (3) Uppenberg, J., Lindqvist, F., Svensson, C., Ek-Rylander, B., Andersson, G. *J. Mol. Biol.* **1999**, *290*, 201.
- (4) Lindqvist, Y., Johansson, E., Kaija, H., Vihko, P., Schneider, G. *J. Mol. Biol.* **1999**, *291*, 135.
- (5) Guddat, L. W., McAlpine, A. S., Hume, D., Hamilton, S., deJersey, J., Martin, J. L. *Structure* **1999**, *7*, 757.
- (6) Strater, N.; Jasper, B.; Scholte, M.; Krebs, B.; Duff, A. P.; Langley, D. B.; Han, R.; Averill, B. A.; Freeman, H. C.; Guss, J. M. *J. Mol. Biol.* **2005**, *351*, 233.
- (7) Schenk, G.; Gahan, L. R.; Carrington, L. E.; Mitic, N.; Valizadeh, M.; Hamilton, S. E.; deJersey, J.; Guddat, L. W., McAlpine, A. S., Hume, D., Hamilton, S., deJersey, J., Martin, J. L. *Proc. Natl. Acad. Sci. U.S.A.* **2005**, *102*, 273.
- (8) Strater, N.; Lipscomb, W. N.; Klabunde, T.; Krebs, B. *Angew. Chem. Int. Ed.* **1996**, *35*, 2024.
- (9) Wilcox, D. E. *Chem. Rev.* **1996**, *96*, 2435.
- (10) Wang, X.; Ho, R. Y. N.; Whiting, A. K.; Que, L., Jr. *J. Am. Chem. Soc.* **1999**, *121*, 9235.
- (11) Kimura, E. *Curr. Opin. Chem. Biol.* **2000**, *4*, 207.
- (12) Smoukov, S. K.; Quaroni, L.; Xuedong, W.; Doan, P. E.; Hoffman, B. M.; Que, L., Jr. *J. Am. Chem. Soc.* **2002**, *124*, 2595.
- (13) Smith, S. J.; Casellato, A.; Hadler, K. S.; Mitic, N.; Riley, M. J.; Bortoluzzi, A. J.; Szpoganicz, B.; Schenk, G.; Neves, A.; Gahan, L. R. *J. Biol. Inorg. Chem.* **2007**, *12*, 1207.
- (14) Neves, A., Lanznaster, M., Bortoluzzi, A. J., Peralta, R. A., Casellato, A., Castellano, E. E., Herrald, P., Riley, M. J., Schenk, G. *J. Am. Chem. Soc.* **2007**, *129*, 7486.

- (15) Aquino, M. A. S.; Lim, J. S.; Sykes, A. G. *J. Chem. Soc., Dalton Trans.* **1994**, 429.
- (16) Twitchett, M. B.; Sykes, A. G. *Eur. J. Inorg. Chem.* **1999**, 2105.
- (17) Dietrich, M.; Munstermann, D.; Suerbaum, H.; Witzel, H. *Eur. J. Biochem.* **1991**, *199*, 105.
- (18) Schenk, G.; Boutchard, C. L.; Carrington, L. E.; Noble, C. J.; Moubaraki, B.; Murray, K. S.; DeJersey, J.; Hanson, G. R.; Hamilton, S. *J. Biol. Chem.* **2001**, *276*, 19084.
- (19) Itoh, T.; Hisada, H.; Usui, Y.; Fujii, Y. *Inorg. Chim. Acta* **1998**, *238*, 51.
- (20) Koike, T., Kimura, E. *J. Am. Chem. Soc.* **1991**, *113*, 8935.
- (21) Bonfa, L.; Gatos, M.; Mancin, F.; Tecilla, P.; Tonellato, U. *Inorg. Chem.* **2003**, *42*, 3943.
- (22) Merckx, M.; Averill, B. A. *Biochemistry* **1998**, *37*, 8490.
- (23) d'Hardemare, A. d. M.; Jarjayes, O.; Mortini, F. *Synth. Commun.* **2004**, *34*, 3975
- (24) Yang, X.-P.; Su, C.-Y.; Kang, B.-S.; Feng, X.-L.; Xiao, W.-L.; Liu, H.-Q. *J. Chem. Soc., Dalton Trans.* **2000**, 3253.
- (25) Chiu, Y.-H.; Canary, J. W. *Inorg. Chem.* **2003**, *42*, 5107.
- (26) McLendon, G.; Motekaitis, R. J.; Martell, A. E. *Inorg. Chem.* **1975**, *14*, 1993.
- (27) Ceccato, A.; Neves, A.; Brito, M.; Drechsel, S.; Mangrich, A.; Werner, R.; Haase, W.; Bortoluzzi, A. *J. Chem. Soc., Dalton Trans.* **2000**, *2000*, 1573.
- (28) Jarjayes, O.; Mortini, F.; d'Hardemare, A. d. M.; Philouze, C.; Serratrice, G. *Eur. J. Inorg. Chem.* **2005**, *2005*, 4417.
- (29) Ginzburg, G. *Talanta* **1977**, *23*, 149.
- (30) Gold, V. *Adv. Phys. Org. Chem.* **1967**, Academic Press: New York.
- (31) Cassano, A. G.; Anderson, V. E.; Harris, M. E. *J. Am. Chem. Soc.* **2002**, *124*, 10964.
- (32) Spartan '08; Wavefunction Inc.: Irvine, CA.

Appendix 2.1. Crystallographic data for 3 – 6.

Table 1. Crystallographic data for compounds 3 – 6.

	3	4	4a	6
Formula	C ₂₀ H ₃₀ Ga ₂ N ₄ O ₁	C ₁₂ H ₃₀ Ga ₂ N ₄ O ₁	C ₁₂ H ₂₆ ClGa ₂ N ₄ O	C ₂₈ H ₃₆ Ga ₂ N ₈ O ₁
<i>M_r</i>	689.92	593.84	491.54	864.09
Crystal colour and habit	colourless block	colourless block	colourless plate	colourless cube
Crystal size (mm)	0.20 x 0.20 x 0.10	0.30 x 0.30 x 0.20	0.20 x 0.15 x 0.05	0.30 x 0.20 x 0.15
Crystal system	monoclinic	monoclinic	orthorhombic	monoclinic
Space group	P2 ₁ /c	P2 ₁ /c	Pccn	P2 ₁ /c
unit cell dimensions				
<i>a</i> [Å]	8.8492(3)	7.8500(7)	12.3409(7)	12.1675(4)
<i>b</i> [Å]	10.4470(4)	10.085(1)	16.974(1)	10.1530(3)
<i>c</i> [Å]	14.0948(5)	13.983(2)	9.6776(6)	14.3743(3)
β [°]	90.216(2)	97.36(1)		94.478(2)
<i>V</i> [Å ³]	1303.02(8)	1097.9(2)	2027.3(2)	1770.33(9)
<i>Z</i>	2	2	4	2
<i>D</i> _{calc} (g cm ⁻³)	1.758	1.796	1.61	1.621
μ (Mo K α) ($\mu\mu^{-1}$)	2.146	2.53	1.546	1.603
<i>F</i> (000)	704	608	1016	884
2 θ range (°)	5.8 - 52.7	5.9 - 52.7	5.9 - 52.7	5.2 - 52.7
No. measd. reflections	8736	7619	14392	9049
No. unique reflections (<i>R</i> _{int})	2653 (2.9 %)	2235 (2.5 %)	2072 (9.5%)	3536 (2.2%)
No. of observed reflections	2087 (<i>I</i> > 2 σ (<i>I</i>))	1896 (<i>I</i> > 2 σ (<i>I</i>))	1470 (<i>I</i> > 2 σ (<i>I</i>))	2751 (<i>I</i> > 2 σ (<i>I</i>))
No. of parameters	181	145	129	238
Final <i>R</i> ₁ , <i>wR</i> ₂	<i>R</i> ₁ = 3.0%,	<i>R</i> ₁ = 2.6%,	<i>R</i> ₁ = 5.6%,	<i>R</i> ₁ = 3.9%,
(observed reflections) ^a	<i>wR</i> ₂ = 8.4%	<i>wR</i> ₂ = 7.2%	<i>wR</i> ₂ = 15.7%	<i>wR</i> ₂ = 11.5%
Final <i>R</i> ₁ , <i>wR</i> ₂	<i>R</i> ₁ = 4.1%,	<i>R</i> ₁ = 3.1%,	<i>R</i> ₁ = 8.1%,	<i>R</i> ₁ = 5.4%,
(all reflections) ^a	<i>wR</i> ₂ = 8.6%	<i>wR</i> ₂ = 7.3%	<i>wR</i> ₂ = 16.9%	<i>wR</i> ₂ = 12.0%
Goodness-of-fit (observed reflections)	1.042	1.062	1.074	1.013

^a $R_1 = \sum ||F_o| - |F_c|| / \sum |F_o|$; $wR_2 = [\sum w(F_o^2 - F_c^2)^2 / \sum w(F_o^2)^2]^{1/2}$; $w^{-1} = \sigma^2(F_o^2) + (aP)^2$; $P = (F_o^2 + 2F_c^2)/3$.

Chapter 3. Hydrolysis of an RNA Mimic by Mg^{II} and Zn^{II} Complexes in Non-Aqueous Media.

3.1. Introduction.

As described in section 1.2, the susceptibility of RNA towards cleavage is greatly increased relative to DNA. This is due to the presence of the 2' hydroxyl group. It is well positioned to act as an internal nucleophile, leading to transesterification of the phosphate ester.

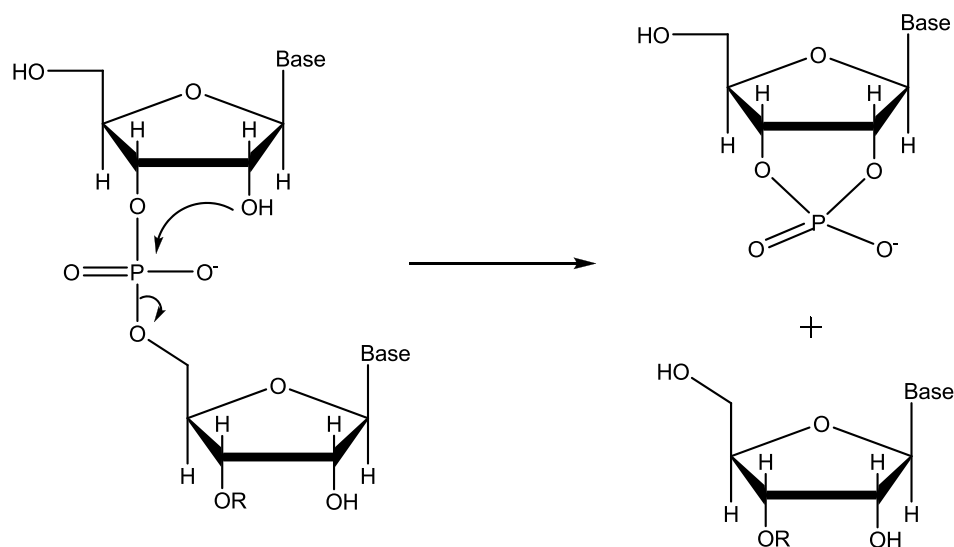


Figure 3.1: Intramolecular transesterification of RNA by 2'-OH group.

The pseudo-first-order rate constant for the cleavage of UpU, is estimated to be $2 \times 10^{-10} \text{ s}^{-1}$ at pH 7 and 25°C . This translates to a half-life of about 110 years.¹ It is clear that RNA is very stable with respect to hydrolysis. Many enzymes involved in the biochemistry of nucleic acids require the presence of a divalent metal ion, most commonly magnesium. This fact might be explained by the high natural abundance and favourable chemical properties of magnesium. Magnesium is redox inactive, has a small ionic radius resulting in a high charge density and has slow solvent exchange rates.²

Enzymes that employ magnesium as a metal cofactor in RNA transformations include ribonuclease H, ribonuclease III and ribonuclease P. Divalent zinc is also known to act as a metal cofactor in RNA cleavage, for example in P1 nuclease.³

3.1.1. Ribonucleases.

3.1.1.a. Ribonuclease A.

Ribonuclease A (RNase A) is one of the most widely studied nucleases.⁴ It is a pancreatic enzyme that cleaves single stranded RNA. RNase A operates through a two-step mechanism (**Figure 3.2**).⁵ Two catalytic histidines, His12 and His119 are central to the reaction mechanism. In the first step, nucleophilic attack on phosphorus by the 2'-OH group is aided by the deprotonation of the alcohol by His12 acting as a general base. Concomitantly, His119 acting as a general acid protonates the 5' oxygen leaving group. In the second step, deprotonation of a solvent water by the basic His119 generates OH⁻ nucleophile which targets the phosphorus of the 2'-3' cyclic phosphate intermediate. His12 acts as a general acid and protonates the 2' oxygen leaving group.

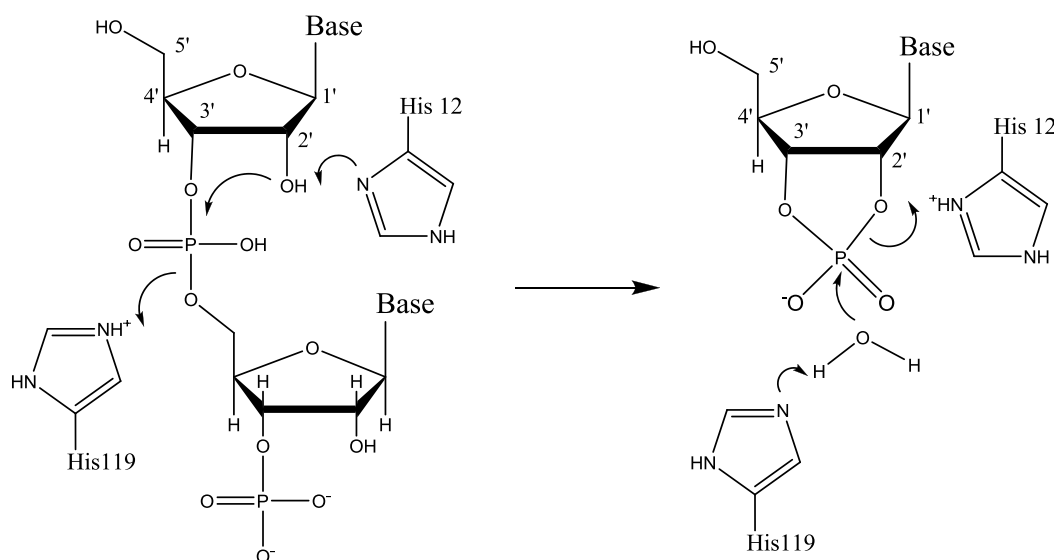


Figure 3.2: Mechanism of hydrolysis of RNA catalysed by ribonuclease A.

3.1.1.b. Ribonuclease H.

Ribonuclease H is an endonuclease that relies upon divalent magnesium as a metal cofactor. RNase H cleaves the RNA strand of RNA-DNA hybrids.⁶ RNase H is present in a broad range of organisms from *Escherichia coli* to humans. The mechanism of catalysis by RNase H is unclear, a number of different mechanisms being suggested.⁶⁻⁹ One mechanism proposed for the catalytic mechanism of *E. coli* RNase H, is shown in **Figure 3.3**.⁹

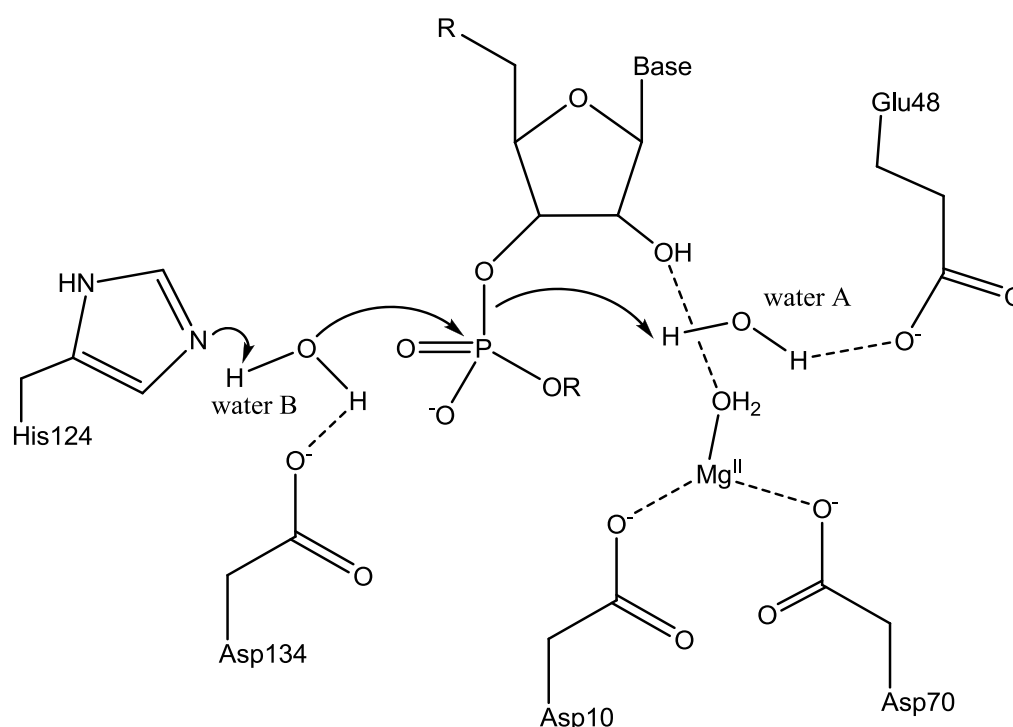


Figure 3.3: Mechanism of catalysis by Ribonuclease H.

This is a general acid-base mechanism for the hydrolysis of the P-O_{3'} bond of an RNA substrate. Water A acts as a general acid, protonating the liberated 3' oxygen of the leaving group. Water A is held in position by a hydrogen bond with Glu48. Water B, hydrogen bonded to Asp134, acts as a general base. Deprotonation of water B by His124 generates a hydroxide nucleophile. In this model, outer sphere interactions between Mg^{II} and the 2'-hydroxyl group serve to stabilise the transient intermediate. An outersphere interaction is supported by the work of Jou and Cowan¹⁰ who were able to

show that $[\text{Co}(\text{NH}_3)_6]^{III}$ and $[\text{Co}(\text{en})_3]^{III}$ also act as metal cofactors. It is unlikely that these substitutionally inert complexes are degraded *in situ* and thus an outer sphere interaction in the catalytic mechanism is inferred.

3.1.1.c. Ribonuclease P.

Ribonuclease P is a widely occurring endonuclease, present in Bacteria, Eukarya and Archaea.¹¹ The function of RNase P is to cleave a specific phosphate diester bond in precursor tRNAs. This action generates the mature 5' termini of all cellular and organellar transfer RNA molecules.¹² Ribonuclease P is distinct from other ribonucleases in that it is a ribonucleoprotein composed of a single large RNA and at least one protein section. The RNA section alone of the ribonucleoprotein is sufficient to hydrolyse the phosphate diester bond of the precursor tRNA and release products.^{13,14} Thus, RNase P is classed a ribozyme. Steitz and Steitz¹⁵ proposed a mechanism of action for RNase P involving two-metal-ion activation. However, currently, the mechanism of catalysis is thought to be a variation on this, involving three divalent magnesium ions (**Figure 3.4**).¹¹

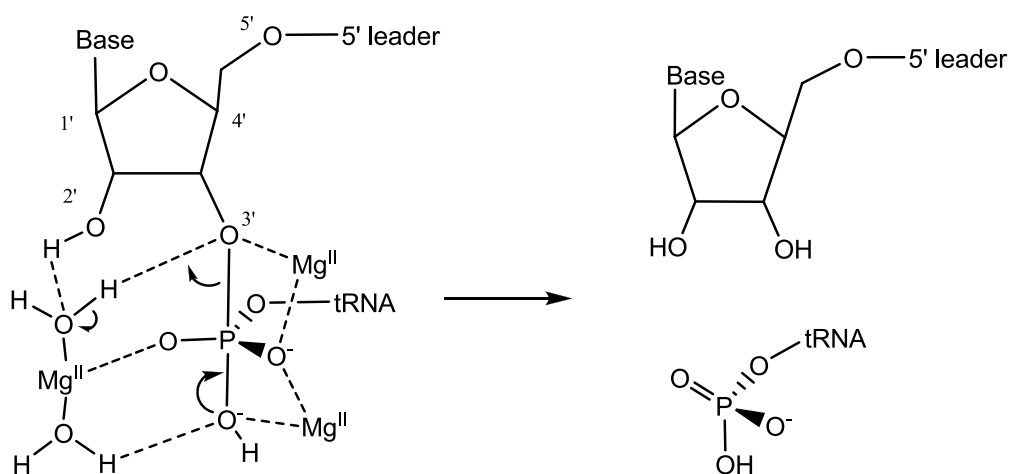


Figure 3.4: Mechanism of catalysis by RNase P.

In the catalytic scheme shown above, phosphate oxygen bridges two magnesium ions. The attacking nucleophile is thus activated and positioned suitably. Coordination of the 3' oxygen leaving group to Mg^{II} stabilizes the developing negative charge and lowers the energy of the transition state. Coordinated water of the third Mg^{II} ion plays an

important role in this mechanism, by lowering the pK_a of coordinating water ligand, proton transfer to the 3' oxygen of the leaving group is facilitated.

3.1.2. Model Systems.

The activity of divalent magnesium with respect to phosphate ester hydrolysis in model systems is greatly reduced relative to enzymatic systems.¹⁶⁻¹⁸ The medium effects of the metal ion plays a very important role in determining its catalytic efficiency. In organic media, hydrolysis rates are greatly improved. Medium effects in solvents of low polarity can enhance transformations in a number of possible ways including:¹⁹

1. In organic media, the association of hydroxide ions to Mg is greatly increased for solutions of comparable basicity, resulting in a higher concentration of active metal-hydroxide species relative to aqueous media.
2. In apolar media, the association of Mg^{II} to negatively charged substrate species will also be increased.
3. Solvation of the ionic components by apolar solvent molecules is preferable for catalysis over polar solvent molecules. The reactivity of a metal-bound hydroxo group towards nucleophilic attack on phosphate is greatly increased when surrounded by non-polar solvent molecules.

Organic solvents such as alcohols or DMSO are considered to better represent the environment inside the active site of an enzyme.¹⁹ The dielectric constant at the active site can be as low as 4.²⁰ In general, the active sites of enzymes are relatively non-polar, though often containing several charged and polar groups that serve to increase the local dielectric constant, but not to the value of water.²¹ A number of studies involving the hydrolysis or alcoholysis of a range of DNA/RNA model substrates by a range of different metals in apolar media have been published.²²⁻³⁴ Of particular interest is the study concerning the phosphodiesterase activity of the alkaline earth metals in 90% DMSO.^{19,22} It was found that first-order rate constants for phosphodiester hydrolysis in the presence of 1 - 2 mM Mg^{II} or Ca^{II} were 10^8 - 10^{11} times higher than the rates for

background hydrolysis at the same pH in water. Up to 50 mM Mg^{II} or Ca^{II} in water produced < 100-fold accelerations.

3.1.3. Aims.

In model systems, the activity of zinc towards phosphate diester hydrolysis is very high, with some dinuclear complexes being among the most active reported (**Figure 3.5**).^{35,36}

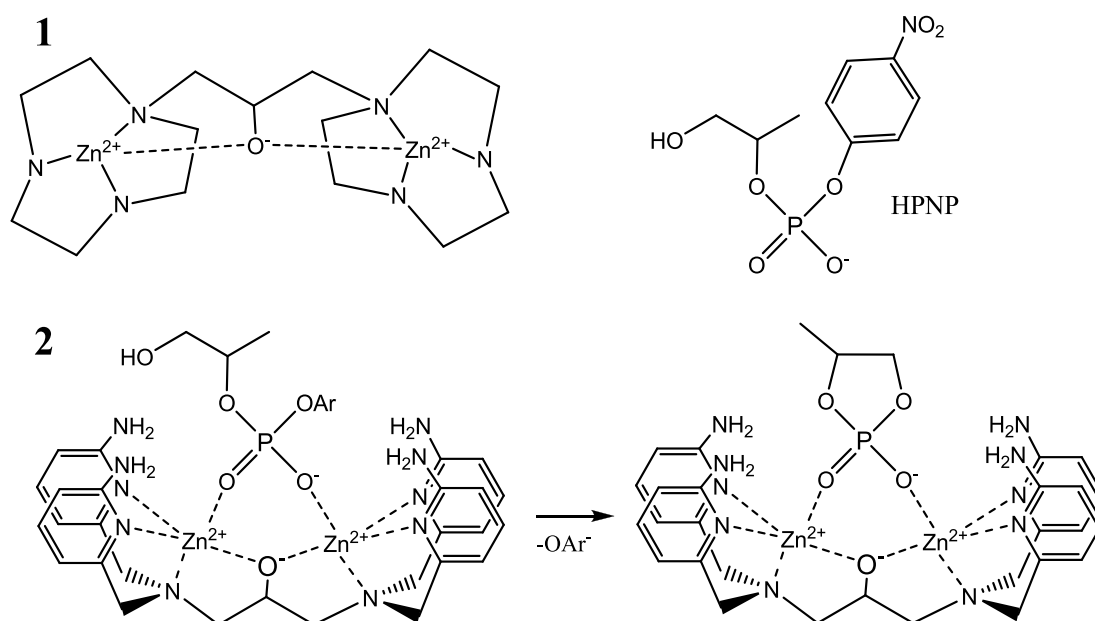


Figure 3.5: Active dinuclear complexes and hydrolysis of the activated phosphate diester 2-hydroxypropyl-4-nitrophenyl phosphate (HPNP).

These complexes are very active with respect to the hydrolysis of the RNA analog HPNP, providing rate enhancements of up to 10^6 fold at neutral pH, in aqueous medium. The mononuclear counterpart of the complex **1** was synthesised,³⁵ comparison of kinetic data with the dinuclear complex revealed positive cooperation of the metal ions.

Although, frequently the metal cofactor in operation in ribonuclease catalytic transformations, magnesium model systems do not provide the same level of rate enhancement delivered by zinc in model systems.¹⁶⁻¹⁸

Arising from this observation, a study was designed to test and compare related dinuclear magnesium and zinc complexes that mimic the active site of nucleases on their phosphoesterase activity in an organic solvent that more accurately mirrors the microenvironment within the active site of an enzyme. The main question to be addressed by this study is the influence of the factors listed in section 3.1.2. on this system.

Dinuclear complexes Mg^{II} and Zn^{II} of the ligand 5-methyl-2-hydroxy-1,3-xylene- α,α -diamine- N,N,N',N' -tetraacetic acid (HXTA) (**Figure 3.6**) were synthesised and their activities towards the transesterification of the RNA analog HPNP (**Figure 3.5**) in anhydrous DMSO investigated.

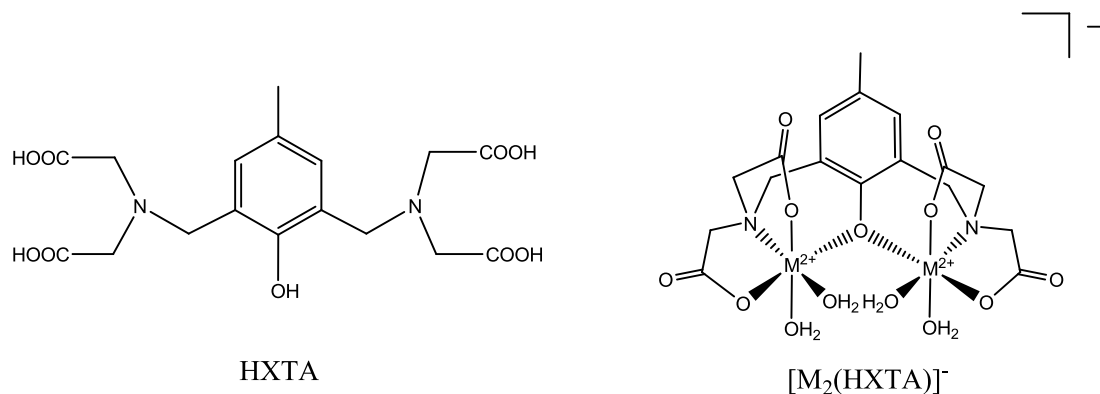


Figure 3.6: HXTA ligand and dinuclear complex of the ligand.

The ligand HXTA is known to form dinuclear complexes by bridging metal ions through the phenolate oxygen. This mode of binding in which metal ions are in close proximity is very useful for catalysis and has been shown to be effective in model systems.³⁵⁻³⁷ The design of magnesium complexes that catalyse the cleavage of phosphate ester bonds is challenging. Negatively charged oxygen donors are needed for efficient binding. However these reduce Lewis acidity and lower binding of anionic phosphate diester substrates. It was hoped that despite the overall negative charge (**Figure 3.6**), M^{II} complexes of HXTA would be active.

HPNP was chosen as a model substrate on the basis of its widespread use and availability. The reaction involved is an intramolecular transesterification (**Figure 3.5**) leading to the formation of p-nitrophenol(ate) and a cyclic phosphate and proceeds in the absence of water. The reaction can be conveniently followed by measuring the increase in absorbance at 400 nm due to the reaction product p-nitrophenolate or at 318 nm due to p-nitrophenol.

3.2. Results.

3.2.1. Synthesis and Characterisation of the Mg^{II} and Zn^{II} Complexes of HXTA.

The ligand HXTA was prepared in a Mannich reaction according to the procedure of Que et al. (**Figure 3.7**).³⁷

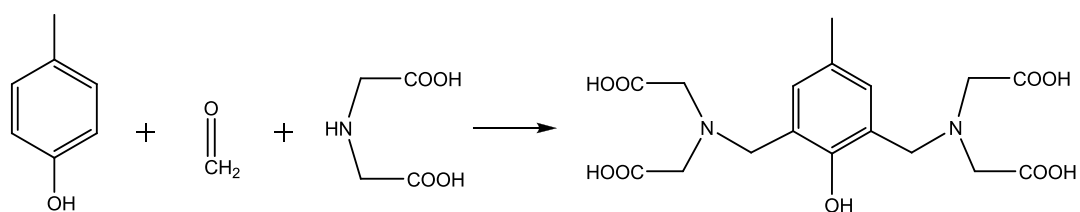


Figure 3.7: Synthesis of HXTA.

Dinuclear magnesium and zinc complexes of HXTA were isolated from aqueous solution in crystalline form. Crystals suitable for X-ray diffraction of the dinuclear Mg^{II} complex were prepared by mixing 2 equiv. $MgCl_2$ with Na_4 -HXTA and standing in an open beaker at neutral pH for a few days. Crystals of the zinc complex of HXTA were obtained by mixing two equivalents of $ZnCl_2$ with one equivalent of sodium acetate and HXTA and allowing to stand in an open beaker at pH 6 for a few days (**Figure 3.8**).

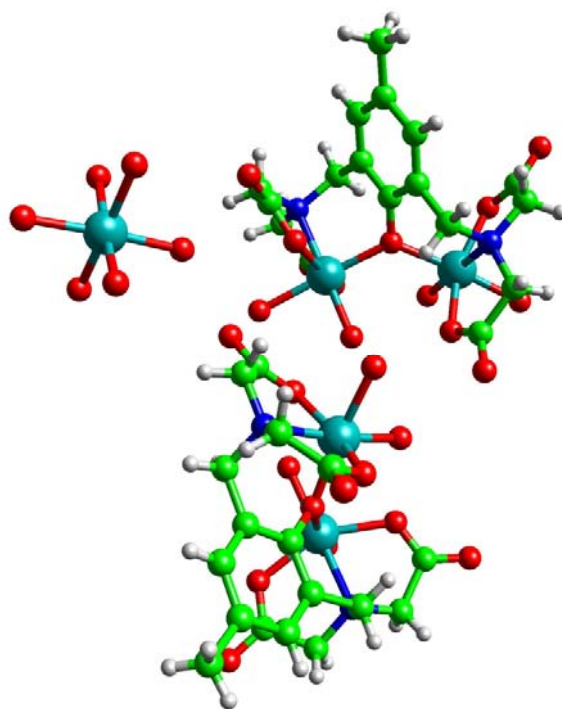


Figure 3.8a: Molecular structure of $[\text{Mg}(\text{H}_2\text{O})_6][\text{Mg}_2(\text{HXTA})_2] \cdot 4\text{H}_2\text{O}$.

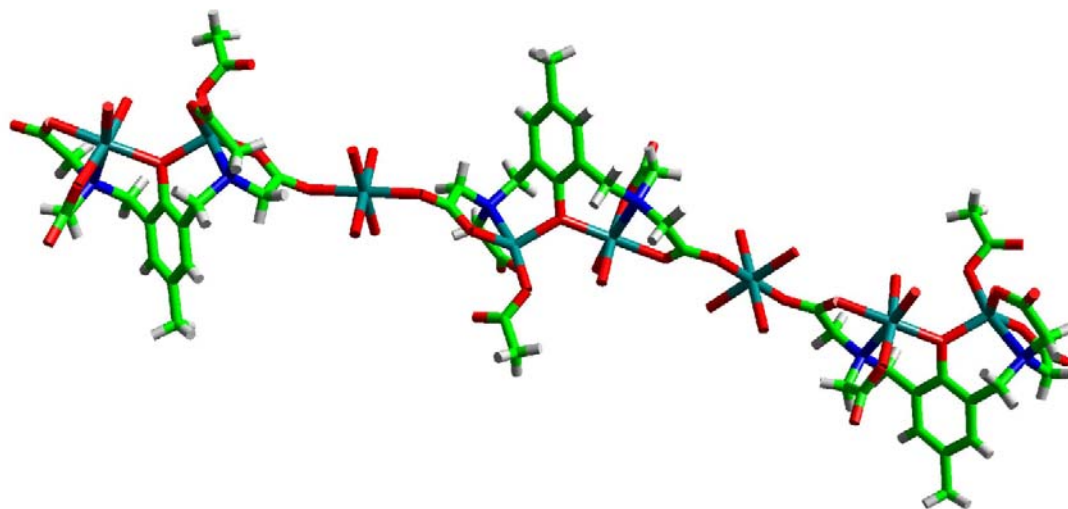


Figure 3.8b: Molecular structure of polymeric $[\text{Zn}_2(\text{HXTA})(\text{ac})(\text{H}_2\text{O})_2\text{Zn}(\text{H}_2\text{O})_4]_n$.

For the dinuclear Mg^{II} complex (**Figure 3.8a**) (complex **1**), each magnesium is located in a slightly distorted octahedral coordination environment, bridged by phenolate and each ion containing a $\text{N}_{\text{tert.am}}(\text{COO})_2\text{O}_{\text{Phe}}$ donor set. Two remaining coordination sites on each Mg^{II} are occupied by water ligands. The counteranion for **1** is $[\text{Mg}(\text{H}_2\text{O})_6]^{2+}$. Each dinuclear unit carries a charge of -1, requiring $\frac{1}{2} \text{Mg}^{\text{II}}$ as counteranion, giving a ligand-to-metal ratio of 2 : 5.

Complex **2** (**Figure 3.8b**) was crystallised at pH 6 with one equivalent of acetate. As with complex **1**, two zinc ions are chelated by HXTA. A notable feature of the molecular structure is the asymmetric coordination mode; one penta-coordinate and one hexa-coordinate Zn. 6-coordinate Zn sits in a slightly distorted octahedral coordination environment and has a $\text{N}_{\text{tert.am}}(\text{COO})_2\text{O}_{\text{Phe}}$ donor set. The two remaining coordination sites are occupied by aqua ligands. 5-coordinate Zn has the ligand donor set $\text{N}_{\text{tert.am}}(\text{COO})_2\text{O}_{\text{Ph}}$, the remaining coordination site is occupied by acetate. Assigning its geometry is not clear-cut. The model of Addison *et al.*³⁸, is used whereby the geometric parameter τ distinguishes between trigonal bipyramidal and square pyramidal geometries. Perfect bipyramidal geometry will give a τ value of unity with perfect square pyramidal geometry having a value of zero. In this case, $\tau = 0.49$ and so the geometry around 5-coordinate Zn is best described as being intermediate between trigonal bipyramidal and square pyramidal. A third octahedral Zn is coordinated monodentately by bridging carboxylate groups of two $\text{Zn}_2(\text{HXTA})$ moieties and links the complex units to form a 1D coordination polymer.

Crystallographic data are presented Appendix 3.1.

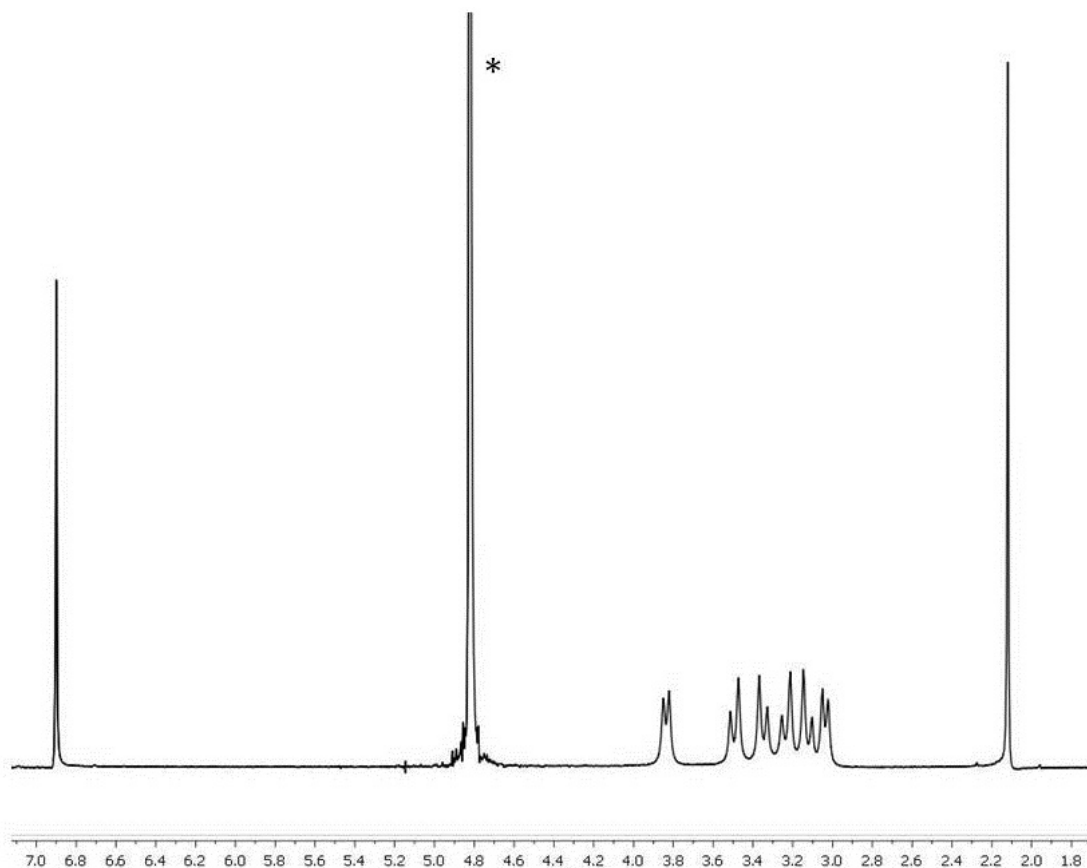


Figure 3.9: ^1H NMR of crystalline $[\text{Mg}(\text{H}_2\text{O})_6][\text{Mg}_2(\text{HXTA})]_2 \cdot 4\text{H}_2\text{O}$ dissolved in D_2O , pD 10 (* = HDO).

The ^1H NMR for complex **1** is shown in **Figure 3.9**. A binding study was undertaken, using ^1H NMR to follow binding with varying relative amounts of ligand and metal under conditions of constant pD 10, and 15 mM HXTA (**Figure 3.10**). It can be seen that formation of the dinuclear complex is favourable; it is completely formed at a metal-to-ligand ratio of 2:1. Even at a 1:1 metal-to-ligand ratio, some formation of the dinuclear complex is observed.

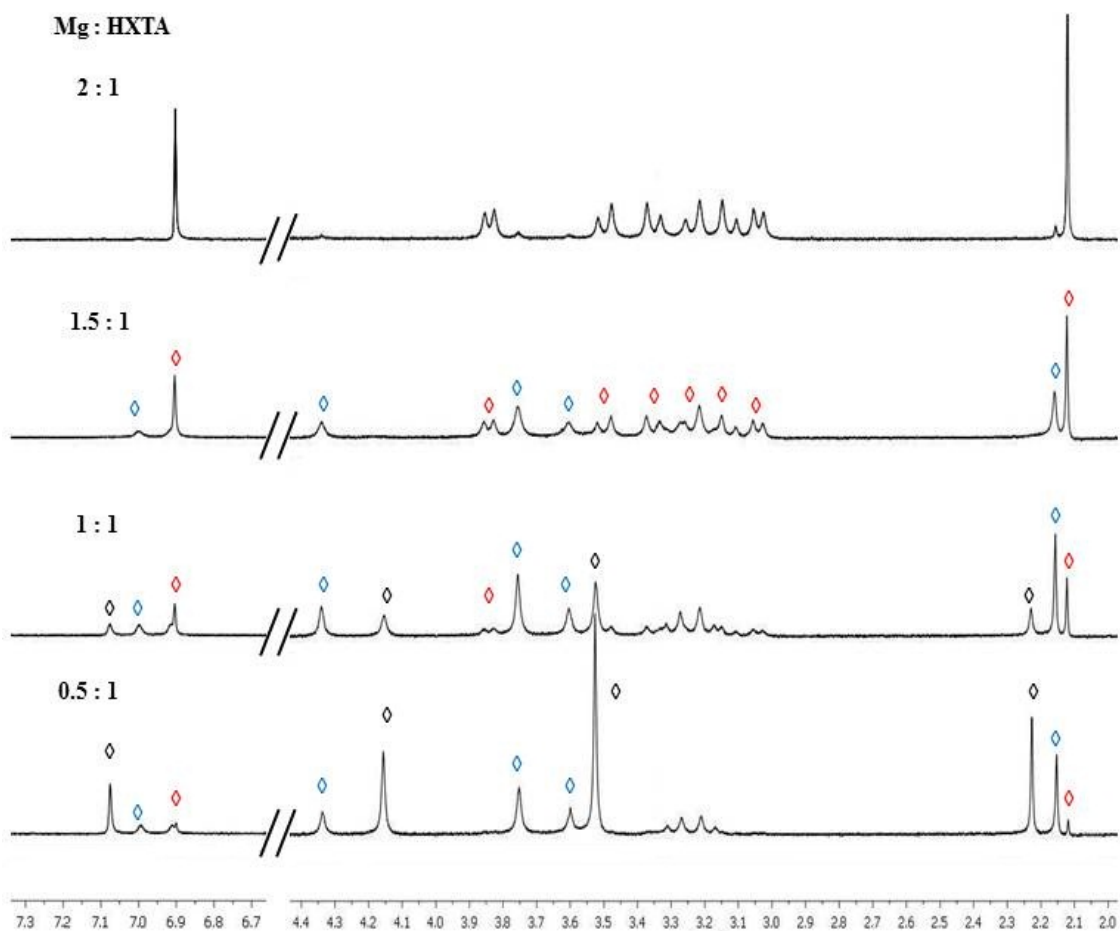


Figure 3.10: ^1H NMR binding study with varying ratios of Mg : HXTA. Free ligand signals are labeled with \diamond , mononuclear complex signals with \diamond and dinuclear complex signals are represented by \diamond (D_2O , $\text{pD} = 10$).

3.2.2. Phosphodiesterase Activity.

Complexes **1** and **2** were generated in situ in anhydrous DMSO by mixing 2 equivalents of metal salt with the sodium salt of HXTA to give 1 mM complex. HPNP was then added to give a concentration of 50 μM , and a 20-fold excess of complex. However, no increase in absorbance due to phenol or phenolate reaction products was observed at 40°C over 10 hours. Small aliquots of base were added in order to deprotonate the attacking nucleophile (**Figure 3.11**). Yet, still no catalysis was observed.

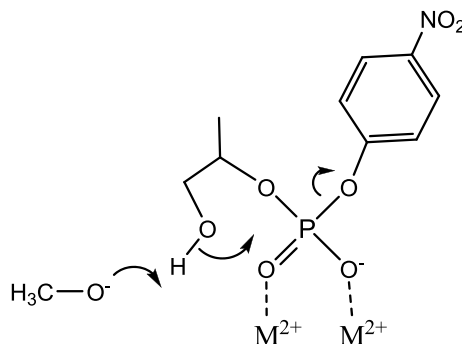


Figure 3.11: Addition of base to catalyse transesterification.

Phosphate diester binding to **1** and **2** in DMSO was investigated using ^1H and ^{31}P NMR using the unreactive phosphate diester diphenyl phosphate (DPP). However, no set of signals for bound phosphate diester were observed.

3.3. Discussion.

Zn^{II} and Mg^{II} complexes of the bis-nucleating ligand HXTA have been isolated and fully characterised. The activities of these complexes towards the transesterification of an activated RNA model substrate, HPNP, in a medium that more accurately mirrors the environment in the active site of an enzyme has been investigated. However, these complexes proved inactive towards mediating this reaction.

Substrate binding to these complexes in DMSO was investigated using the unreactive phosphate diester DPP. ^1H and ^{31}P NMR were used to study binding, however no new or shift of signals representing bound phosphate were observed. It is clear that association of the anionic substrate with **1** and **2** is unfavourable. Rationalising this, the electrophilicity of the divalent zinc and magnesium ions is reduced upon coordination to HXTA. Each metal ion has in its coordination sphere the ligand donor set $\text{N}_{\text{tert.am}}(\text{COO})_2\text{O}_{\text{Phe}}$ and $\text{N}_{\text{tert.am}}(\text{COO})_2\text{O}_{\text{PheO}_{\text{acetate}}}$ in the case of the second zinc ion. Negatively charged carboxylate and phenolate donor groups are strong electron donors.

In order to design a new catalyst in this mould, a more neutral ligand donor set, for example substituting a carboxylate donor for an amine donor group, would firstly

increase the electrophilicity of divalent cations. This would improve coordination of the anionic phosphate diester substrate and secondly, upon binding, would enable higher Lewis acid activation of the substrate. However, a more neutral ligand donor set may compromise the stability of the complex.

3.4. References.

- (1) Williams, N. H.; Takasaki, B.; Wall, M.; Chin, J. *Acc. Chem. Res.* **1999**, *32*, 485.
- (2) Cowan, J. A. *Chem. Rev.* **1998**, *98*, 1067.
- (3) Wilcox, D. E. *Chem. Rev.* **1996**, *96*, 2435.
- (4) Raines, R. T. *Chem. Rev.* **1998**, *98*, 1045.
- (5) Richards, F. M.; Wyckoff, H. W. *The Enzymes* **1971**, *4*, 647.
- (6) Oda, Y.; Yoshida, M.; Kanaya, S. *J. Biol. Chem.* **1993**, *268*, 88.
- (7) Yang, W.; Hendrickson, W. A.; Crouch, R. J.; Satow, Y. *Science* **1990**, *249*, 1398.
- (8) Nakamura, H.; Oda, Y.; Iwai, S.; Inoue, H.; Ohtsuka, E.; Kanaya, S.; Kimura, S.; Katsuda, C.; Katayanagi, K.; Morikawa, K. *Proc. Natl. Acad. Sci. U.S.A.* **1991**, *88*, 11535.
- (9) Kanaya, S.; Oobatake, M.; Liu, Y. *J. Biol. Chem.* **1996**, *271*, 32729.
- (10) Jou, R.; Cowan, J. A. *J. Am. Chem. Soc.* **1991**, *113*, 6685.
- (11) Kazantsev, A. V.; Pace, N. R. *Nat. Rev. Microbiol.* **2006**, *4*, 729.
- (12) Li, X.; Gegenheimer, P. *Biochemistry* **1997**, *36*, 2425.
- (13) Pannucci, J. A.; Haas, E. S.; Hall, T. A.; Harris, J. K.; Brown, J. W. *Proc. Natl. Acad. Sci. U.S.A.* **1999**, *96*, 7803.
- (14) Guerrier-Takada, C. A.; Gardiner, K.; Marsh, T.; Pace, N. R.; Altman, S. *Cell* **1983**, *35*, 849.
- (15) Steitz, T. A.; Steitz, J. A. *Proc. Natl. Acad. Sci. U.S.A.* **1993**, *90*, 6498.
- (16) Morrow, J. R.; Buttrey, L. A.; Berback, K. A. *Inorg. Chem.* **1992**, *31*, 16.
- (17) Milburn, R. M.; Gautam-Basak, M.; Tribolet, R.; Sigel, H. *J. Am. Chem. Soc.* **1985**, *107*, 3315.
- (18) Herschlag, D.; Jencks, W. P. *J. Am. Chem. Soc.* **1987**, *109*, 4665.
- (19) Taran, O.; Medrano, F.; Yatsimirsky, A. K. *Dalton Trans.* **2008**, 6609.
- (20) Mertz, E. L.; Krishtalik, L. I. *Proc. Natl. Acad. Sci. U.S.A.* **2000**, *97*, 2081.
- (21) Richard, J. P.; Amyes, T. L. *Bioorg. Chem.* **2004**, *32*, 354.
- (22) Taran, O.; Yatsimirsky, A. K. *Chem. Commun.* **2004**, 1228.
- (23) Nagelkerke, R.; Thatcher, G. R. J.; Buncel, E. *Org. Biomol. Chem.* **2003**, *1*, 163.

- (24) Buncel, E.; Nagelkerke, R.; Thatcher, G. R. J. *Can. J. Chem.* **2003**, *81*, 53.
- (25) Neverov, A. A.; Lu, Z.-L.; Maxwell, C. I.; Mohamed, M. F.; White, C. J.; Tsang, J. S. W.; Brown, R. S. *J. Am. Chem. Soc.* **2006**, *128*, 16398.
- (26) Bunn, S. E.; Liu, C. T.; Lu, Z.-L.; Neverov, A. A.; Brown, R. S. *J. Am. Chem. Soc.* **2007**, *129*, 16238.
- (27) Liu, C. T.; Neverov, A. A.; Brown, R. S. *Inorg. Chem.* **2007**, *46*, 1778.
- (28) Neverov, A. A.; Brown, R. S. *Inorg. Chem.* **2001**, *40*, 3588.
- (29) Tsang, J. S. W.; Neverov, A. A.; Brown, R. S. *J. Am. Chem. Soc.* **2003**, *125*, 1559.
- (30) Tsang, J. S.; Neverov, A. A.; Brown, R. S. *J. Am. Chem. Soc.* **2003**, *125*, 7602.
- (31) Selmeczi, K.; Michel, C.; Milet, A.; Gautier-Luneau, I.; Philouze, C.; Pierre, J.-L.; Schnieders, D.; Rompel, A.; Belle, C. *Chem.-- Eur. J.* **2007**, *13*, 9093.
- (32) Mohamed, M. F.; Neverov, A. A.; Brown, R. S. *Inorg. Chem.* **2009**, *48*, 11425.
- (33) Mohamed, M. F.; Brown, R. S. *J. Org. Chem.* **75**, 8471.
- (34) Gomez-Tagle, P.; Vargas, I.; Taran, O.; Yatsimirsky, A. K. *The J. Org. Chem.* **2006**, *71*, 9713.
- (35) Iranzo, O.; Kovalevsky, A. Y.; Morrow, J. R.; Richard, J. P. *J. Am. Chem. Soc.* **2003**, *125*, 1988.
- (36) Feng, G.; Natale, D.; Prabakaran, R.; Mareque-Rivas, J. C.; Williams, N. H. *Angew. Chem. Int. Ed.* **2006**, *45*, 7056.
- (37) Branum, M. E.; Tipton, A. K.; Zhu, S.; Que, L. *J. Am. Chem. Soc.* **2001**, *123*, 1898.
- (38) Addison, A. W.; Rao, T. N.; Reedijk, J.; van Rijn, J.; Verschoor, G. C. *J. Chem. Soc., Dalton Trans.* **1984**, 1349.

Appendix 3.1. X-Ray diffraction tables for compounds **1** and **2**.

Table 1. Crystallographic data for **1** and **2**.

	1	2
Formula	C ₃₄ H ₆₀ Mg ₅ N ₄ O ₃₉	C ₁₉ H ₃₆ N ₂ O ₂₅ Zn ₃
<i>M_r</i>	1270.2	888.71
Crystal colour and habit	colourless block	colourless block
Crystal size (mm)	0.30 x 0.35 x 0.35	0.25 x 0.25 x 0.30
Crystal system	Triclinic	Triclinic
Space group	P-1	P-1
unit cell dimensions		
<i>a</i> [Å]	11.2917(4)	10.0293(11)
<i>b</i> [Å]	11.4723(4)	13.3481(10)
<i>c</i> [Å]	23.4046(6)	14.0680(11)
α [°]	95.485(3)	93.554(6)
β [°]	95.467(2)	99.509(8)
γ [°]	106.102(3)	109.992(9)
<i>V</i> [Å ³]	2875.99(17)	1731.2(3)
<i>Z</i>	2	2
<i>D</i> _{calc} (g cm ⁻³)	1.437	1.674
μ (Mo K α) (mm ⁻¹)	0.18	2.156
<i>F</i> (000)	1276	876
2 θ range (°)	6.4 - 50.8	6.4 - 51.4
No. measd. reflections	19261	11269
No. unique reflections (<i>R</i> _{int})	9996 (2.9 %)	6564 (4.8 %)
No. of observed reflections	6957 (<i>I</i> > 2 σ (<i>I</i>))	5065 (<i>I</i> > 2 σ (<i>I</i>))
No. of parameters	748	445
Final <i>R</i> ₁ , <i>wR</i> ₂ (observed reflections)	<i>R</i> ₁ = 5.79%, <i>wR</i> ₂ = 17.1%	<i>R</i> ₁ = 7.1%, <i>wR</i> ₂ = 20.8%
Goodness-of-fit (observed reflections)	1.043	1.075

Table 2. Selected bond lengths [\AA] and angles [$^\circ$] for **1** and **2**.

1			
Mg(1) - O(1)	2.043(2)	Mg(2) - O(1)	2.017(2)
Mg(1) - O(2)	2.053(2)	Mg(2) - O(6)	2.071(3)
Mg(1) - O(4)	2.082(3)	Mg(2) - O(8)	2.109(3)
Mg(1) - O(10)	2.134(3)	Mg(2) - O(12)	2.055(3)
Mg(1) - O(11)	2.021(3)	Mg(2) - O(13)	2.134(2)
Mg(1) - N(1)	2.201(3)	Mg(2) - N(2)	2.247(3)
Mg(3) - O(102)	2.036(3)	Mg(4) - O(101)	2.066(3)
Mg(3) - O(104)	2.111(3)	Mg(4) - O(106)	2.071(2)
Mg(3) - O(110)	2.025(3)	Mg(4) - O(112)	2.028(3)
Mg(3) - O(111)	2.124(4)	Mg(4) - O(113)	2.118(3)
Mg(3) - N(101)	2.237(3)	Mg(4) - N(102)	2.215(3)
Mg(3) - O(101)	2.044(3)	Mg(4) - O(108)	2.054(3)
2			
Zn(1) - O(1)	1.979(3)	Zn(1) - O(2)	2.093(4)
Zn(1) - O(4)	2.030(4)	Zn(1) - O(10)	1.984(4)
Zn(1) - N(1)	2.149(5)	Zn(2) - O(1)	2.044(3)
Zn(2) - O(6)	2.081(4)	Zn(2) - O(8)	2.117(4)
Zn(2) - O(17)	2.073(4)	Zn(2) - O(16)	2.150(4)
Zn(2) - N(3)	2.122(5)	Zn(3) - O(5)	2.083(4)
Zn(3) - O(12)	2.061(4)	Zn(3) - O(13)	2.099(5)
Zn(3) - O(5_b)	2.083(4)	Zn(3) - O(12_b)	2.061(4)
Zn(3) - O(13_b)	2.099(5)	Zn(4) - O(9)	2.093(4)
Zn(4) - O(14)	2.179(4)	Zn(4) - O(15)	2.087(4)
Zn(4) - O(9_a)	2.093(4)	Zn(4) - O(14_a)	2.179(4)
Zn(4) - O(15_a)	2.087(4)		

Chapter 4. Hydrolysis of Phosphate Esters: Selective Hydrolysis of Phosphate Monoesters over Diesters by Zirconium(IV) Complexes.

4.1. Introduction.

Most studies on phosphate ester hydrolysis are carried out with phosphate diesters as substrates. However, it is equally important to study phosphate monoester hydrolysis. Phosphate monoester hydrolysis is one of the most fundamental reactions in molecular biology and biotechnology.¹ There are several enzymes that catalyze phosphate monoester hydrolysis, including alkaline phosphatase, fructose 1,6-biphosphatase, inositol monophosphatase, and purple acid phosphatase (described in Chapter 2) for example. Common to each enzyme is the requirement for at least two divalent metal ions in the active site. Hydrolysis of dianionic phosphate monoesters by water is much slower than for monoanionic phosphate diesters. The half-life for attack by water on alkyl phosphate dianions is estimated to be in the region of 10^{12} years at 25°C.² Water attack on phosphate monoester dianions is very slow, enzymes that catalyze water attack on this substrate are said to exceed other known enzymes in the rate enhancements that they produce.³ Mechanisms of catalysis by alkaline phosphatase and purple acid phosphatase are described in Chapters 1 and 2. Inositol monophosphatase contains two magnesium metal ions in the active site. Unlike alkaline phosphatase, the catalytic mechanism of inositol monophosphatase is not considered to proceed through a phosphoenzyme intermediate. Metal ions are involved in activating a solvent nucleophile, stabilising the trigonal bipyramidal phosphorus intermediate and interacting with the products (**Figure 4.1**).⁴

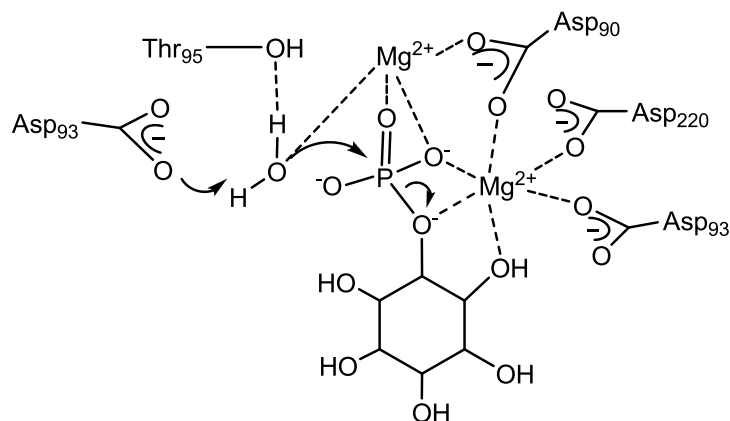


Figure 4.1: Inositol monophosphatase-catalysed phosphate monoester hydrolysis.

4.1.1. Mechanisms of Phosphate Monoester Hydrolysis.

Described in section 1.3., are dissociative, associative and concerted mechanisms of phosphate ester hydrolysis. The mechanism of hydrolysis for different types of phosphate ester varies. Theoretical studies have shown that phosphate triesters, for example *O,O'*-diethyl *p*-nitrophenyl phosphate (paraoxon), react with hydroxide in an associative mechanism, giving a penta-coordinate intermediate.^{5,6} Similarly, theoretical work has shown that the hydrolysis of the phosphate diester, dineopentyl phosphate proceeds via a penta-coordinate intermediate.⁷ Monoester hydrolysis in aqueous solution, in the absence of metal ions is generally accepted as following a dissociative pathway.^{6,8,9} Metalloenzyme mediated phosphate monoester hydrolysis, however favours an associative pathway, while phosphate monoesterases that operate in the absence of metal ions, catalyse via a dissociative pathway.⁶ For dianionic phosphate monoesters, Kirby and Jencks have proposed a dissociative mechanism (**Figure 4.2**).¹⁰ A small, positive entropy of activation coupled with an insensitivity to the nature of solvent and a small or negligible solvent deuterium isotope effect, support this scheme. In a theoretical study, a change in the nature of the transition state from dissociative to associative upon increasing the pK_a of the leaving group is suggested. A 2-dimensional More O'Ferrall-Jencks plot¹¹ representing the different routes to substituted phosphate is

shown in **Figure 4.2**. Association of the nucleophile is represented by the vertical axis and dissociation of the leaving group is represented by the horizontal axis.

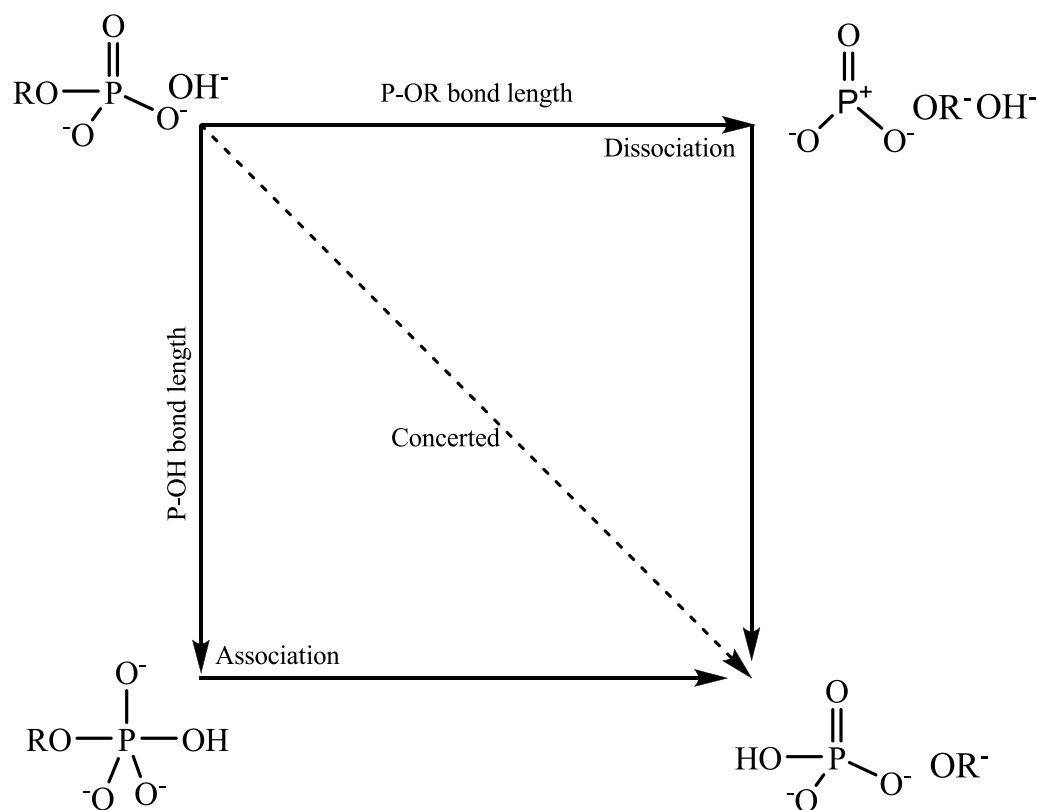


Figure 4.2: More O'Ferrall-Jencks 2-dimensional plot of the different routes to substituted phosphate.

4.1.2. Metal-Catalysed Phosphate Monoester Hydrolysis.

The objectives of studies on metal-mediated phosphate ester hydrolysis include the elucidation of mechanistic information for the natural phosphatases (Chapter 2) and the search for highly efficient catalysts. Much effort has been dedicated to the design of small molecule metal catalysts as highly active phosphohydrolases. The main focus of this effort has been directed towards the hydrolysis of the phosphate diester bond, the bond linking deoxyribose and ribose and phosphate in the backbone of DNA and RNA respectively. Several transition metal and lanthanide complexes have been reported.¹²⁻¹⁴

Studies directed at understanding and improving phosphate monoester hydrolysis are comparatively few.

Often, model studies aimed at understanding phosphomonoesterases are carried out using diesters. This reflects the high stability of phosphate monoesters and the challenge to find efficient catalysts. The study of phosphate monoester hydrolysis is important. Of particular interest are catalysts that selectively hydrolyse phosphate monoester bonds, e.g. for the removal of terminal phosphate groups from oligonucleotides. Some selected examples are described in 4.1.2.a – 4.1.2.d.

4.1.2.a.

Hydrolysis of the unactivated substrate, methyl phosphate, by the Co^{III} complex of triethylene tetraamine ligand (trien) was reported.¹⁵ Complexation of Co^{III} with the tetradentate ligand trien results in two unoccupied coordination sites cis to each other. Two mechanisms of hydrolysis are proposed; monodentate coordination of phosphate monoester and nucleophilic attack by the aqua ligand in the cis position (**Figure 4.3 A**), and bidentate coordination by the phosphate ester followed by subsequent nucleophilic attack by solvent water. At 78°C, by extrapolation, a 130- fold rate acceleration of rate is reported over spontaneous hydrolysis of $\text{HPO}_4\text{CH}_3^-$, the species with the highest rate of hydrolysis in the aqueous methyl phosphate system. (**Figure 4.3 B**).

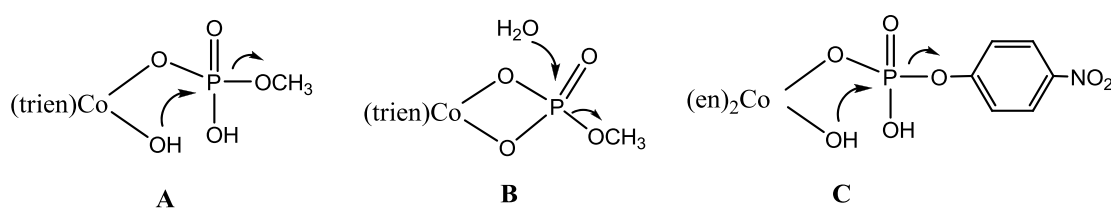


Figure 4.3: Mechanisms of hydrolysis of methyl phosphate by $\text{Co}^{\text{III}}(\text{trien})$ (**A + B**) and $\text{Co}^{\text{III}}(\text{en})_2$ (**C**).

In the same study, the activity of electronically analogous $\text{Co}^{\text{III}}(\text{NH}_3)_5$, which contains only one free binding site, was tested towards methyl phosphate hydrolysis and found to

be two orders of magnitude less active. The necessity for two vacant coordination sites cis to each other is clearly demonstrated.

The activity of Co^{III} (trien) towards the diester, dimethyl phosphate was also investigated. No production of methanol was observed. The authors conclude that bidentate coordination of the phosphate monoester is stronger than for the diester. Bidentate coordination of the diester would require coordination of the phosphoryl oxygen, a weak donor.

In a later study, Sargeson *et al.*, used ^{18}O tracer experiments to study the hydrolysis of p-nitrophenyl phosphate by the cobalt(III) complex of ethylenediamine (en), and were able to show that intra-molecular nucleophilic attack by cis hydroxide is taking place. **(Figure 4.3 C).**¹⁶

4.1.2.b.

Chin *et al.* synthesised a dinuclear Co^{III} complex that provides 11 orders of magnitude rate acceleration in the hydrolysis of the unactivated phosphate monoester, phenyl phosphate. **(Figure 4.4).**¹⁷ In this study, the phosphate ester- bridged complex was first synthesised, followed by measurement of rates of hydrolysis.

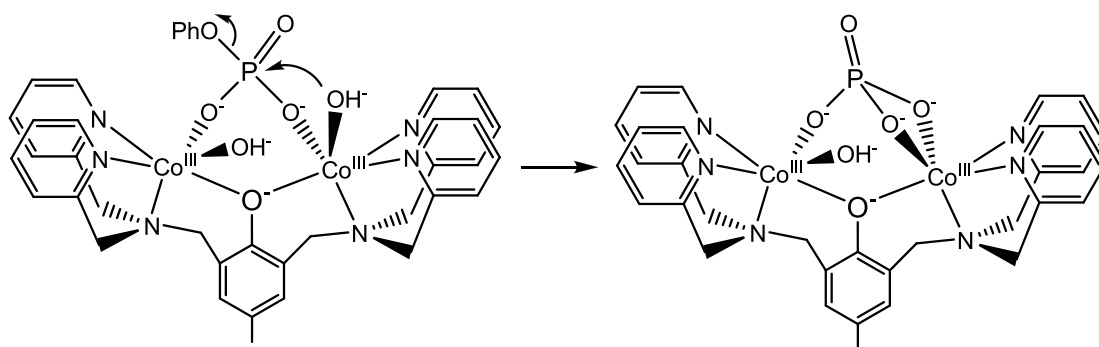


Figure 4.4: Hydrolysis of phenyl phosphate by dinuclear Co^{III} complex.

A crystal structure of the phenylphosphonate analog of this complex revealed the phosphate to bidentately bridge the metal ions. The mechanism of hydrolysis involves intramolecular nucleophilic attack on phosphorus by metal-bound hydroxide.

4.1.2.c.

A dizinc cryptate which selectively catalyses phosphate monoester hydrolysis has been reported. In a manner analogous to alkaline phosphatase, in which a serine residue acts as nucleophile on phosphorus, the reaction-initiating nucleophile which leads to P-OR bond scission, is a secondary amine of the macrocyclic ligand (**Figure 4.5**).¹⁸

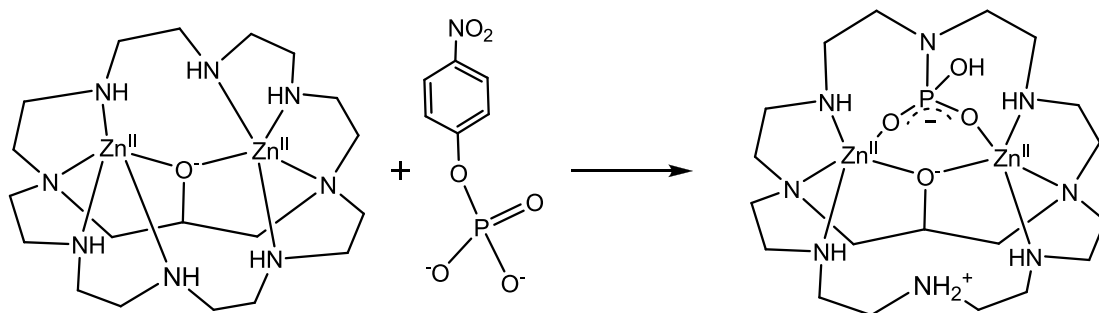


Figure 4.5: Phosphate monoester hydrolysis by dizinc cryptate.

Catalytic turnover is not observed in this complex as the phosphoramidate formed is stable. Hydrolytic activity of this complex is selective for phosphate ester polyanions, for example ATP or phosphate monoester dianions. No activity is observed towards monoanionic phosphate diesters or neutral triesters.

4.1.2.d.

The selective hydrolysis of phosphate monoesters by cerium(IV) ions in concentrated buffer solution has been reported.¹ Up to 580- fold rate accelerations for phosphate mono- over diester hydrolysis is described for the nucleotide dAp over d(ApA), in 500 mM Tris buffer. In 50 mM Tris buffer, the rate acceleration for mono- over diester hydrolysis is reduced to 90- fold. This enhanced activity in concentrated buffer is attributed to buffer-induced suppression of phosphate diester hydrolysis. There is competition between monoanionic phosphate diesters and buffer with respect to Ce^{IV}

coordination sites and this competition at higher buffer concentration results in the suppression of phosphate diester hydrolysis. Binding of dianionic phosphate monoesters is affected to a lesser degree. A proposed mechanism for the hydrolysis of d(pApA) is shown in **Figure 4.6**. Formation of Ce^{IV} clusters is expected and coordination of the mono- and diester moieties is shown. Strong coordination of the terminal monophosphate enables coordination of the diester and subsequent hydrolysis.

In another study, the hydrolysis and β -elimination of terminal phosphate from polypeptide substrates in cerium(IV) and other trivalent lanthanide ion solutions, buffered by bis-tris propane (BTP) (**Figure 4.6**) is reported by Schepartz *et al.*¹⁹ Lanthanide ions form dinuclear polyhydroxo complexes with BTP of the type $\text{M}_2(\text{BTP})_2(\text{OH})_n$ (where $n = 2, 4, 5, \text{ or } 6$).²⁰

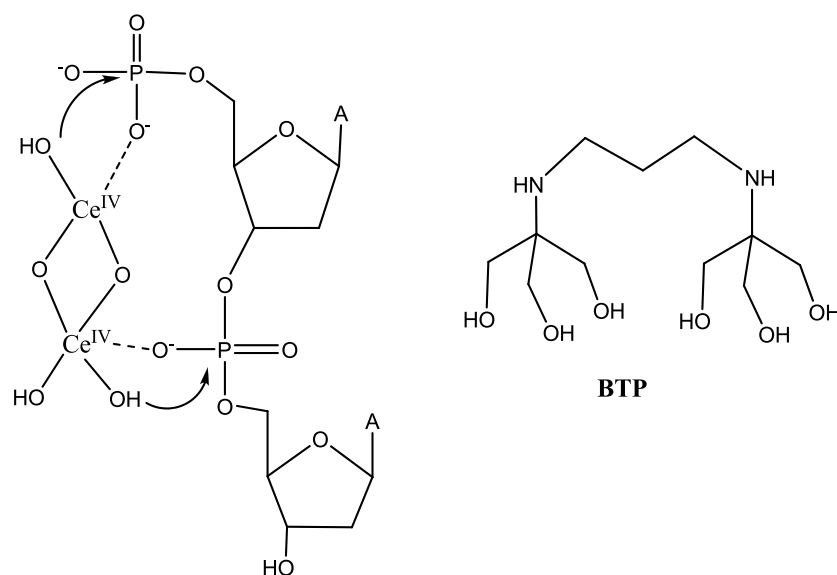


Figure 4.6: Proposed mechanism of phosphate mono- and diester hydrolysis by Ce^{IV} hydroxide cluster in solution¹ and BTP.

4.1.3. Zr^{IV} -Mediated Phosphate Ester Hydrolysis.

The phosphoesterolytic activity of Zr^{IV} was first noticed by Kennedy *et al.* while measuring the activity of an alkaline phosphatase immobilised on zirconium

hydroxide.²¹ This observation was further explored in a later work by the same group.²² Heterogenous catalysis of the hydrolysis of the activated phosphate monoester, 4-nitrophenyl phosphate (4-NPP) by gelatinous zirconium(IV) hydroxide is described. In the pH range 7 – 9, greatest activity was observed at pH 7. However, only modest rate accelerations of *ca.* 30- fold were observed for the hydrolysis of 4-NPP relative to the uncatalysed reaction. It was also found that the rate of hydrolysis was not linear with respect to time, owing to an initial induction period involving substrate-catalyst coordination.

Homogenous catalysis by Zr^{IV} was also observed and published.²³ In this study, the activity of the Zr^{IV} ion and some of its complexes were tested towards the hydrolysis of the activated phosphate diester bis (4-nitrophenyl) phosphate (BNPP) (**Figure 4.7**) and the dinucleotide thymidyl(3'→5')thymidine.

Uncomplexed Zr^{IV} was found to greatly promote phosphate diester hydrolysis between pH values ~2 – 5 (insoluble zirconium hydroxide gels are formed above pH 5), with a rate maximum occurring at pH 4. A 5×10^8 – fold rate acceleration over the uncatalysed reaction ($k_{obs} = 10^{-11} s^{-1}$, pH 7, 25°C) is provided at this pH. Conversion of the liberated phosphate monoester to nitrophenol and inorganic phosphate is reported to happen at a similar rate ($k_{obs}=3.4 \times 10^{-3} s^{-1}$).

Zr^{IV} is homogenised above pH 5 through coordination with ligands **1** and **2** by mixing $ZrCl_4$ and ligands in 1:1 and 1:2 ratios respectively (**Figure 4.7**).

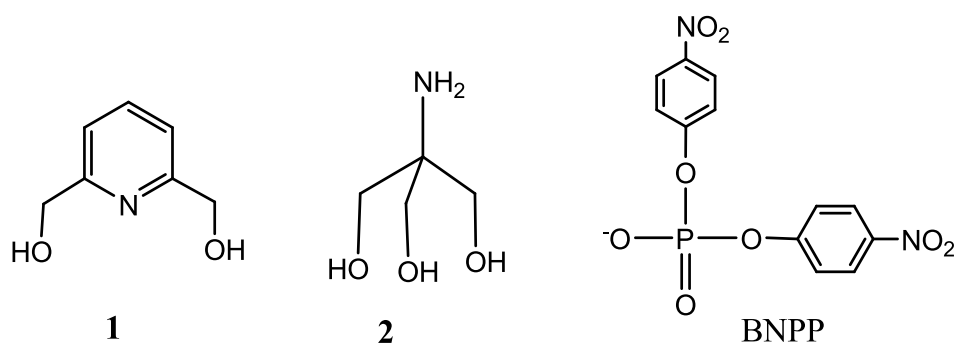


Figure 4.7: Ligands employed to homogenise Zr^{IV} above pH 5, and substrate BNPP.

pH-rate profiles for the hydrolysis of BNPP by these complexes exhibit maxima between pH 3 and 4 and display similar activities to free Zr^{IV} . Upon increasing the pH value, activity lessens, at neutral pH, it is reduced by ~ 1 order of magnitude. k_{obs} for the hydrolysis of thymidyl(3' \rightarrow 5')thymidine by the Zr^{IV} complex of **2** is equal to $2.9 \times 10^{-7} \text{ s}^{-1}$ (20°C, 5 mM $ZrCl_4$, 10 mM **2** and pH 5.5). This translates to a half-life of 28 days.

A similar study was published around the same time, investigating the cleavage of BNPP and the RNA model substrate HPNP by Zr^{IV} and Hf^{IV} ions.²⁴ (See **Figure 4.5**, section **3.1.3**. for the structure of HPNP).

In the most recent study of Zr^{IV} – mediated phosphate ester hydrolysis, a number of complexes were screened for ATPase activity.²⁵ Ligands employed include **1** and **2** (**Figure 4.7**), and those shown in **Figure 4.8**.

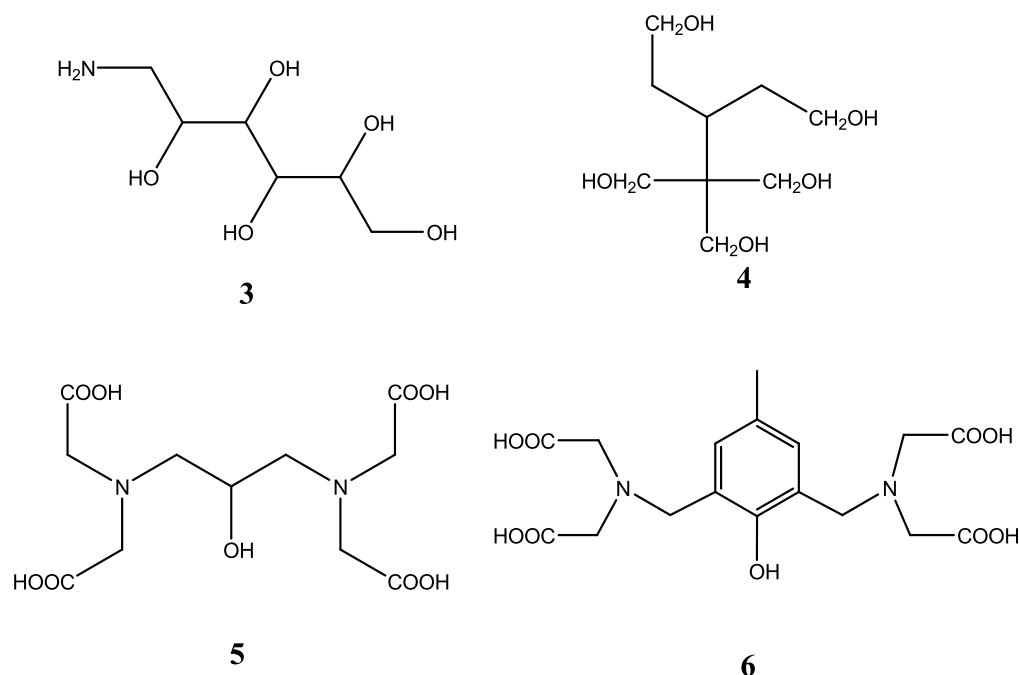


Figure 4.8: Ligands employed as Zr^{IV} chelators.

Two equivalents of ligand were added per equivalent of metal ion. In this screening, carried out at pH 4 and 7, the Zr^{IV} complex of HXTA (**6**, **Figure 4.8**) showed greatest ATPase activity at both pH values. Similar rates for the dephosphorylation of ATP and resultant ADP were detected, while AMP hydrolysis is described as “rather slow”

(Figure 4.9). Cleavage of P-O-P bonds is more facile than cleavage of P-O-R bonds in monoesters.

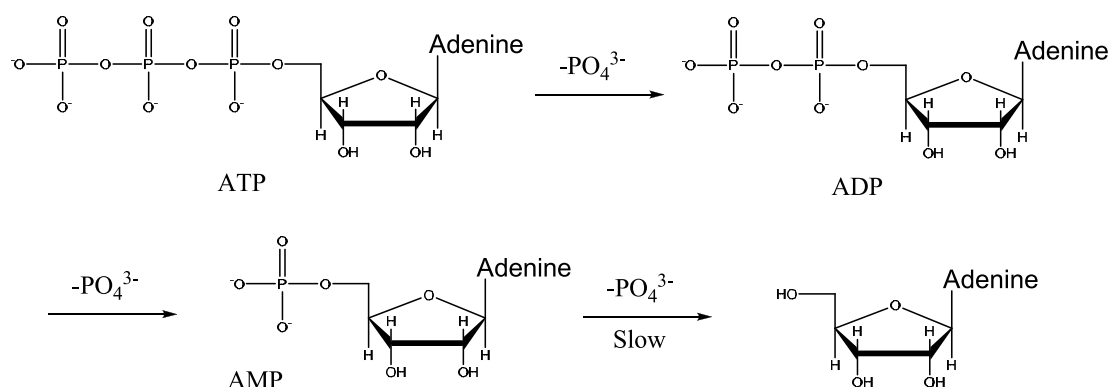


Figure 4.9: Dephosphorylation of ATP.

In other work, Leumann *et al.* have studied the solvolysis of phosphate esters by Zr^{IV} complexes in methanolic media.^{26,27} A 5-fold rate enhancement in the hydrolysis of the activated phosphate monoester 4-nitrophenyl phosphate (4-NPP) by a Zr^{IV} – peptide adduct was reported.²⁸

4.1.4. Aims.

The high charge to ionic radius ratio make zirconium(IV) an ideal mediator of phosphate ester hydrolysis and, behind Ce^{IV} , is among the most active metal ions.²⁴ Cerium is the only lanthanide that can access the +4 oxidation state and many of the most active phosphoesterolytic systems are based on Ce^{IV} . Rate enhancements of $>10^{10}$ for BNPP and $>10^{11}$ for DNA hydrolysis have been detected.²⁹ A dinuclear cerium complex of the ligand HXTA (**6**, **Figure 4.8**), capable of catalysing double-strand DNA hydrolysis at 37°C and pH 8 has been reported.³⁰ The HXTA ligand and HXTA-type ligands (**Figure 4.8**, ligand **5**) provide an ideal structural scaffold for metal ion-mediated phosphate ester hydrolysis, and have been employed to great effect in a number of highly active systems.³⁰⁻³⁴ The phenolate-bridged metal ions are held in close proximity, facilitating positive cooperation.

In the previous study by Ott and Krämer²⁵, Zr^{IV} salt and HXTA were mixed in a 1:2 ratio and the ATPase activity of the resulting solution tested. No attempts were made to characterise active species, but the mononuclear complex can be assumed due to the metal : ligand ratio used. In light of this study, the challenge of generating the 2 : 1 (Zr^{IV} : HXTA) complex and carrying out a detailed investigation into its phosphoesterolytic activity appeared.

In this study, metal ion cooperativity in the dinuclear complex was investigated by generating the 2:1 complex of HXTA and comparing its phosphatase activity with a well-defined mononuclear complex.

In previous studies, phosphate monoester hydrolysis at neutral pH by homogenous Zr^{IV} solutions has not been demonstrated. Monoester hydrolysis by Zr^{IV} ions is described as being at a similar rate to that of the analogous phosphate diester at pH 4.²³ Recalling the work by Komiyama *et al.*¹, an up to 580- fold rate acceleration for monoester-over-diester hydrolysis by cerium(IV) cations is described (**4.1.2.d.**). This rate enhancement is attributed to the higher metal-binding affinity of the dianionic phosphate monoester relative to the monoanionic diester. The chemistry of aqueous Zr^{IV} is complicated in solution and precipitation occurs at neutral pH. Cationic polynuclear polyhydroxo zirconium species are formed.²³ This leads to a reduction in the number of vacant metal coordination sites and the conversion of labile aqua ligands into more tightly-bound hydroxide ligands, reducing substrate binding. To look into this further, the comparison of phosphate mono- versus diester hydrolysis at neutral pH would be investigated.

4.2. Results.

4.2.1. Complexes.

Including HXTA, three ligands were employed as Zr^{IV} chelators (**Figure 4.10**); **H₅L¹** (HXTA) and **H₅L²** (p-OMeHXTA) are closely related bis-nucleating ligands wherein the metal ions are bridged by phenolate. **H₅L²** contains an electron-donating *p*-methoxy group on the phenol ring, conferring upon it greater electron donation potential relative

to $\mathbf{H}_5\mathbf{L}^1$. The mononuclear Zr^{IV} complex of $\mathbf{H}_3\mathbf{L}^3$ was generated and its phosphoesterolytic activity relative to the dinuclear complexes was examined in order to investigate metal ion cooperativity.

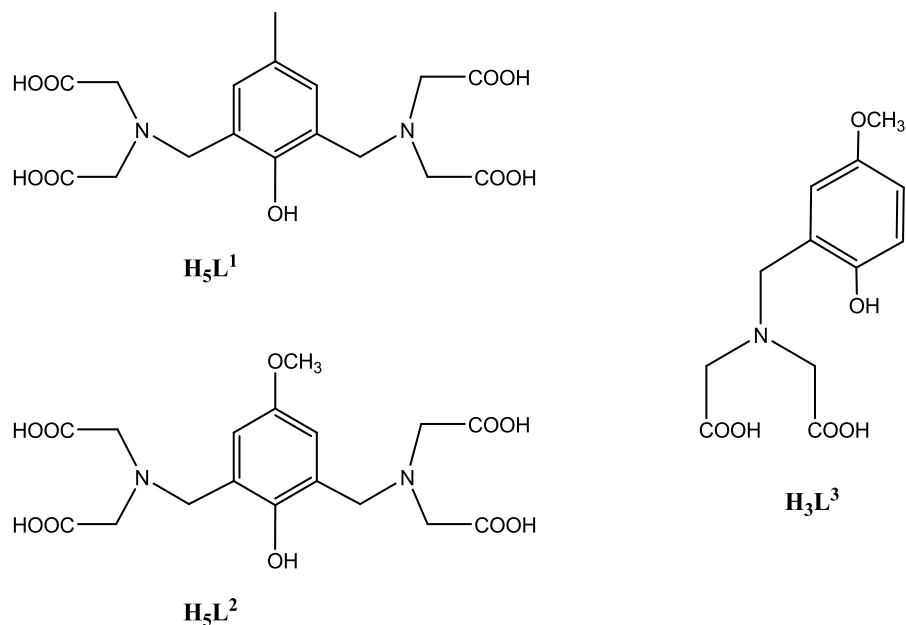


Figure 4.10: Ligands employed as Zr^{IV} chelators; bis-nucleating ligands $\mathbf{H}_5\mathbf{L}^1$ and $\mathbf{H}_5\mathbf{L}^2$ and mononucleating ligand $\mathbf{H}_3\mathbf{L}^3$.

$\mathbf{H}_5\mathbf{L}^1$ and $\mathbf{H}_5\mathbf{L}^2$ were synthesised by the scheme described in **Figure 4.7**, section 3.2.1.³⁰ $\mathbf{H}_3\mathbf{L}^3$ was synthesised in a solvent free Mannich reaction by the scheme described in **Figure 4.10**, section 2.2.1.³⁵

Zirconium complexes were prepared *in situ*. For the bis-nucleating ligands $\mathbf{H}_5\mathbf{L}^1$ and $\mathbf{H}_5\mathbf{L}^2$, the ligand was dissolved in water and the pH adjusted to pH 1 with 2 M HCl. A two-fold excess of zirconyl chloride (zirconyl chloride does not contain an oxide group and is a tetramer of composition $[\text{Zr}(\text{OH})_2 \cdot 4\text{H}_2\text{O}]_4^{8+}$ structure) dissolved in an equal volume of water was added with stirring. The pH value was then raised upwards by dropwise addition of 1 M NaOH with stirring. The same procedure was employed in generating the mononuclear complex, mixing ligand and metal in equimolar amounts.

Complex formation was investigated using ^1H NMR spectroscopy. Complete formation of the dinuclear complexes $\text{Zr}_2\mathbf{L}^1$ and $\text{Zr}_2\mathbf{L}^2$ could not be confirmed, due to a very

complicated and poorly resolved spectrum; in particular, in the CH₂ region, broadening was observed. ¹H NMR spectra were recorded over a range of pD values, with little change in the spectrum observed between pD 10 and pD 5 for both complexes. ¹H NMR spectra of Zr and L¹, mixed 2 : 1, recorded at pD 9.4 and pD 5 are shown in **Figure 4.11**. No signals representing free ligand were observed. Complete binding of mononucleating ligand L³ to Zr is observed in the NMR. Spectra recorded at pD 6.9 and pD 12.2 are shown in **Figure 4.12**. Splitting of CH₂ signals upon complexation is observed. CH₂ protons are magnetically inequivalent due to formation of a chelate ring. For the free ligand, only singlets for CH₂ signals are observed. Below pD 6.9, at this concentration, precipitation of the complex occurs as an extremely fine colourless powder, that was isolated through centrifugation. Similarly, complexes of H₅L¹ and H₅L² were isolated in this way, upon lowering the pH to below pH 3. However, characterisation of the precipitates proved difficult; elemental analysis results were not reproducible. Samples were examined using energy dispersive X-ray spectroscopy (EDX) in order to determine the zirconium content, however, sample consistency was poor.

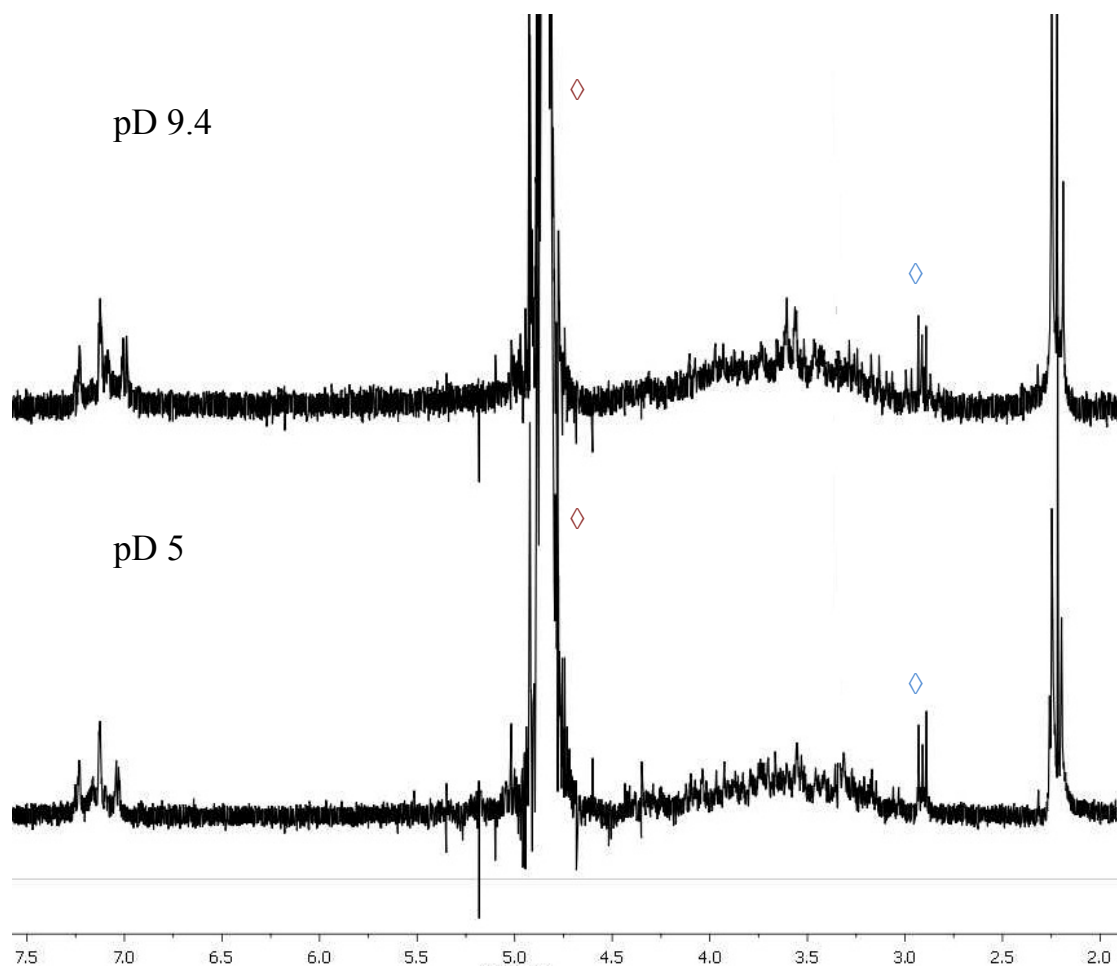


Figure 4.11: ^1H NMR spectra taken of mixtures of ZrOCl_2 and L^1 , at pD 5 and pD 9.4. (\diamond = HDO, \diamond = TSP reference signal).

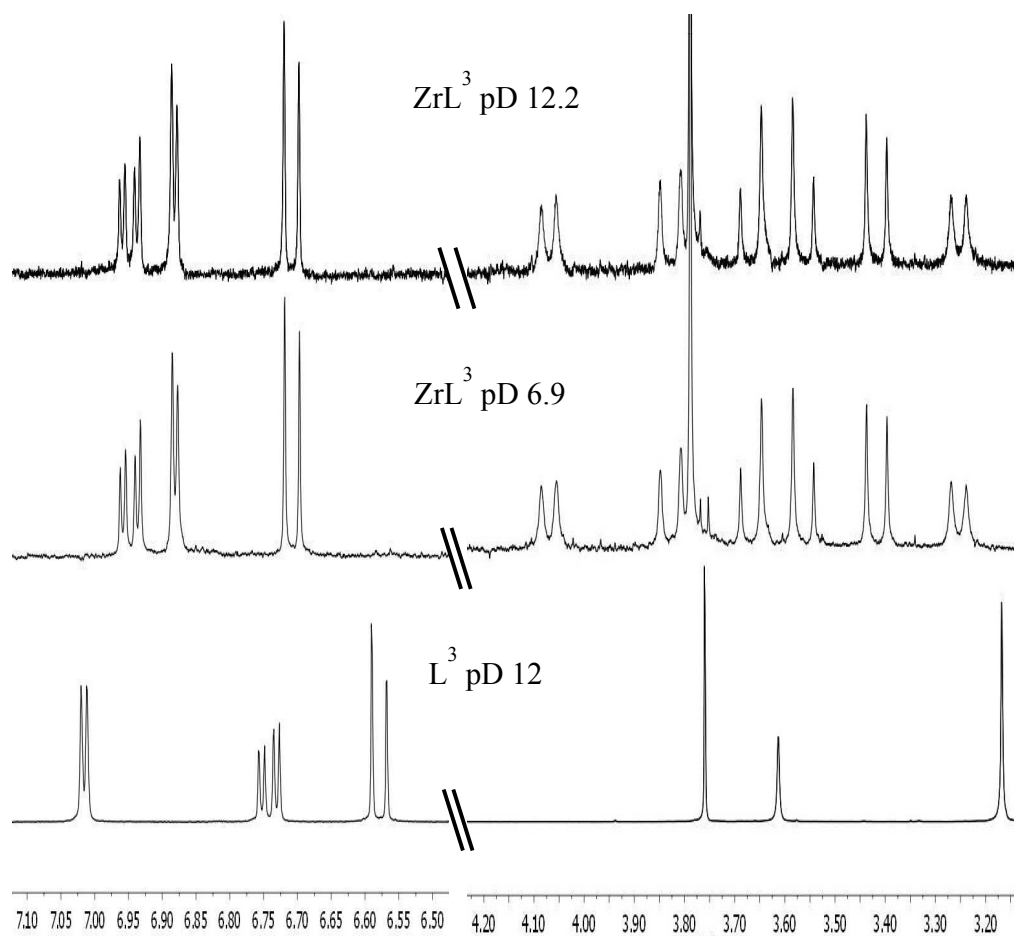


Figure 4.12: ^1H NMR spectra of ZrL^3 at pD 12.2 and pD 6.9 and L^3 at pD 12.

4.2.2. Phosphate Ester Hydrolysis.

The activity of the complexes towards phosphate di- and monoester hydrolysis was studied using the activated phosphate diesters; bis(4-nitrophenyl) phosphate (BNPP) and mono(4-nitrophenyl) monophenyl phosphate (MNPP),³⁶ and the phosphate monoesters, 4-nitrophenyl phosphate (4-NPP) and phenyl phosphate (PP) (**Figure 4.13**).

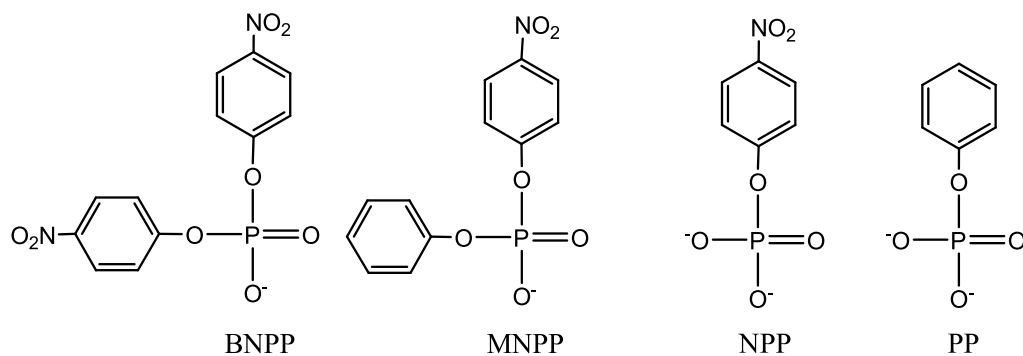


Figure 4.13: Di- and monoester substrates.

The hydrolysis of the nitrophenol-containing substrates was followed by measuring the increase in absorbance with time at 400 nm, due to liberated 4-nitrophenolate. The method of initial rates was used to determine the pseudo-first-order rate constants by following the reaction to < 5 % conversion.

4.2.2.1. Phosphate Diester Hydrolysis.

For phosphate diester substrates, BNPP and MNPP, the measure of accurate rate constants was hampered by a varying induction period, under pseudo-first order conditions. The absorbance versus time trace for the hydrolysis of BNPP by Zr_2L^1 at pH 6.61, shown in **Figure 4.14** is curving upwards during the first 5 % of the reaction. For more absorbance versus time traces, displaying varying induction periods, see **Appendix 4.1**.

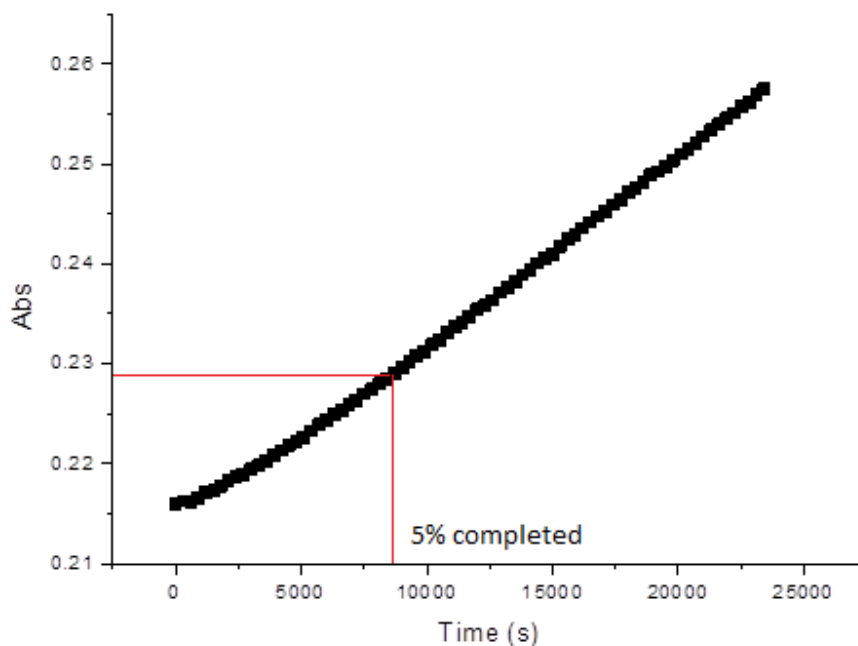


Figure 4.14: Absorbance vs. time plot for hydrolysis of BNPP (5×10^{-5} M) by Zr_2L^1 (1 mM) (25°C , 50 mM HEPES, pH 6.61).

Taking the linear segment of the absorbance versus time plot after the induction period, an approximate rate constant can be determined. The approximate observed rate constant (k_{obs}) for the hydrolysis of BNPP ($5.4 \times 10^{-6} \text{ s}^{-1}$) by Zr_2L^1 is slightly larger than for MNPP ($3.63 \times 10^{-6} \text{ s}^{-1}$) at neutral pH. Induction periods of this type, varying with pH were observed for each complex, making direct comparison of rate constants between complexes difficult.

4.2.2.2. Phosphate Monoester Hydrolysis.

The hydrolysis of the activated phosphate monoester 4-nitrophenyl phosphate (4-NPP) proceeds linearly during the first 5 % of the reaction and thus, it was possible to accurately measure pseudo-first-order rate constants for each complex. pH-rate profiles for the hydrolysis of 4-NPP are displayed in **Figure 4.15**. Upon increasing pH from 5.5 to 9, activity drops off markedly, in each case.

Measurement of rates of cleavage below pH 5.5 was not possible to determine accurately, as the concentration of released 4-nitrophenol in its deprotonated form becomes very small (pK_a 4-nitrophenol = 7.1). Following the increase of the protonated phenol at 318 nm ($E = 10,000 \text{ M}^{-1}\text{cm}^{-1}$)²³ was attempted. However, this is hampered by the disappearance of substrate phosphate ester ($E = 8,900 \text{ M}^{-1}\text{cm}^{-1}$) that also absorbs at this wavelength.

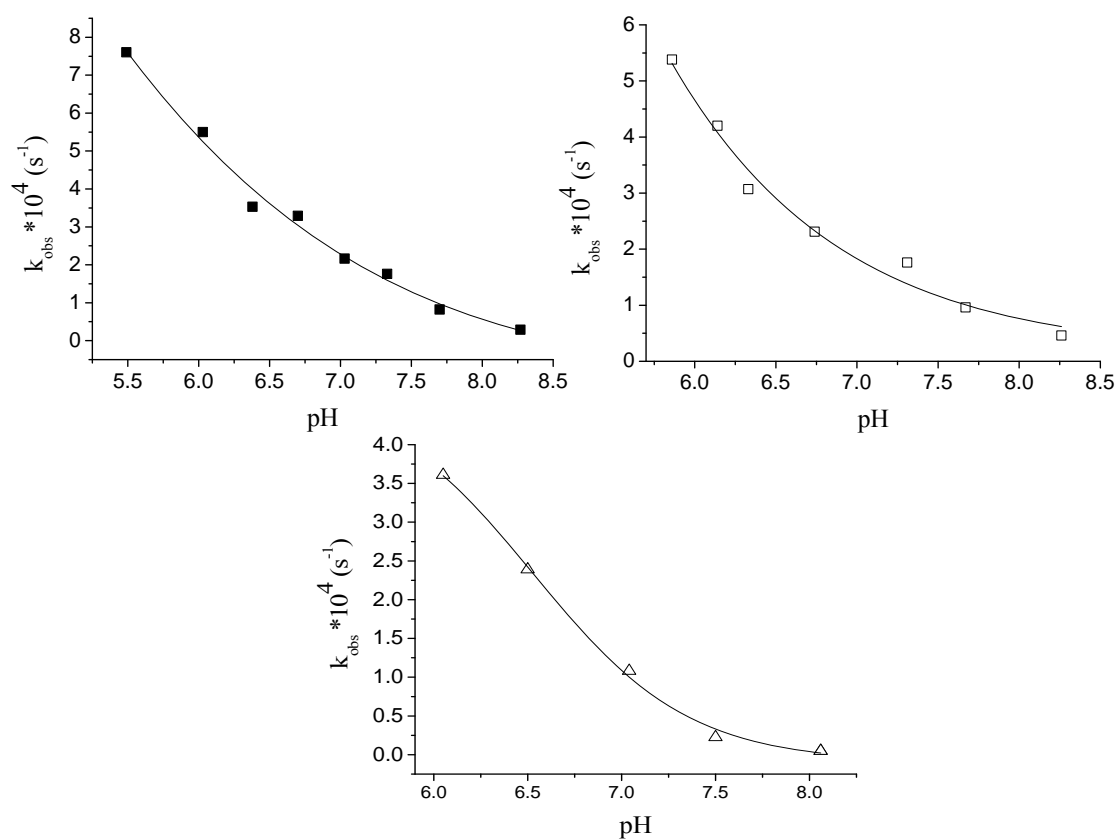


Figure 4.15: Rate-pH profiles for the cleavage of 4-NPP ($5 \times 10^{-5} \text{ M}$) by $[\text{Zr}_2\text{L}^1]^{3+}$ (1 mM) (■), $[\text{Zr}_2\text{L}^2]^{3+}$ (1 mM) (□) and $[\text{ZrL}^3]^+$ (2 mM)(△) at 25°C. [buffer] = 50 mM (HEPES); $I = 0.1 \text{ M}$ (NaCl).

The dependence of the initial rates of 4-NPP hydrolysis with complex concentration at pH 7 was studied. Plots were linear in the concentration range 0.25–2 mM concentration

indicating clean 2nd order kinetics. 2nd order rate constants (k) were calculated; Zr_2L^1 ($0.18 \text{ M}^{-1}\text{s}^{-1}$), Zr_2L^2 ($0.17 \text{ M}^{-1}\text{s}^{-1}$) and ZrL^3 ($0.042 \text{ M}^{-1}\text{s}^{-1}$). 2nd order plots for Zr_2L^1 and ZrL^3 are shown in **Figure 4.16**. For clarity, the 2nd order plot for Zr_2L^2 is not shown in **Figure 4.16**, it is shown in **Appendix 4.2**. Rate constants for 4-NPP hydrolysis by dinuclear complexes are approximately 4- times larger that for the mononuclear complex.

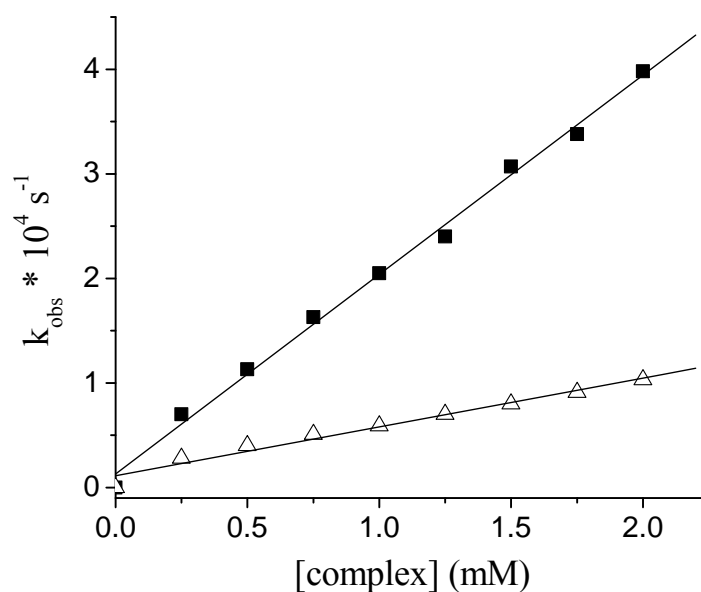


Figure 4.16: Dependence of the rate of cleavage of 4-NPP by Zr_2L^1 (■) and ZrL^3 (△) at 25°C and pH 7. For Zr_2L^1 (■), 4-NPP = $2.5 \times 10^{-6} \text{ M}$ and for ZrL^3 (△), 4-NPP = $1.25 \times 10^{-6} \text{ M}$. [buffer] = 50 mM (HEPES), I = 0.1 M (NaCl).

Phosphate monoester cleavage was also investigated at various substrate concentrations for each complex. Michaelis-Menten behaviour is observed in each case, as shown by a linear relationship between the inverse initial rate ($1/v$) and the inverse substrate concentration ($1/[4\text{-NPP}]$). Lineweaver-Burk plots are shown in **Figure 4.17** and kinetic data are displayed in **Table 1**.

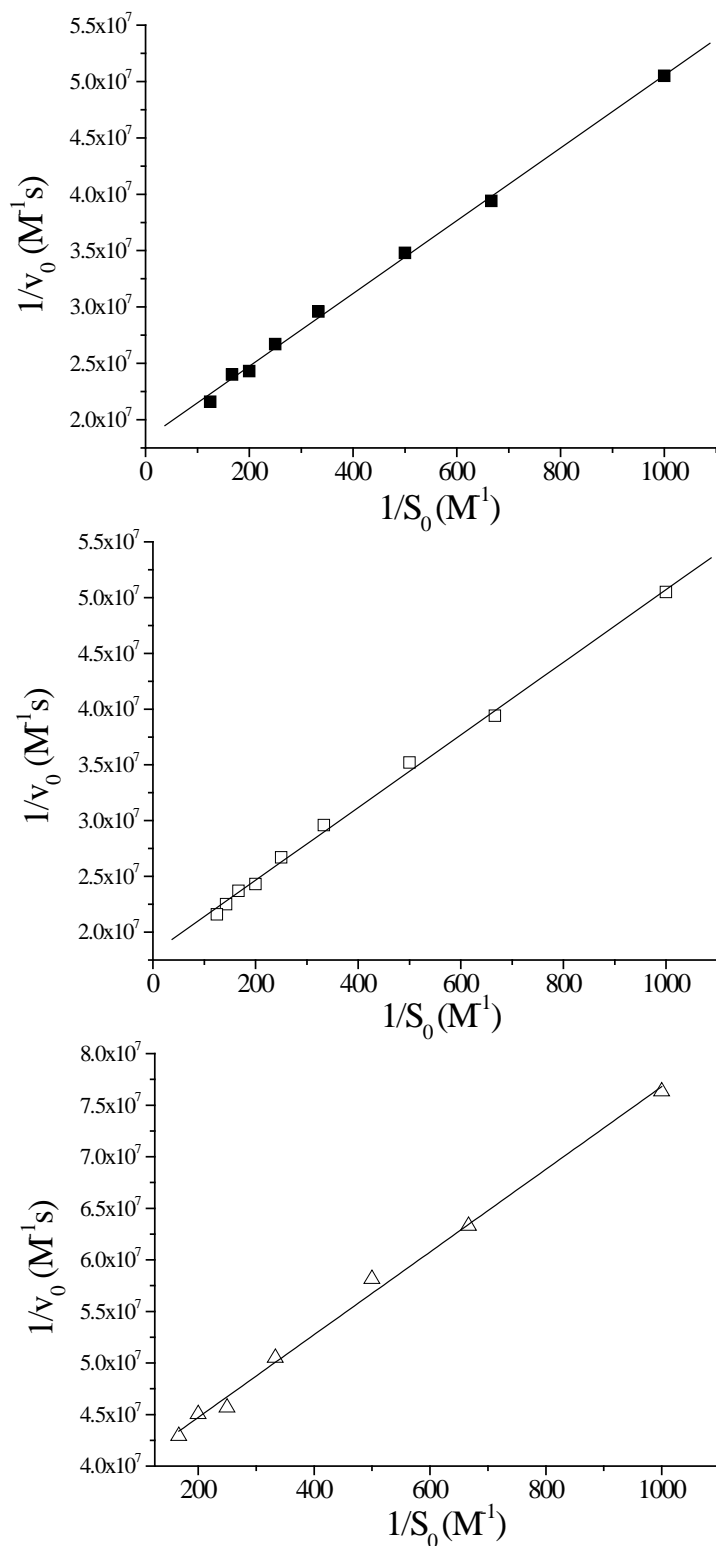


Figure 4.17: Lineweaver-Burk plots for Zr_2L^1 (0.5 mM) (■), Zr_2L^2 (0.5 mM) (□) and ZrL^3 (1 mM)(△) at 25°C and pH 7. [buffer] = 50 mM (HEPES); I = 0.1 M (NaCl).

Michaelis-Menten kinetic studies were performed at constant complex concentration; Zr_2L^1 and Zr_2L^2 at 0.5 mM and ZrL^3 at 1 mM. Initial substrate concentration (S_0) was in the range 1 – 8 mM. However, for ZrL^3 , above 6 mM S_0 , Michaelis-Menten behaviour was not observed.

Table 1: Constants determined from Lineweaver-Burk plots.

Complex	v_{max} ($\times 10^8 Ms^{-1}$)	k_{cat} ($\times 10^4 s^{-1}$)	K_m ($\times 10^3 M$)	$1/K_m$ (M^{-1})
Zr_2L^1	5.47	1.1	1.77	565
Zr_2L^2	5.51	1.1	1.80	556
ZrL^3	2.72	0.272	1.24	806

4.2.2.3. Thermodynamics of Phosphate Ester Hydrolysis.

The Eyring equation is used to relate reaction rate to temperature and from it, activation parameters enthalpy of activation (ΔH^\ddagger) and entropy of activation (ΔS^\ddagger) can be determined. The Eyring equation is given by:

$$\ln\left(\frac{k}{T}\right) = -\frac{\Delta H^\ddagger}{RT} + \ln\left(\frac{k'}{h}\right) + \frac{\Delta S^\ddagger}{R}$$

Plotting of $\ln\left(\frac{k}{T}\right)$ vs. $\frac{1}{T}$, intercept = $\ln\left(\frac{k'}{h}\right) + \frac{\Delta S^\ddagger}{R}$ and gradient = $-\frac{\Delta H^\ddagger}{R}$. k' = Boltzmann constant, h = Planck constant, R = molar gas constant. Eyring plots were generated for the hydrolysis of 4-NPP by each of the complexes and also for the hydrolysis of MNPP by ZrL^3 (**Figure 4.18**). Activation parameters are given in **Table 2**.

Table 2. Activation parameters.

Complex	4-NPP		MNPP	
	ΔS^\ddagger (JK^{-1})	ΔH^\ddagger ($kJmol^{-1}$)	ΔS^\ddagger (JK^{-1})	ΔH^\ddagger ($kJmol^{-1}$)
Zr_2L^1	-98.6	64.1	-129.7	65.0
Zr_2L^2	-75.6	71.4		
ZrL^3	-92.0	67.3		

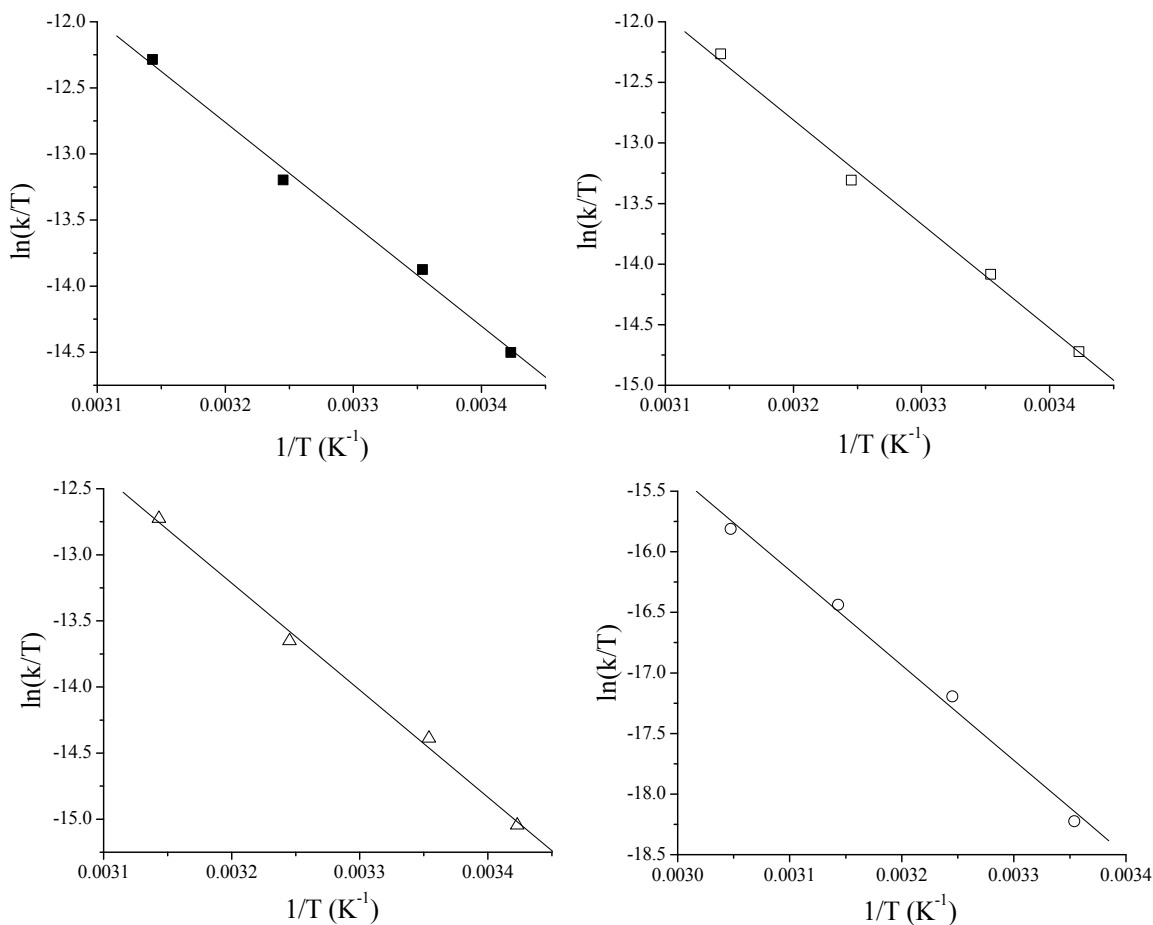


Figure 4.18: Eyring plots for hydrolysis of 4-NPP by Zr_2L^1 (1 mM) (■), Zr_2L^2 (1 mM) (□) and ZrL^3 (2 mM)(△) and for the hydrolysis of MNPP by ZrL^3 (2 mM)(○) at 25°C and pH 7. [buffer] = 50 mM (HEPES); I = 0.1 M (NaCl).

Fitting the same kinetic data to the Arrhenius equation allows the determination of the activation energy (E_a). The Arrhenius equation (in logarithmic form) is given by:

$$\ln k = \ln A - \frac{E_a}{RT}$$

Plotting $\ln k$ vs. T^{-1} gives a slope = $-\frac{E_a}{R}$ and intercept = $\ln A$ where A is a constant (**Figure 4.19**). R = molar gas constant. Activation energies are given in **Table 3**.

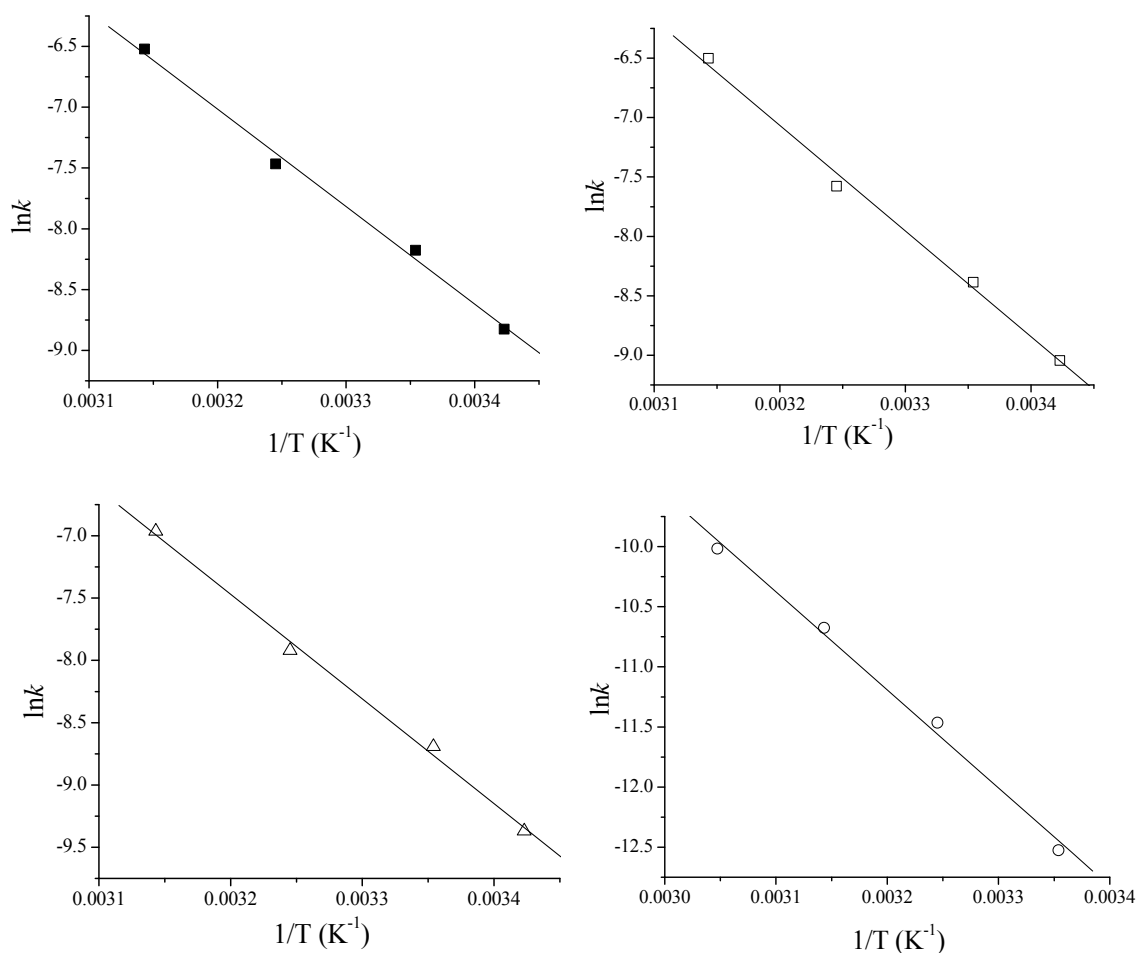


Figure 4.19: Arrhenius plots for hydrolysis of 4-NPP by Zr_2L^1 (1 mM) (■), Zr_2L^2 (1 mM)(□) and ZrL^3 (2 mM)(△) and for the hydrolysis of MNPP by ZrL^3 (2 mM)(○) at 25°C and pH 7. [buffer] = 50 mM (HEPES); I = 0.1 M (NaCl).

Table 3. Activation energies.

Complex	4-NPP	MNPP
	E_a (kJmol ⁻¹)	E_a (kJmol ⁻¹)
Zr_2L^1	66.6	67.8
Zr_2L^2	73.9	
ZrL^3	69.9	

4.2.2.4. Hydrolysis of Phenyl Phosphate.

The water rate for hydrolysis of dianionic phenyl phosphate is $\sim 5 \times 10^{-13} \text{ s}^{-1}$ at 25°C .¹⁷ This corresponds to a half-life of around 44,000 years. ($t_{1/2} = \ln 2/k$). Phenyl phosphate and Zr_2L^1 were mixed together 1 : 1 in D_2O solution in an NMR tube at pD 7. The mixture was heated at 40°C and its ^1H NMR spectrum recorded intermittently over a 10-day period (**Figure 4.20**).

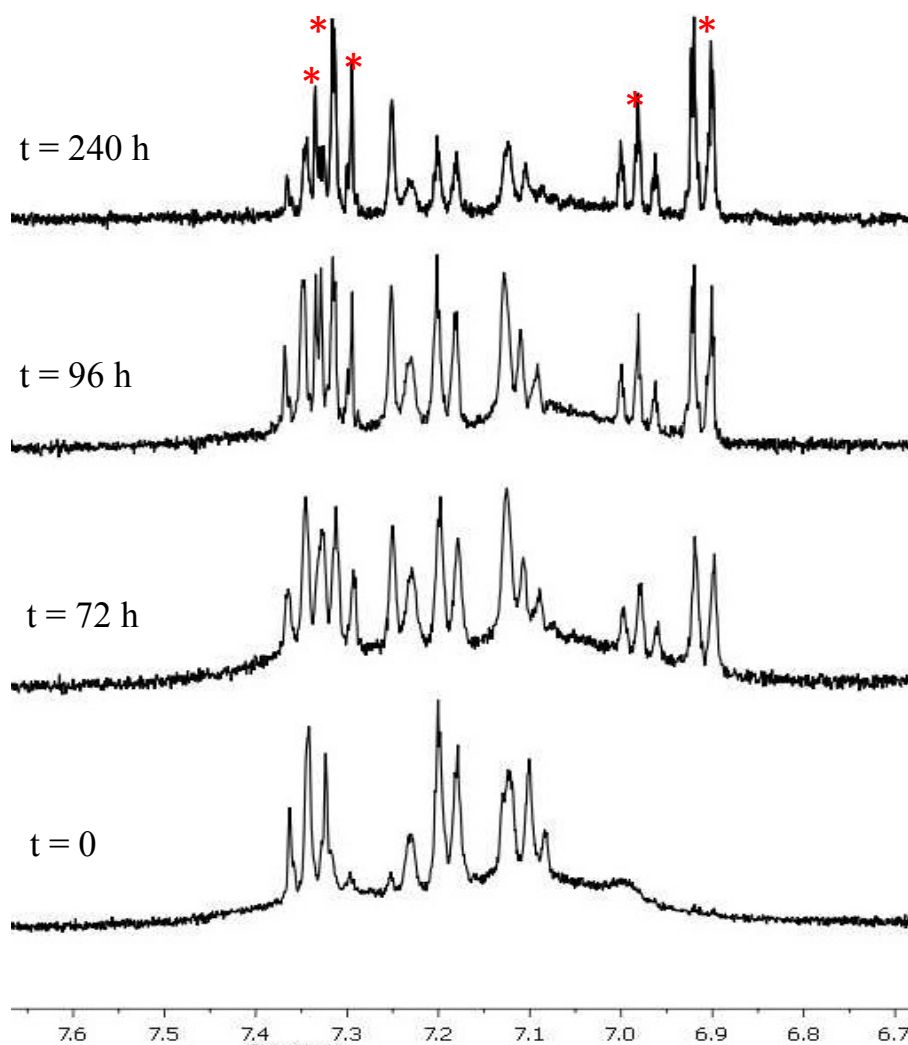


Figure 4.20: Hydrolysis of phenyl phosphate (10 mM) by Zr_2L^1 (10 mM) at pD 7 and 40°C . (* = liberated phenol).

The half-life of phenyl phosphate is greatly reduced in the presence of the dinuclear complex Zr_2L^1 . Measurement of rate constant is hampered due to signal overlap between ligand, substrate and product. However it is reasonable to say that after 96 hours, roughly one half-life has passed.

4.2.2.5. Dependence of the Hydrolysis Rate on the Ligand : Zr^{IV} Ratio.

The ability of the dinucleating ligands to keep in solution more than 2 equivalents of Zr^{IV} and the mononucleating ligand L^3 to keep in solution more than one equivalent Zr^{IV} was considered. It was found, following the procedure described in 4.2.1. that bis-nucleating ligands L^1 and L^2 have the ability to keep 4 equivalents of Zr^{IV} and the mononucleating ligand, L^3 , 2 equivalents in solution at neutral pH. It appears that the Zr complexes form extended zirconium hydroxide networks in solution, with one equivalent of uncoordinated Zr^{IV} per bound Zr^{IV} . Hydrolytic activity of mixtures containing varying amounts of Zr^{IV} at fixed ligand concentration was studied (**Figure 4.21**).

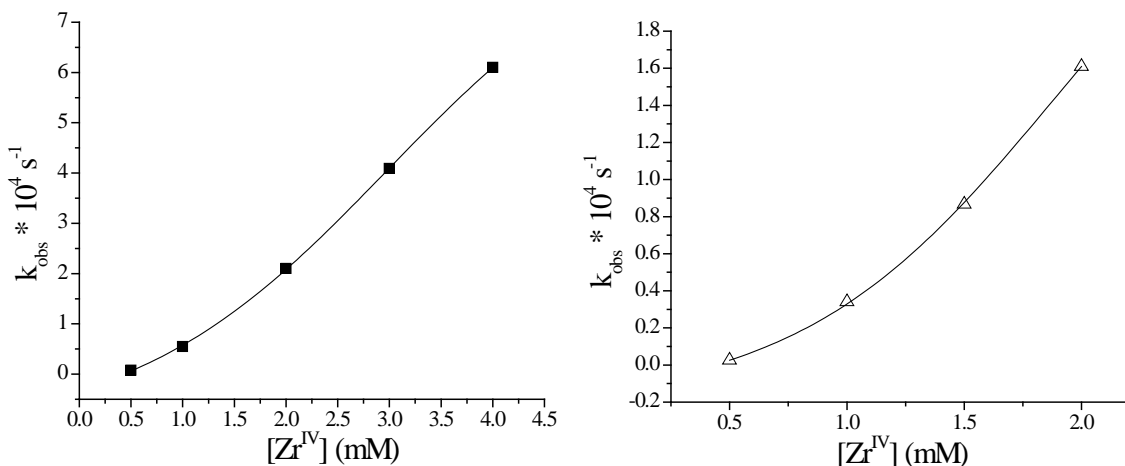


Figure 4.21: Dependence of rate of hydrolysis of 4-NPP ($5 \times 10^{-5} \text{ M}$) upon Zr^{IV} concentration, for L^1 (1 mM) (■) and L^3 (1 mM)(△) at pH 7 and 25°C. [buffer] = 50 mM (HEPES); I = 0.1 M (NaCl).

4.2.2.6. Inhibition by Phosphate.

Free phosphate produced in hydrolysis reduces hydrolytic activity. This may perhaps be due to formation of inactive zirconium-phosphate species. This behaviour has been observed in previous work.²³ To illustrate this, 5×10^{-5} M Zr_2L^1 and 5×10^{-4} M 4-NPP were mixed at 25°C and the reaction followed (**Figure 4.22**). After 1 equivalent of phosphate has been produced per equivalent of complex, the reaction rate is greatly reduced.

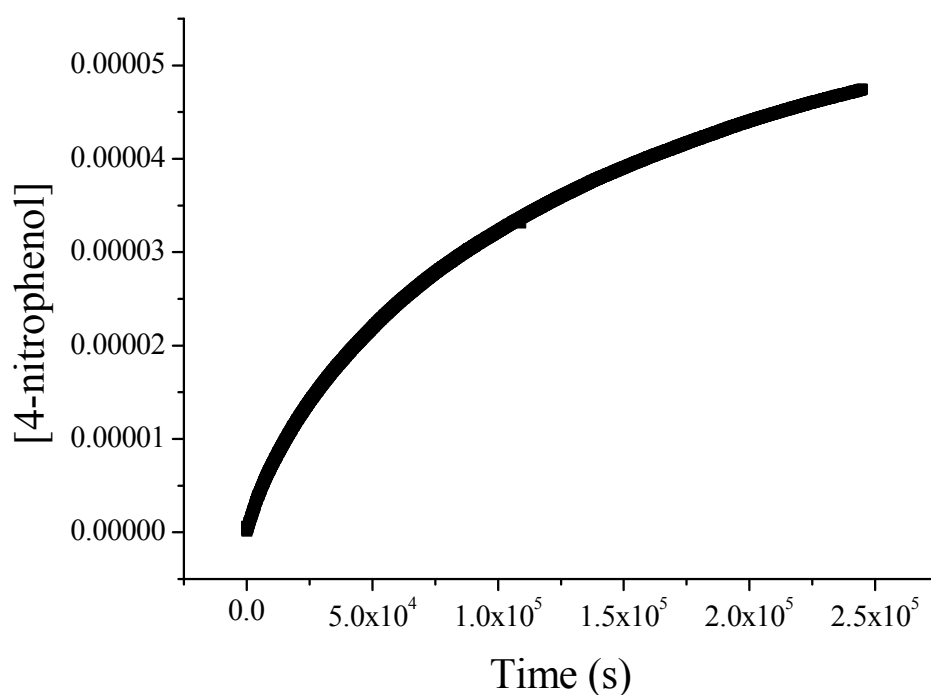


Figure 4.22: Hydrolysis of NPP (5×10^{-4} M) by Zr_2L^1 (5×10^{-5} M).

In another study to demonstrate product inhibition, small amounts of inorganic phosphate were added in order to investigate how this affects the pseudo first order rate constant (**Figure 4.23**).

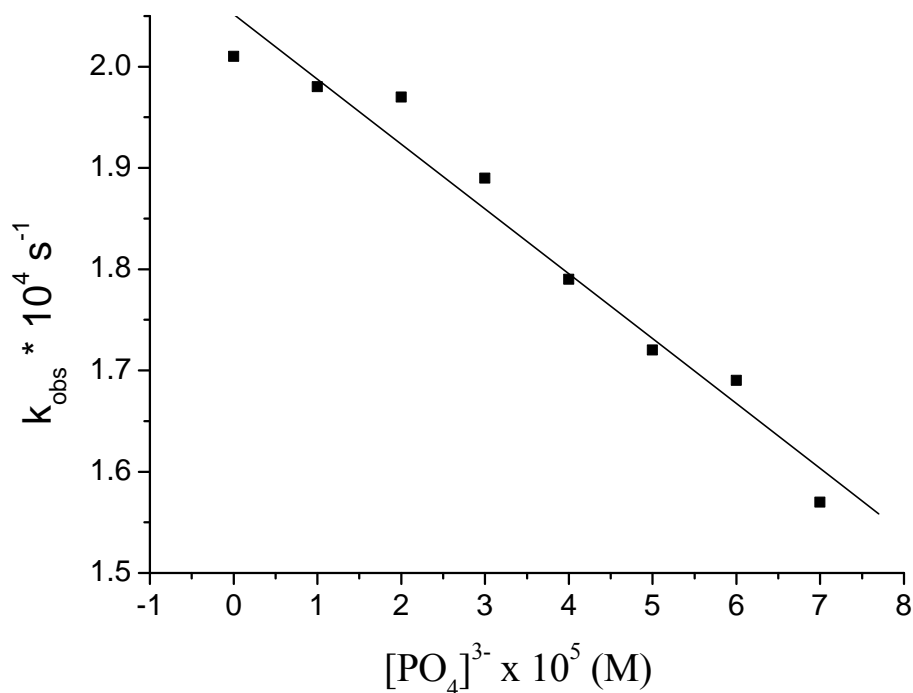


Figure 4.23: Influence of phosphate on reaction rate for 4-NPP (5×10^{-5} M) hydrolysis catalysed by Zr_2L^1 (1 mM). [buffer] = 50 mM (HEPES); I = 0.1 M (NaCl).

4.3. Discussion.

The bis-nucleating ligands HXTA (L^1) and OMeHXTA (L^2) and the mononucleating tripodal ligand (L^3) have been synthesised and their respective complexes with Zr^{IV} studied. ^1H NMR provides strong evidence for metal binding. Also, for tetravalent zirconium, homogenous solutions at neutral pH indicate complexation. In the absence of ligand, zirconium-hydroxo species are insoluble at this pH. Upon increasing pH from acid pH, precipitation of zirconium-hydroxo species occurs at pH 4.5.²⁴

For the dinuclear complexes, complete binding cannot be confirmed. However, no free ligand signals in the ^1H NMR spectrum, in the pD range 5–9.4 are observed. As confirmed by NMR, formation of the mononuclear complex ZrL^3 is complete in the pD range 6.9 – 12.

Evidence for formation of extended complex-zirconium-hydroxo species in solution is the fact that each bis-nucleating ligand keeps 4 equiv. Zr^{IV} in solution and the mononuclear complex keeps 2 equiv. of Zr^{IV} in solution at neutral pH.

Activity of each complex towards phosphate mono- and diester hydrolysis was examined. In studying phosphate diester hydrolysis, the activated substrates BNPP and MNPP were used. Induction periods, in which the rate of hydrolysis is increasing with time, evidenced by a gradual “curving upwards” of the abs. vs. time trace were observed. The length of the induction period varied between systems and no discernible pattern relating induction period length and severity could be established. After a period, linearity is established. Approximate rate constants can be determined by measuring the slope of the linear segment. The approximate observed rate constant (k_{obs}) for the hydrolysis of BNPP ($5.4 \times 10^{-6} \text{ s}^{-1}$) by Zr_2L^1 (1 mM) is larger than that for MNPP ($3.63 \times 10^{-6} \text{ s}^{-1}$); pH 7, 25°C. The increased rate of BNPP hydrolysis relative to MNPP hydrolysis can be ascribed to it containing two electron withdrawing 4-nitrophenol groups, which better-activate phosphorus towards nucleophilic attack relative to MNPP. Also, liberated 4-nitrophenylphosphate from BNPP hydrolysis will itself be hydrolysed to give an inflated value for diester hydrolysis. The rate constant for the spontaneous hydrolysis of BNPP at pH 7 and 25°C is $= 10^{-11} \text{ s}^{-1}$.³⁷ A ~5- orders of magnitude rate acceleration relative to BNPP spontaneous hydrolysis is provided by 1 mM Zr_2L^1 .

Phosphate monoester hydrolysis by these complexes proceeds linearly during the initial 5 % of the reaction and so, the method of initial rates was employed to elucidate kinetic data in the pH range 5.5 – 8.5. As observed in previous studies on zirconium-mediated phosphate di and monoester hydrolysis,²²⁻²⁴ highest activity is observed at lower pH. Rate-pH profiles for both dinuclear complexes (Zr_2L^1 and Zr_2L^2) are almost identical, while lower activity (~4- fold) is observed for the mononuclear complex. Some cooperation between metal ions in the dinuclear complex is evident.

The presence of an electron donating methoxy group on phenol in L^2 has little effect on the activity of its Zr^{IV} complex with respect to Zr_2L^1 in the pH range studied; pH – rate profiles are practically identical. In chapter 2, ligand effects on the kinetics of

phosphate diester hydrolysis mediated by Ga^{III} complexes of tripodal ligands was studied. The Ga^{III} complex of the ligand containing the strongly electron donating *p*-methoxy phenol group is more reactive than that of the electron withdrawing nitro group. From this and other data, it was concluded that the efficiency of a gallium-bound hydroxide nucleophile is more important than the Lewis acid activation of the substrate. No enhanced activity was conferred by the more strongly donating Zr_2L^2 relative to Zr_2L^1 . Zr^{IV} is more labile than Ga^{III} , and thus the Zr-bound hydroxide is expected to be a more reactive nucleophile. Perhaps the inherently greater activity of this nucleophile relative to $\text{Ga}^{\text{III}} - \text{OH}$ means that additional activation by electron-donating ligands is unnecessary.

Comparison of rates of phosphate monoester hydrolysis by mononuclear ZrL^3 and dinuclear complexes, for the same concentration of Zr^{IV} , reveals some positive cooperation between metal ions, with the dinuclear complexes being approximately 2-times more active across the pH range under investigation, at the same metal ion concentration. Values of 2nd order rate constants for the dinuclear complexes Zr_2L^1 ($0.18 \text{ M}^{-1}\text{s}^{-1}$) and Zr_2L^2 ($0.17 \text{ M}^{-1}\text{s}^{-1}$) are approximately 4- times that for the mononuclear complex ZrL^3 ($0.042 \text{ M}^{-1}\text{s}^{-1}$) at neutral pH.

Michaelis-Menten behaviour was observed for each complex in phosphate monoester hydrolysis, indicating the instant establishment of an equilibrium between catalyst and substrate and catalyst-substrate complex. With substrate in excess, after the hydrolysis of one equivalent of phosphate per equivalent of complex, the reaction becomes very slow, possibly due to the formation of unreactive zirconium-phosphate species. Catalytic turnover is not observed.

The most important finding of this study pertains to the relative rates of phosphate monoester versus diester hydrolysis. Comparison of rates of phosphate monoester and approximate rates of phosphate diester hydrolysis shows monoester hydrolysis to be much more efficient. In **Figure 4.23**, the absorbance versus time traces are plotted for phosphate mono- and diester hydrolysis catalysed by Zr_2L^1 (1 mM). Under the same experimental conditions, the pseudo-first order rate constant for monoester hydrolysis ($2.1 \times 10^{-4} \text{ s}^{-1}$) is approx. 60- fold faster than phosphate diester hydrolysis ($3.6 \times 10^{-6} \text{ s}^{-1}$).

A possible explanation for this observation is that monoanionic phosphate diesters are weak ligands and so, binding to the catalyst is poor relative to phosphate monoesters. Strong coordination of metal ions to phosphate monoester compared to diester has been described previously.^{1,15}

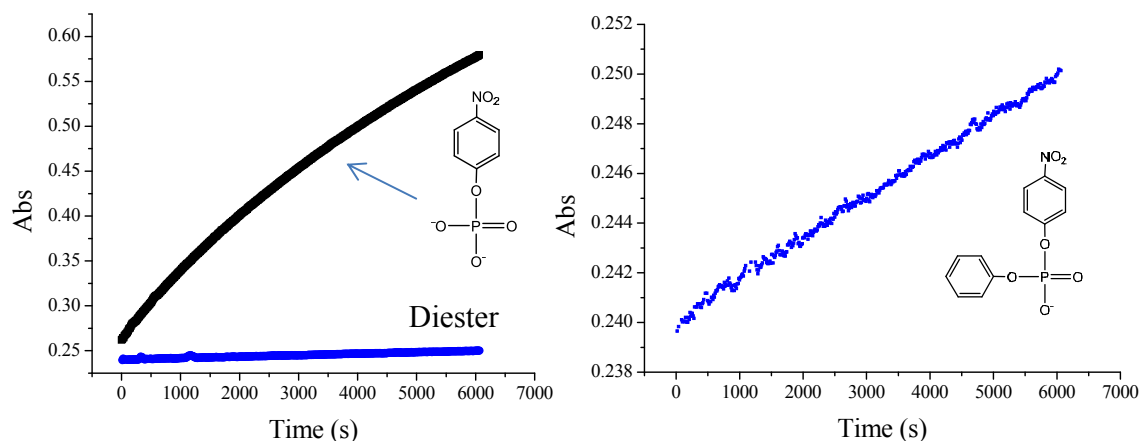


Figure 4.23: 4-NPP versus BNPP (5×10^{-5} M), catalysed by Zr_2L^1 (1 mM) at neutral pH and 25°C. [buffer] = 50 mM (HEPES); I = 0.1 M (NaCl).

Cleavage of the hydrolytically stable phosphate monoester phenyl phosphate is possible with these catalysts. Under mild experimental conditions (40°C and pH 7), and in the presence of 1 equivalent of Zr_2L^1 , the reaction proceeds with an estimated half-life of 4-5 days. This is a remarkable rate enhancement; ~ 7 orders of magnitude relative to the water rate for hydrolysis of dianionic phenyl phosphate of $5 \times 10^{-13} \text{ s}^{-1}$ at 25°C.¹⁷

Thermodynamic parameters; enthalpy of activation (ΔH^\ddagger) and entropy of activation (ΔS^\ddagger) were determined from Eyring plots, for di- and monoester hydrolysis. Activation energies were calculated from the Arrhenius equation. As described in 4.1.1., the mechanisms of uncatalysed phosphate monoester and diester hydrolysis proceed by dissociative and associative pathways respectively.⁷⁻⁹ The activation entropies for hydrolysis of 4-NPP by Zr_2L^1 (-98.6 JK^{-1}), Zr_2L^2 (-75.6 JK^{-1}) and ZrL^3 (-92 JK^{-1}) are very close in value to the value for hydrolysis of the phosphate diester MNPP (-129.7 JK^{-1}) by Zr_2L^1 . These small negative values for entropy of activation suggest possibly an

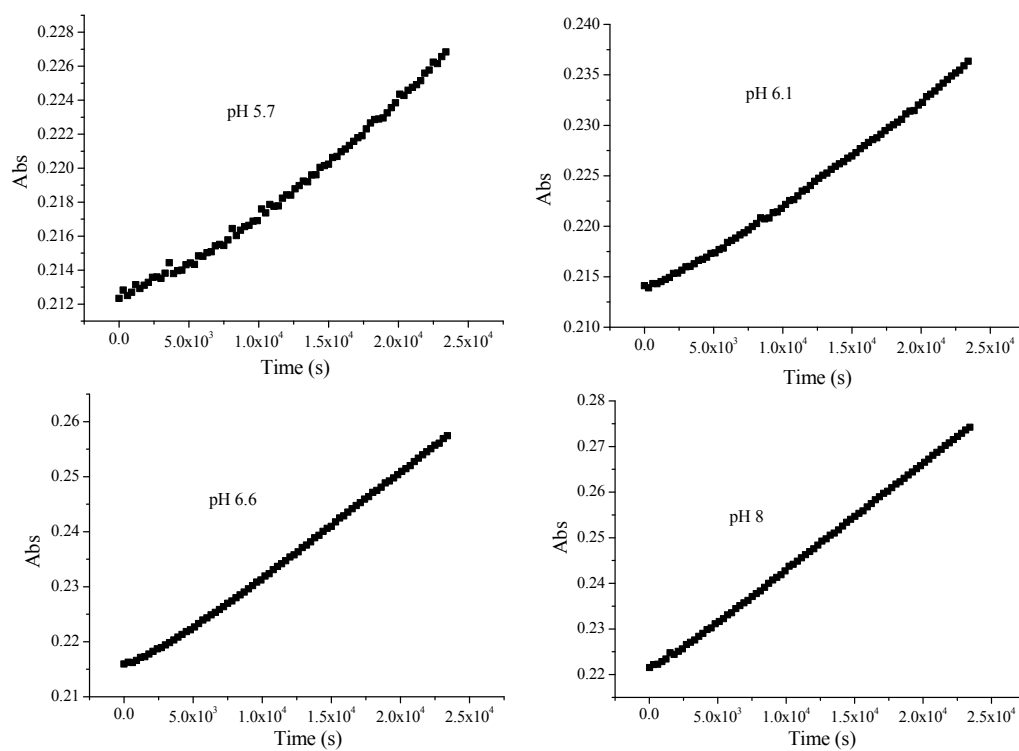
interchange associative pathway, for both phosphate di- and monoester hydrolysis, though it is not possible to say conclusively. Also, given the similar enthalpies ($64 < \Delta H^\ddagger < 71 \text{ kJmol}^{-1}$) of activation, overall activation energies ($66 < E_a < 70 \text{ kJmol}^{-1}$) (from Arrhenius plots) and the small but negative entropies of activation, for diester and monoester hydrolysis, an associative mechanism common to each system might be suggested. This points towards the higher affinity of the monoester for binding to Zr^{IV} relative to the diester as the cause of the observed selectivity.

4.4. References.

- (1) Miyama, S.; Asanuma, H.; Komiyama, M. *J. Chem. Soc., Perkin Trans. 2*, **1997**, 1685.
- (2) Lad, C.; Williams, N. H.; Wolfenden, R. *Proc. Natl. Acad. Sci. U.S.A.* **2003**, *100*, 5607.
- (3) Wolfenden, R.; Zhao, F. *J. Am. Chem. Soc.* **2004**, *126*, 8646.
- (4) Wilcox, D. E. *Chem. Rev.* **1996**, *96*, 2435.
- (5) Zheng, F.; Zhan, C.-G.; Ornstein, R. L. *J. Chem. Soc., Perkin Trans. 2*, **2001**, 2355.
- (6) Souza, B. S.; Brandão, T. A. S.; Orth, E. S.; Roma, A. C.; Longo, R. L.; Bunton, C. A.; Nome, F. *J. Org. Chem.* **2009**, *74*, 1042.
- (7) Kamerlin, S. C. L.; Williams, N. H.; Warshel, A. *J. Org. Chem.* **2008**, *73*, 6960.
- (8) Souza, B. S.; Brandão, T. A. S.; Orth, E. S.; Roma, A. C.; Longo, R. L.; Bunton, C. A.; Nome, F. *J. Org. Chem.* **2008**, *74*, 1042.
- (9) Kamerlin, S. C. L.; Wilkie, J. *Org. Biomol. Chem.* **2007**, *5*, 2098.
- (10) Kirby, A. J.; Jencks, W. P. *J. Am. Chem. Soc.* **1965**, *87*, 3209.
- (11) Jencks, W. P. *Chem. Rev.* **1972**, *72*, 705.
- (12) Hegg, E. L.; Burstyn, J. N. *Coord. Chem. Rev.* **1998**, *173*, 133.
- (13) Komiyama, M.; Sumaoka, J. *Curr. Opin. Chem. Biol.* **1998**, *2*, 751.
- (14) Cowan, J. A. *Curr. Opin. Chem. Biol.* **2001**, *5*, 634.
- (15) Farrell, F. J.; Kjellstrom, W. A.; Spiro, T. G. *Science* **1969**, *164*, 320.
- (16) Jones, D. R.; Lindoy, L. F.; Sargeson, A. M. *J. Am. Chem. Soc.* **1983**, *105*, 7327.
- (17) Seo, J. S.; Sung, N.-D.; Hynes, R. C.; Chin, J. *Inorg. Chem.* **1996**, *35*, 7472.
- (18) Koike, T.; Inoue, M.; Kimura, E.; Shiro, M. *J. Am. Chem. Soc.* **1996**, *118*, 3091.
- (19) Luedtke, N. W.; Schepartz, A. *Chem. Commun.* **2005**, 5426.
- (20) Gómez-Tagle, P.; Yatsimirsky, A. K. *Inorg. Chem.* **2001**, *40*, 3786.
- (21) Kennedy, J. F.; Barker, S. A.; Humphreys, J. D. *J. Chem. Soc., Perkin Trans. 1* **1976**, 962.
- (22) Kennedy, J. F.; Barker, S. A.; Humphreys, J. D. *J. Chem. Soc., Perkin Trans. 1* **1977**, 753.

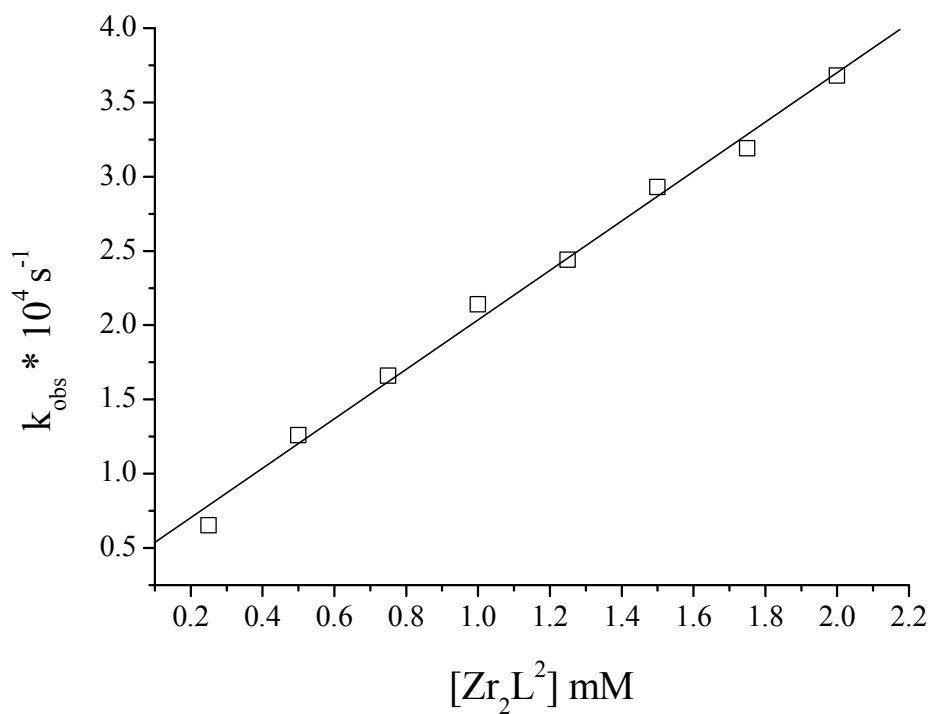
- (23) Ott, R.; Krämer, R. *Angew. Chem. Int. Ed.* **1998**, *37*, 1957.
- (24) Moss, R. A.; Zhang, J.; Ragunathan, K. G. *Tetrahedron Lett.* **1998**, *39*, 1529.
- (25) Jagoda, M.; Krämer, R. *Inorg. Chem. Commun.* **2005**, *8*, 697.
- (26) Stulz, E.; Leumann, C. *Chem. Commun.* **1999**, 239.
- (27) Stulz, E.; Burgi, H.-B.; Leumann, C. *Chem. Eur. J.* **2000**, *6*, 523.
- (28) Berkessel, A.; Héroult, D. A. *Angew. Chem. Int. Ed.* **1999**, *38*, 102.
- (29) Franklin, S. J. *Curr. Opin. Chem. Biol.* **2001**, *5*, 201.
- (30) Branum, M. E.; Tipton, A. K.; Zhu, S.; Que, L. *J. Am. Chem. Soc.* **2001**, *123*, 1898.
- (31) Iranzo, O.; Kovalevsky, A. Y.; Morrow, J. R.; Richard, J. P. *J. Am. Chem. Soc.* **2003**, *125*, 1988.
- (32) Feng, G.; Natale, D.; Prabakaran, R.; Mareque-Rivas, J. C.; Williams, N. H. *Angew. Chem. Int. Ed.* **2006**, *45*, 7056.
- (33) Selmeçzi, K.; Giorgi, M.; Speier, G.; Farkas, E.; Réglie, M. *Eur. J. Inorg. Chem.* **2006**, 1022.
- (34) Neves, A.; Lanznaster, M.; Bortoluzzi, A. J.; Peralta, R. A.; Casellato, A.; Castellano, E. E.; Herrald, P.; Riley, M. J.; Schenk, G. *J. Am. Chem. Soc.* **2007**, *129*, 7486.
- (35) d'Hardemare, A. d. M.; Jarjayes, O.; Mortini, F. *Synth. Commun.* **2004**, *34*, 3975.
- (36) Moss, R. A.; Ragunathan, K. G. *Tetrahedron Lett.* **2000**, *41*, 3275.
- (37) Chin, J.; Banaszczyk, M.; Jubian, V.; Zou, X. *J. Am. Chem. Soc.* **1989**, *111*, 186.

Appendix 4.1. Kinetic Plots for Phosphate Diester Hydrolysis.



Zr₂L¹ (1 mM), 4-NPP (5 x 10⁻⁵ M), 25°C, [buffer] = 50 mM (HEPES); I = 0.1 M (NaCl).

Appendix 4.2. 2nd order plot for the hydrolysis of 4-NPP by Zr₂L².



Zr₂L¹ (1 mM), 4-NPP (0.25 – 2 mM), pH 7, 25°C, [buffer] = 50 mM (HEPES), I = 0.1 M (NaCl).

Chapter 5. Experimental.

5.1. General Information.

^1H and ^{13}C NMR spectra were recorded on Jeol ECX-400 and Varian 500 AR spectrometers and referenced to TSP ($\delta = 0.00$) and methanol ($\delta = 49.5$), respectively. The pD values of D_2O solutions were measured by use of a glass electrode and addition of a value of 0.4 to the pH meter reading.¹² The pD values were adjusted using concentrated DNO_3 and NaOD solutions.

UV/Vis measurements were carried out using a Varian Cary 50 scan spectrophotometer coupled to a Grant thermostated water circulation bath. FT-IR spectra were recorded on a PerkinElmer FT-IR spectrometer fitted with an ATR accessory. Elemental analyses (carbon, hydrogen and nitrogen) were performed with a PerkinElmer 2400 Series II analyser.

Potentiometric titrations were performed on a Jenway 3510 pH meter fitted with a Reflex Sensors Ltd. EC-1910-11 glass electrode. The program HYPERQUAD was used to calculate the deprotonation constants from the titration data.³ Species diagrams were computed using a program based on the COMICS algorithm.⁴ Standardised NaOH solutions were purchased from Aldrich chemical company.

Single crystal X-ray diffraction data for all structures were collected at room temperature on an Oxford Diffraction Xcalibur CCD diffractometer using graphite-monochromated Mo-K_α radiation ($\lambda = 0.71069 \text{ \AA}$).⁵ The structures were solved by direct methods and subsequent Fourier syntheses and refined by full-matrix least squares on F^2 using SHELXS-97, SHELXL-97⁶ and Oscaleil.⁷ The scattering factors were those given in the SHELXL program. Hydrogen atoms except those for the water molecules of crystallization were generated geometrically and refined as riding atoms with isotropic displacement factors equivalent to 1.2 times those of the atom to which they were attached (1.5 for methyl groups). Graphics were produced with ORTEX.⁸

DFT Calculations. All DFT geometry optimizations were done in water at the B3LYP/6-31G* level using Spartan08.⁹

5.2. Kinetic Studies.

The hydrolysis of BDNPP, BNPP, 4-NPP and MNPP were followed by measuring the increase in absorbance at 400 nm due to the production of 2,4-dinitrophenolate or 4-nitrophenolate. Rate constants were obtained by the initial rate method (< 5 % conversion). Concentrations of 2,4-dinitrophenolate and 4-nitrophenolate were calculated from their extinction coefficients $12,100 \text{ M}^{-1}\text{cm}^{-1}$ and $18,700 \text{ M}^{-1}\text{cm}^{-1}$ respectively. Concentrations were corrected for the degree of ionization of 2,4-dinitrophenol and 4-nitrophenol at the respective pH value using pK_a (2,4-dinitrophenol) = 4.0 and pK_a (4-nitrophenol) = 7.15. The pH of the metal complex solutions were adjusted with 1 M NaOH and HCl solutions. Solutions were buffered with 50 mM PIPBS (pH 4 – 5), MES (pH 5 – 6.7), HEPES (pH 6.8 – 8), EPPS (pH 7.5 – 8.5) and CHES (pH 8.5 – 9.5). In a typical experiment, 15 μl of 10 mM substrate was added to 3 ml of buffered complex solution. The ionic strength was maintained at 0.1 M with NaClO_4 or NaCl. In the case of BDNPP, hydrolysis rates have been corrected for the spontaneous hydrolysis of the substrate by following two identical parallel reactions except for the absence of metal complex in one of them. Kinetic runs were run in duplicate to give a reproducibility of $\pm 20 \%$. To determine the solvent deuterium isotope effect, analogous kinetic experiments were performed in H_2O and 99.9 % D_2O . Fitting of the kinetic data was carried out using a non-linear least squares program based on the NIHH23 algorithm.¹⁰

5.3. Materials.

Pyridine-2-carboxaldehyde, imino diacetate, diethyl iminodiacetate, glycine, 2-(chloromethyl)pyridine hydrochloride, p-methoxyphenol, p-cresol, ZnCl_2 , MgCl_2 , ZrOCl_2 , BNPP and $\text{Ga}(\text{NO}_3)_3$ were purchased from Aldrich and used as supplied. All of the other chemicals and solvents were of analytical or spectroscopic grade,

purchased from commercial sources and used without further purification. Deuterated solvents were obtained from Apollo Scientific. BDNPP,¹¹ MNPP¹² and HPNP¹³ were prepared according to published procedures.

5.3.1. Chapter 2: Synthetic Procedures.

[GaL¹(H₂O)₂],¹⁴ H₃L²,¹⁵ H₃L³,¹⁶ H₂L⁴,¹⁷ H₃L⁵,¹⁸ and HL⁶¹⁶ were prepared according to literature procedures. [GaL²(H₂O)₂] and [GaL⁵(H₂O)₂] were generated in situ by mixing equimolar amounts of Ga(NO₃)₃ and the respective ligand.

Preparation of [GaL³(μ-OH)]₂·4H₂O (3). Ga(NO₃)₃·8H₂O (2.92 g, 7.3 mmol) was dissolved in 50 mL water. H₂L³ (1.64 g, 7.3 mmol) was dissolved in 50 mL water and the two solutions were combined. The pH value was adjusted to 2.5 with 5 M NaOH. Slow evaporation of the solution over a period of two weeks yielded cubic crystals. Yield: 1.67 g (66 %). ¹H NMR (D₂O): δ 8.72 (d, ³J = 5.3 Hz, 1H), 8.29 (td, J = 7.8, 1.6 Hz, 1H), 7.82 (t, ³J = 5.7 Hz, 1H), 7.77 (d, ³J = 8.0 Hz, 1H), 4.76 (s, 2H), 3.92 (dd, ²J = 17.6 Hz, 4H). ¹³C NMR (D₂O): δ 174.7, 150.9, 145.9, 144.1, 127.1, 126.2, 62.6, 62.1. IR (cm⁻¹): 3222(br), 1666(m), 1622(s), 1445(w), 1378(s), 1340(m), 1309(m), 1269(w), 1153(w), 1104(w), 1027(w), 970(w), 911(m), 831(w), 773(m), 748(s), 728(m). Anal. calcd (%) for C₂₀H₃₀Ga₂N₄O₁₄: C, 34.82; H, 4.38; N, 8.12; found: C, 34.90; H, 4.18; N, 8.54 %.

Preparation of [GaL⁴(μ-OH)]₂·4H₂O (4). Ga(NO₃)₃·8H₂O (2.92 g, 7.3 mmol) was dissolved in water (50 mL) and added to an aqueous solution (50 mL) of H₂L⁴ (1.28 g, 7.3 mmol). The pH value of the solution was adjusted to 5 with 5 M NaOH. Slow evaporation of the solution over a period of two weeks yielded small needles suitable for X-ray analysis. Yield: 980 mg (46 %). ¹H NMR (D₂O): δ 3.69 (m, 4H), 3.03 (s, br, 2H), 2.87 (s, br, 2H). ¹³C NMR (D₂O): δ 176.3, 60.7, 58.23, 36.2. IR (cm⁻¹): 3225(br), 3091(w), 2987(w), 1608(s), 1393(m), 1301(m), 1210(w), 1175(w), 1100(w), 1070(m), 1053(m), 1000(w), 981(w), 917(m), 878(w), 789(w), 734(m). Anal. calcd (%) for C₁₂H₃₀Ga₂N₄O₁₄: C, 24.27; H, 5.00; N, 9.49; found: C, 24.22; H, 4.41; N, 9.56 %.

Preparation of [Ga(HL⁴)₂]Cl·2H₂O (4a). A solution of Ga(NO₃)₃·8H₂O (2.92 g, 7.3 mmol) in 50 mL water was mixed with a solution of H₂L⁴ (1.28 g, 7.3 mmol) in 50 mL water. The pH value was adjusted to 3 using 5 M NaOH. Slow evaporation of the solution over a period of two weeks gave colourless cubes of **4a** which were insoluble in all common solvents. Yield: 1.12 g (62%). IR (cm⁻¹): 2913(br), 1638(s), 1523(w), 1381(s), 1364(s), 1348(m), 1315(m), 1251(w), 1176(w), 1107(w), 1051(m), 1000(m), 969(m), 942(m), 928(m), 907(s), 765(s). Anal. calcd (%) for C₁₂H₂₆ClGa₄N₄O₁₀: C, 29.26; H, 5.33; N, 11.37; found: C, 28.53; H, 5.0; N, 11.30 %.

Preparation of [GaL⁶(μ-OH)]₂(NO₃)₂·3H₂O (6). Ga(NO₃)₃·8H₂O (2.92 g, 7.3 mmol) was dissolved in 50 mL water and added to a solution of HL⁶ (1.87 g, 7.3 mmol) in water (50 mL). The pH value of the solution was adjusted to 2.5 using 5 M NaOH. Slow evaporation of the solution over a two week period yielded small needles of the dimer. Yield: 950 mg (30 %). ¹H NMR (D₂O): δ 8.83 (d, ³J = 5.24 Hz, 2H), 8.33 (td, J = 8.0, 1.6 Hz, 2H), 7.85 (m, 4H), 5.00 (d, ²J = 16.48 Hz, 2H), 4.76 (d, ²J = 16.48 Hz, 2H), 3.88 (s, 2H). ¹³C NMR (D₂O): δ 174.6, 150.8, 145.9, 144.3, 127.2, 126.3, 61.8, 61.6. IR (cm⁻¹): 3092(br), 1611(s), 1469(w), 1450(w), 1369(s), 1336(s), 1306(s), 1269(m), 1160(w), 1098(m), 1053(w), 1031(m), 966(w), 908(m), 829(w), 767(s), 746(m). Anal. Calcd (%) for C₂₈H₃₆Ga₂N₈O₁₅: C, 38.92; H, 4.19; N, 12.97; found: C, 38.47; H, 4.07; N, 13.09 %.

5.3.2. Chapter 3: Synthetic Procedures.

Preparation of [Mg(H₂O)₆][Mg₂(HXTA)]₂·4H₂O. MgCl₂·6H₂O (406 mg, 2 mmol) and Na₄HXTA (0.54 g, 1 mmol) were dissolved in 15 ml water. The pH was adjusted to 7 and the solution was left to stand in an open beaker. After 1 – 2 weeks, crystals in the form of colourless blocks had appeared (0.751 g, 0.583 mmol). ¹H NMR (400 MHz, D₂O): δ 6.90 (s, 2H), 3.84 (d, J = 28.1 Hz, 2H), 3.50 (d, J = 15.8 Hz, 2H), 3.35 (d, J = 16 Hz, 2H), 3.24 (d, J = 16.7 Hz, 2H), 3.14 (d, J = 17.2 Hz, 2H), 3.05 (d, J = 11.2 Hz, 2H), 2.12 (s, 3H). Anal. Calcd. for C₃₄H₇₆Mg₅N₄O₃₉: C, 31.74; H, 5.95; N, 4.35; found: C, 31.52; H, 5.95; N, 4.32.

Preparation of $[\text{Zn}_2(\text{HXTA})(\text{ac})(\text{H}_2\text{O})_2\text{Zn}(\text{H}_2\text{O})_4]_n$. ZnCl_2 (273 mg, 2 mmol), Na_4HXTA (0.54 g, 1 mmol) and sodium acetate (82 mg, 1 mmol) were dissolved in 15 ml water. The pH was adjusted to 6 and the solution was left to stand in an open beaker. After 1 – 2 weeks, crystals in the form of colourless blocks had appeared (0.41 g, 0.54 mmol). ^1H NMR (400 MHz, D_2O): δ 6.95 (s, 2 H), 3.3 (br s, 12H), 2.15 (s, 3 H). Anal. Calcd. for $\text{C}_{34}\text{H}_{76}\text{Mg}_5\text{N}_4\text{O}_{39}$: C, 31.74; H, 4.26; N, 3.70; found: C, 30.16; H, 4.22; N, 3.68. Anal. Found (calcd. for $\text{C}_{19}\text{H}_{32}\text{N}_2\text{O}_{17} \text{Zn}_3$): C, 31.36 (30.16); H, 4.22 (4.26); N, 3.68 (3.70).

5.3.3. Chapter 4: Synthetic Procedures.

The zirconium complexes of H_5L^1 , H_5L^2 and H_3L^3 were prepared *in situ* according to the procedure described in 4.2.1.

5.4. References

- (1) Glasoe, P. K.; Long, F. A. *J. Phys. Chem.* **1960**, *64*, 188.
- (2) Mikkelsen, K.; Nielsen, S. O. *J. Phys. Chem.* **1960**, *64*, 632.
- (3) Gans, P.; Sabatini, A.; Vacca, A. *Talanta* **1996**, *43*, 1739.
- (4) Ginzburg, G. *Talanta* **1977**, *23*, 149.
- (5) CrysAlisPro, Oxford Diffraction Ltd., Version 1.171.33.31 (release 08-01-2009 CrysAlis171.NET).
- (6) Sheldrick, G. M. SHELXS-97. Program for crystal structure solution, University of Göttingen, Germany, 1997. (b) Sheldrick, G. M. SHELXL-97, Program for crystal structure refinement, University of Göttingen, Germany, 1997. (c) Sheldrick, G. M. SHELXTL-PLUS (VMS), siemens Analytical X-ray Instruments, Inc., Madison, WI, 1990.
- (7) Mc Ardle, P.; Gilligan, K., Cunningham, D.; Dark, R.; Mahon, M. *CrystEngComm*, **2004**, *6*, 303-309.
- (8) McArdle, P. PC Windows version, *J. Appl. Cryst.* **1995**, *28*, 65-65.
- (9) Spartan '08, Wavefunction, Inc. Irvine, CA.
- (10) Fletcher, J. E.; Shrager, R. I. National Institute of Health, MD, USA.
- (11) Bunton, C. A.; Farber, S. J. *J. Org. Chem.* **1969**, *34*, 767-772.
- (12) Ross, R. A.; Ragunathan, K. G. *Tet. Lett.* **2000**, *42*, 3275.

- (13) Brown, D. M.; Usher, D. A. *J. Chem. Soc.* **1965**, 6558.
- (14) Jarjayes, O.; Mortini, F.; du Moulinet d'Hardemare, A.; Philouze, C.; Serratrice, G. *Eur. J. Inorg. Chem.* **2005**, 4417-4424.
- (15) Du Moulinet d'Hardemare, A.; Jarjayes, O.; Mortini, F. *Synth. Commun.* **2004**, *34*, 3975-3988.
- (16) Chiu, Y.-H.; Canary, J. W. *Inorg. Chem.* **2003**, *42*, 5107-5116.
- (17) McLendon, G.; Motekaitis, R. J.; Martell, A. E. *Inorg. Chem.* **1975**, *14*, 1993-1996.
- (18) Ceccato, A. S.; Neves, A.; de Brito, M. A.; Drechsel, S. M.; Mangrich, A. S.; Werner, R.; Haase, W.; Bortoluzzi, A. J. *J. Chem. Soc., Dalton. Trans.* **2000**, 1573-1577.